JOHANNES GUTENBERG UNIVERSITÄT MAINZ

JG|U

ASTROPARTICLE PHYSICS

Luca Doria

Institut für Kernphysik
J.J. Becher-Weg 45 55128 Mainz (Germany)
doria@uni-mainz.de

Vertiefende Kapitel der Teilchenphysik
Sommersemester 2020

Fachbereich Physik, Mathematik und Informatik
der Johannes Gutenberg-Universität Mainz

March 2020

Chapter 1 | Preface

This document contains the notes of the "Astroparticle Physics" course held in the 2020 Summer Term at the Johannes Gutenberg University in Mainz (Germany). The course is aimed at last year Bachelor and Master students. With the term “astroparticle”,we refer to particle physics applied to astrophysical sources: stars, galaxies, interstellar medium, and even black holes. Astrophysical objects generate and send around the universe many kinds of particles which we can detect: photons, leptons, hadrons and nuclei, and neutrinos. The groundbreaking recent detection of gravitational waves opens a completely new opportunity for complementing a *multimessenger astronomy* approach, where an astrophysical source can be observed detecting many different emission patterns.

Contents

1 Preface **i**

2 General Relativity **1**
2.1 The Equivalence Principle 1
2.2 Free-Falling Bodies 2
2.3 Non-Relativistic Limit 3
2.4 Energy-Momentum Tensor 4
2.5 The Einstein Equations 5
2.6 Trace-Reversed Form of the Einstein Equations 7
2.7 Geodesic Deviation 7
2.8 Summary 8

3 Cosmological Models **11**
3.1 The Cosmological Principle 11
3.2 Metric of Homogeneous and Isotropic Space-times 12
3.3 Properties of the FLRW Universe 14
3.4 Friedmann Equations 15
3.5 The Cosmological Parameters 18
3.6 Cosmological Models 19
3.6.1 The Einstein Universe 19
3.6.2 The Matter-dominated Universe 20
3.6.3 The Radiation-dominated Universe 20
3.6.4 Vacuum-Dominated Universe 21
3.6.5 Mixed Models 22
3.7 Cosmological Red Shift 22
3.8 Age of the Universe 24

4 Elements of Nuclear Physics **27**
4.1 General Properties of Nuclei 27
4.2 A simple nuclear model: Weizsäcker Semiempirical Mass Formula 29

5 Early Universe Thermodynamics and Freeze-Out **33**
5.1 Equilibrium 33
5.2 Statistical Mechanics Recap 34
5.3 Entropy and its Density 36
5.4 Thermal Decoupling 38
5.5 The Boltzmann Equation 39
5.6 Freeze Out 42

6 Nucleosynthesis **45**
6.1 Introduction 45
6.2 Protons and Neutrons 46
6.3 Nuclear Reactions at Equilibrium 47
6.4 Nucleosynthesis of the Light Elements 49
6.5 Predictions of Big Bang Nucleosynthesis 51
6.6 Observations 52

7 Cosmic Rays **57**
7.1 Introduction 57
7.2 Cosmic Ray Flux 58
7.3 Primary Cosmic Rays 58
7.4 Secondary Cosmic Rays and Showers 59
7.5 Diffusion 64
7.6 Acceleration Mechanisms 68
7.6.1 Magnetic Mirrors 69
7.6.2 Second Order Fermi Acceleration 71
7.6.3 First Order Fermi Acceleration 73
7.7 Supernovae as Sources of Shock Waves 75
7.8 The Knee 76
7.9 After the Knee 78
7.10 Can be a (binary) pulsar a candidate source for high-energy cosmic rays? 79
7.11 Ultra-High Energy Cosmic Rays 80
7.12 The GZK Effect 81

8 The Gamma Ray Sky **85**
8.1 Hadronic Sources . . . 85
8.2 Leptonic Sources . . . 86
8.3 The 511 keV Line . . . 88
8.4 The Crab Nebula . . . 90
8.5 An interesting gamma source: Geminga . . . 91
8.6 Gamma ray bursts . . . 92
8.7 The "TeV Sky" . . . 93

9 Neutrino Astronomy **95**
9.1 Neutrino Basics . . . 95
9.2 Neutrino Sources and the Waxman-Bahcall Bound . . . 98
9.3 Short Digression: Neutrino freeze-out . . . 99
9.4 Solar Neutrinos . . . 100
9.5 Solar Neutrino Spectrum . . . 102
9.6 The Solar Neutrino Problem . . . 104
9.7 How to detect Solar Neutrios . . . 105
9.8 Radiochemical Experiments . . . 105
9.9 Real-time Experiments . . . 106
9.10 Supernova Neutrinos . . . 109
9.11 How to detect supernova neutrinos . . . 113
9.12 SN 1987A . . . 114
9.13 Diffuse Supernove Neutrino Background . . . 116

10 Dark Matter **117**
10.1 Galaxy Rotation Curves . . . 118
10.2 Barionic Mass Estimation with X-ray Halos . . . 118
10.3 Gravitational Mass Estimation with Weak Lensing . . . 120
10.4 Dark Matter from Astrophysical Measurements . . . 122
10.5 Dark Matter and Structure Formation . . . 124
10.6 Dark Matter Properties . . . 124
10.7 Dark Matter as a Thermal Relic . . . 125
10.8 Hot Thermal Relics and the Example of Neutrinos . . . 126
10.9 Cold Thermal Relics and WIMPs . . . 126
10.10 Mass Ranges for Cold Thermal Relics . . . 129
10.11 Direct Searches for Dark Matter . . . 130

10.12 Velocity Distribution Models 131

11 Dark Energy **135**
11.1 Introduction 135
11.2 Cosmological Constant 136
11.3 Cosmological Constant and the Vacuum 137
11.4 Modified Gravity 138
11.5 Coupling gravity with quantum fields 139
11.6 Dark Energy Measurements 140
11.7 Experimental Details 143

12 Gravitational Waves **145**
12.1 Brief History 145
12.2 Linearized General Relativity 146
12.3 Plane Waves 150
12.4 The TT gauge 151
12.5 Effect on Particles 152
12.6 Observation of gravitational waves with laser interferometers 153
12.7 Gravitational wave energy and amplitude 155
12.8 Gravitational Wave Sources 156

13 Cosmological Perturbations **159**
13.1 Introduction 159
13.2 Classical Newton's theory for non-relativistic matter 159
13.3 First order perturbations for non-relativistic matter 161
13.4 Linear perturbations in comoving coordinates 162
13.5 Perturbations Analysis 163
13.6 Large perturbations in an expanding matter-dominated Universe 165
13.7 Large perturbations in an expanding radiation-dominated Universe 166

14 The Cosmic Microwave Background **167**
14.1 Recombination 168
14.2 Multipole Decomposition of the CMB 168
14.3 Angular Scales 170
14.4 CMB Polarization 171
14.5 CMB Anisotropies 174

14.5.1 Primary Anisotropies 177

Chapter 2 | General Relativity

In this chapter, we briefly review the central concepts at the foundations of General Relativity (GR) and derive its fundamental equations.

2.1 The Equivalence Principle

Gravity has the unique property of impressing the same acceleration to bodies regardless from their mass. This observation leads to the indistinguishably between gravity or an accelerated reference frame. Following an ideal experiment suggested by Einstein, if we are inside an uniformly accelerated elevator, we might think to be immersed in a gravitational field (or the other way around: we think that the elevator is accelerating, but it just hangs still over the surface of a planet). There is a key observation to make here: if the elevator is large enough, we can understand if it is accelerated or at rest into a gravitational field. In the latter case, we could for example note that the acceleration vectors in the elevator are not all parallel. For example, if the elevator is immersed in the gravitational field of a planet, the field lines converge to a single point (the center of the planet). Therefore, an accelerated reference frame or a gravitational field are indistinguishable only *locally*.
We can state now the so called **(strong) Equivalence Principle (EP)**: *at every space-time point in a gravitational field, it is possible to choose a locally inertial coordinate system such that in a sufficiently small neighborhood of that point the laws of nature are expressed in the same form as in an unaccelerated Cartesian (flat) coordinate system.* There is also a weaker version of the principle, called **(weak) Equivalence Principle** which instead of referring to all the laws of nature, it refers only to the laws of motion of free-falling bodies. Clearly the strong version implies the weak on but not vice-versa.

2.2 Free-Falling Bodies

Let's try to translate in mathematical formulas the ideas contained in the EP. Consider a free-falling body: according to the EP, there must exist locally a coordinate system where the effect of gravitation vanishes (inside Einstein's elevator) and the equation of motion in flat space time is

$$\frac{d^2\xi^\mu}{d\tau^2} = 0 \quad , \tag{2.1}$$

where $d\tau^2 = -\eta_{\mu\nu} d\xi^\mu d\xi^\nu$ is the proper time and $\eta_{\mu\nu}$ the Lorentz metric. Let's get out from the elevator and change to new coordinates x^μ, which can be whatever we want (a curvilinear system, an accelerated or rotating system, etc..)

$$\frac{d}{d\tau}\left(\frac{\partial\xi^\alpha}{\partial x^\mu}\frac{dx^\mu}{d\tau}\right) = \frac{\partial\xi^\alpha}{\partial x^\mu}\frac{d^2x^\mu}{d\tau^2} + \frac{\partial^2\xi^\alpha}{\partial x^\mu \partial x^\nu}\frac{dx^\mu}{d\tau}\frac{dx^\nu}{d\tau} = 0 \quad . \tag{2.2}$$

Multiplying the last equation by $\partial x^\lambda / \partial \xi^\alpha$ and recognizing the presence of the Christoffel symbol [1]

$$\frac{d^2x^\lambda}{d\tau^2} + \Gamma^\lambda_{\mu\nu}\frac{dx^\mu}{d\tau}\frac{dx^\nu}{d\tau} = 0 \quad . \tag{2.4}$$

The last result is quite interesting: the presence of the gravitational field can be seen as a curvature of space-time where free-falling particles follow a geodetic in that space. From the coordinate transformation formula and $d\tau = -\eta_{\mu\nu} d\xi^\mu d\xi^\nu$, it is clear that the metric tensor of the curved space is related to the Lorentzian flat space by

$$g_{\mu\nu} = \frac{\partial\xi^\alpha}{\partial x^\mu}\frac{\partial\xi^\beta}{\partial x^\nu}\eta_{\alpha\beta} \quad . \tag{2.5}$$

[1] Only the metric is needed for calculating the Chistoffel symbols:

$$\Gamma^\sigma_{\mu\nu} = \frac{1}{2} g^{\sigma\rho}\left(\partial_\mu g_{\nu\rho} + \partial_\nu g_{\rho\mu} - \partial_\rho g_{\mu\nu}\right) \quad . \tag{2.3}$$

2.3 Non-Relativistic Limit

So far our calculations were relativistic and now we would like to see if what we derived can be reduced to the know non-relativistic result, which should be classical Newtonian gravity. The non-relativistic limit refers to velocities smaller than the speed of light ($v \ll c$) and weak, stationary gravitational fields. Remembering the composition of the velocity four-vector $dx^\mu/d\tau = (dt/d\tau, dx/d\tau)$, in this limit $dx/d\tau \ll dt/d\tau$ so the only non-zero component of the velocity is $\mu = 0$ and therefore

$$\frac{d^2x^\mu}{d\tau^2} + \Gamma^\mu_{00}\left(\frac{dt}{d\tau}\right)^2 = 0 \quad . \tag{2.6}$$

For a weak stationary gravitational field, the space-time geometry must be almost flat: $g_{\alpha\beta} = \eta_{\alpha\beta} + h_{\alpha\beta}$ with $|h_{\alpha\beta}| \ll 1$.
Substituting this metric tensor into the Christoffel symbol we obtain

$$\Gamma^\alpha_{00} = -\frac{1}{2}\eta^{\alpha\beta}\frac{\partial g_{00}}{\partial x_\beta} \quad . \tag{2.7}$$

Reinserting the Christoffel symbol in Eq. 2.6 and separating the $\mu = 0$ "time" and $\mu = 1, 2, 3$ "space" parts we have

$$\frac{d^2t}{d\tau^2} = 0 \quad ; \quad \frac{d^2\mathbf{x}}{d\tau^2} - \frac{1}{2}\left(\frac{dt}{d\tau}\right)^2 \nabla h_{00} = 0 \quad . \tag{2.8}$$

The first equation tells us that $dt/d\tau$ is a certain constant K and we choose K=1. Substituting the first equation in the second and comparing it with the equation of motion with the gravitational potential $d^2x/dt^2 = -\nabla\phi$ we find $h_{00} = -2\phi + C$ where C is another constant. Since the potential must be zero at infinity, we can fix also the second constant C=0. Reinserting the result for h in the original metric tensor we finally have

$$g_{00} = -(1 + 2\phi) \tag{2.9}$$

which is its the only non-zero component in the low-velocity, low-gravitational field approximation. We have showed here that there is a choice of the metric tensor which in the non-relativistic limit makes the relativistic geodesic equation is consistent with Newtonian gravity.

2.4 Energy-Momentum Tensor

Our aim is to find general relativistic equations for the gravitational field which are valid in every reference frame (not only the inertial ones). Such equation must have tensorial character, and since gravitational fields are created by matter and energy distributions, it it meaningful to find a (relativistic) tensorial description for them. The object we are looking for is the energy-momentum tensor. We know already from electrodynamics that in the 4-dimensional formalism charge density and current vector can be organized in a single four-vector. We are going to do something similar for the 4-momenta p^α of a system of N particles labeled with the index n. The momentum density is

$$T^{\alpha 0} = \sum_n p_n^\alpha \delta^3(x - x_n) \quad . \tag{2.10}$$

Note that in this definition we are already thinking at the density as the zeroth-component of a tensor T. In this case T is a tensor with two indices, since one index spans the 4-vector components, while the other one will label the density and the three components of the current which we define as

$$T^{\alpha i} = \sum_n p_n^\alpha \frac{dx_n^i}{dt} \delta^3(x - x_n) \quad . \tag{2.11}$$

where the latin index i runs only on the "space" coordinates 1,2,3. Merging the last two equations into a single tensor

$$T^{\alpha\beta} = \sum_n p_n^\alpha \frac{dx_n^\beta}{dt} \delta^3(x - x_n) = \sum_n \frac{p_n^\alpha p_n^\beta}{E_n} \delta^3(x - x_n) \quad , \tag{2.12}$$

where we used the known relativistic result $v = p/E$. From the last expression, it is clear that $T^{\alpha\beta} = T^{\beta\alpha}$, and therefore the energy-momentum tensor is symmetric.
As in classical physics the time derivative of the momentum gives the force, in this context we have

$$\frac{\partial T^{\alpha\beta}}{\partial x^\beta} = F^\alpha \quad , \tag{2.13}$$

where F^α is a density of forces' 4-vector. In absence of forces, $\partial T^{\alpha\beta}/x^\beta = 0$ and this represents the energy-momentum conservation law. On a generic

curved space, the partial derivative is substituted by the covariant one: $\nabla_\alpha T_{\alpha\beta} = 0$.

2.5 The Einstein Equations

We are now in the position to derive the generally covariant equations for the gravitational field. The distribution of matter and energy exerts a gravitational force, and we have seen that gravitation itself is related to the space-time metric. So we expect that the energy matter distribution is somehow related to space-time geometry. For guessing the correct equations, we can list first the requirements they have to obey:

1. The equations have to be tensor equations, thus retaining their form in any coordinate system. This requirement is connected to the equivalence principle.
2. In analogy to the other field equations of physics, they have to be partial differential equations of (at most) second order in the variable expressing the gravitational potential. In this case such variable is $g_{\mu\nu}$, the metric tensor, as we have seen in the approximate case of the Newtonian non-relativistic limit.
3. The equations must reduce to the Poisson equation for the gravitational potential in the non-relativistic weak-field limit.
4. $T^{\mu\nu}$ must be the source of the gravitational field, since it encodes the energy-matter distribution.
5. If the space-time is flat (no gravitational field), then $T^{\mu\nu} = 0$.

From requirements 1. and 4., the equations must have a form like

$$G^{\mu\nu} \propto T^{\mu\nu} \quad . \tag{2.14}$$

Since we know that from energy-momentum conservation $\nabla_\mu T^{\mu\nu} = 0$, we require that $\nabla_\mu G^{\mu\nu} = 0$. Moreover, since T is symmetric, also G must be symmetric. A symmetric, two-indices tensor which contains $g_{\mu\nu}$ and its derivatives up to second order is the Einstein tensor. So we can guess the following form

$$R_{\mu\nu} - \frac{1}{2} g_{\mu\nu} R = k \cdot T_{\mu\nu} \quad . \tag{2.15}$$

where now we use covariant indices, $R_{\mu\nu}$ is the Ricci tensor, R is the Ricci scalar and k is a constant. We have to check now if requirement 3. holds. We have to use the weak-field and $v \ll c$ approximations together with stationarity $\partial g_{\mu\nu}/\partial t = 0$. In this limit, the only non-zero component of the Ricci tensor is R_{00}. The energy-momentum tensor reduces also to only the energy density component T_{00} which in the non-relativistic limit is just the matter density ρ. The approximate equation is therefore

$$R_{00} = \frac{1}{2}\nabla^2 h_{00} = k\rho \quad , \tag{2.16}$$

which has to be compared to the Poisson equation for the gravitational potential

$$\nabla^2 \phi = 4\pi G\rho \quad . \tag{2.17}$$

where G is the Newton constant. Calculating the constant k, we can write the general relativistic Einstein equation (in natural units $G = c = 1$)

$$R_{\mu\nu} - \frac{1}{2}g_{\mu\nu}R = 8\pi T_{\mu\nu} \quad . \tag{2.18}$$

In "normal units", $8\pi \to 8\pi G/c^4$.
The equation has been checked against many astronomical data, and laboratory and satellite experiments, always finding good agreement up to now.
Eq. 2.18 is not the most general form allowed by our requirements. Since the covariant derivative of both sides of the equation vanishes and this happens also for the metric tensor, we can also add a term which is proportional to $g_{\mu\nu}$

$$R_{\mu\nu} - \frac{1}{2}g_{\mu\nu}R + \Lambda g_{\mu\nu} = 8\pi T_{\mu\nu} \quad . \tag{2.19}$$

The new constant Λ is called **cosmological constant**.
Given the symmetry of the tensors in the equation, there are only 10 independent components. This means that the Einstein equation represents a coupled system of 10 non-linear second-order partial differential equations and finding analytical general solutions is possible only in few cases characterized by high symmetry content. Besides the trivial flat solution, a particularly important space-time satisfying the Einstein equations is the **Schwarzschild solution** which finds wide applications in physics problems involving a spherically symmetric gravitational field.

2.6 Trace-Reversed Form of the Einstein Equations

There is another equivalent form for Eq. 2.19 which can be obtained taking first its trace

$$-R + 4\Lambda = 8\pi T \quad , \tag{2.20}$$

where R and T are the traces of the Ricci tensor and energy-momentum tensor respectively. Multiplying the last trace formula by $g_{\mu\nu}/2$ and substituting the result again in Eq. 2.19, we obtain the "trace-reversed" form of the Einstein equations

$$R_{\mu\nu} - \Lambda g_{\mu\nu} = 8\pi(T_{\mu\nu} - \frac{1}{2}T g_{\mu\nu}) \quad . \tag{2.21}$$

This version of the equation allows some interesting observations. First, in absence of the cosmological constant, matter and energy we have $R_{\mu\nu} = 0$, which represent a Ricci-flat space-time. Ricci-flat spacetimes are the solutions of GR for the completely empty space. The flat space-time is a trivial example of Ricci-flat space-time. A classical non-trivial example of vacuum solution is the Schwarzschild solution describing the space-time around a spherical mass. In absence of matter and energy, and $\Lambda \neq 0$ we have

$$R_{\mu\nu} = \Lambda g_{\mu\nu} \quad , \tag{2.22}$$

and it is tempting to do the identification $T_{\mu\nu} = \Lambda g_{\mu\nu}$ and thinking at the cosmological constant as the energy content of the vacuum itself.

2.7 Geodesic Deviation

There is another interpretation of the role played by the Riemann tensor in General Relativity. If a free-falling observer observes a nearby free-falling object, if there is no gravity, he should see it at rest. If gravity is present, the observer and the object should move with respect to each other. The free-falling observer follows the trajectory

$$\frac{d^2x^\mu}{d\tau^2} + \Gamma^\mu_{\nu\lambda}\frac{dx^\nu}{d\tau}\frac{dx^\lambda}{d\tau} = 0 \quad . \tag{2.23}$$

Another observer is closeby, at $x^\mu(\tau) + \delta x^\mu(\tau)$ thus following the trajectory

$$\frac{d^2}{d\tau^2}(x^\mu + \delta x^\mu) + \Gamma^\mu_{\nu\lambda}(x^\mu + \delta x^\mu)\frac{d}{d\tau}(x^\nu + \delta x^\nu)\frac{d}{d\tau}(x^\lambda + \delta x^\lambda) = 0 \quad . \tag{2.24}$$

The difference between the last two equations at first order in δx^μ is

$$\frac{d^2\delta x^\mu}{d\tau^2} + \frac{\partial\Gamma^\mu_{\nu\lambda}}{\partial x^\rho}\delta x^\rho\frac{dx^\nu}{d\tau}\frac{dx^\lambda}{d\tau} + 2\Gamma^\mu_{\nu\lambda}\frac{dx^\nu}{d\tau}\frac{dx^\lambda}{d\tau} = 0 \quad , \tag{2.25}$$

which in terms of a covariant derivative along a curve [2] can be written as

$$\frac{D^2}{D\tau^2}\delta x^\lambda = R^\lambda_{\nu\mu\rho}\delta x^\mu\frac{dx^\nu}{d\tau}\frac{dx^\rho}{d\tau} \quad . \tag{2.26}$$

In absence of gravity, the Riemann tensor is identically zero and two close geodetics stay "parallel" to each other. If gravity is present, two nearby particles will not conserve their distance along the motion. In this sense, the Riemann tensor can be regarded as quantifying the amount of *geodesic deviation*. The relative acceleration detected among two nearby particles can be thought to be caused by a *tidal force*.

2.8 Summary

Eq. 2.18 was written first by Einstein in 1915 (with Riemann almost contemporarily providing a derivation based on a variational method). General Relativity can thus be summarized as follows:

Space-time is described by a manifold M equipped with a Lorentz metric. The curvature of M (computable from the metric) is related to the matter/energy distribution in M by the Einstein equation.

Eq. 2.18 represent 10 non-linear partial differential equations of the hyperbolic kind (like the wave equation) and they are the gravitational analog to the Maxwell equations written with the relativistic formalism where

[2] If V^μ is a vector, its derivative along a curve x^μ parameterized by a parameter τ is $DV^\mu/D\tau = dA^\mu/d\tau + \Gamma^\mu_{\nu\lambda}dx^\lambda/d\tau A^\nu$.

the scalar and vector potentials are arranged into a fourvector A_μ and charge density and current into a four-vector J_μ: $\partial^2 A_\mu = -4\pi J_\mu$. A fundamental difference among these two theories is the following: while in Maxwell theory once the charges/currents are given, all the potentials can be calculated, in General Relativity the metric enters on both sides of the equation. This means that we cannot specify $T_{\mu\nu}$ and then calculate $g_{\mu\nu}$, since also for constructing $T_{\mu\nu}$ we need the metric. Intuitively this means that gravitation influences the matter/energy distribution, which in turn modifies the gravitational field ("backreaction"). A famous quote summarizing the complexity of Einstein equation is *"Space tells matter how to move, matter tells space how to curve"* (from Gravitation, Misner, Thorne, Wheeler).

Chapter 3 | Cosmological Models

In this chapter, we will apply the Einstein equations to the Universe as a whole discussing some possible models and their consequences. The standard cosmological model presently favored by the available data will be presented.

3.1 The Cosmological Principle

The Einstein equations allow to calculate the space-time geometry if the distribution of matter is known. This task is in general quite complex if we would like to find analytical solutions. Symmetry principles can simplify the problem greatly. In cosmological applications, the so-called **Cosmological Principle**:

The Universe is spatially homogeneous and isotropic

is assumed. With "homogeneous" we mean that the universe is invariant under spatial translations, while with "isotropic" we assume that the universe looks the same in every direction, or that it is spherically symmetric around us. The principle implies that every observer at every point of the universe observes the same properties (a modern version of the Copernican principle which stated that we do not occupy any privileged position in the Universe.). Another way to state the principle, is that the universe can be foliated in space-like surfaces which are spherically symmetric

about any point.
Of course, on a small scale the universe is not homogeneous, since there are stars, galaxies and even clusters of galaxies. The Cosmological Principle is assumed to be approximately realized on scales larger than - say - 10^8 or 10^9 light-years where many galaxy clusters are contained. The Cosmological Principle is not a completely proved fact, but it is supported (besides from our philosophical beliefs) by observations of the matter distribution on the largest scales and by the existence of a rather homogeneous cosmic microwave background (which is of cosmological origin).
If you like to be more mathematically precise, then a space-time is said to be spatially homogeneous if there exist a one-parameter family of space-like hypersurfaces Σ_t foliating the space-time, such that for every t, P and Q in Σ_t, there exists an isometry[1] of the space-time metric which maps P into Q.
A space-time is said to be spatially isotropic at each point if there exists a congruence of time-like curves[2] ("observers"), with tangents denoted by v^α filling the space-time and satisfying the following property. Given any point P and any two unit spatial tangent vectors (orthogonal to v^α) s_1^α, s_2^α there is an isometry of the metric which leaves p and u^α at P fixed, but rotates s_1^α, s_2^α. This means that if isotropy is assumed, it is not possible to construct a preferred tangent vector orthogonal to v^α. Constructing a preferred vector is possible of the tangent space to Σ_t does not coincide to the tangent space containing the vectors orthogonal to u^α. This fact also shows that isotropy requires that Σ_t is orthogonal to u^α.

3.2 Metric of Homogeneous and Isotropic Space-times

The requirements of homogeneity and isotropy from the Cosmological Principle greatly constrain the class of metrics compatible with it.
The spatial isotropy requirement implies that $g_{0i} = 0$ ($i = 1, 2, 3$): in this way no direction is privileged (we have no "mixing" between directions

[1] An isometry is a transformation which preserves the lengths.

[2] A congruence of curves is the set of integral curves of a nowhere-vanishing vector field.

and time). We assume that all the observers on a spatial surface are able to measure the time ("cosmic time") in the same way, so we can choose $g_{00} = -1$ (a constant not depending on the space-time point). It turns out that all these requirements lead to a space-time with constant curvature (in particular such space-times are called *maximally symmetric*[3]). It can be showed that the requirements of homogeneity and isotropy in four dimensions lead to the following metric

$$-ds^2 = g(v)dv^2 + f(v)\left[d\mathbf{u}^2 + \frac{k(\mathbf{u}d\mathbf{u})^2}{1-k\mathbf{u}^2}\right] \quad , \tag{3.1}$$

where v is a coordinate and $\mathbf{u}$ is a vector of three coordinates and f an unknown function of v only. This metric is clearly rotationally invariant as required. Introducing new "spherical coordinates" r, θ, ϕ for the "space" variables $\mathbf{u}$ and a time coordinate $t = \int -\sqrt{-g(v)}dv$ we obtain

$$ds^2 = dt^2 - R^2(t)\left[\frac{dr^2}{1-kr^2} + r^2 d\theta^2 + r^2 \sin^2\theta d\phi^2\right] \quad , \tag{3.2}$$

where $R(t)$ function of time to be determined, and k is a constant representing the curvature. This metric is invariant under the rescaling

$$\begin{aligned} R &\to \frac{R}{\lambda} \\ r &\to \lambda r \\ k &\to \frac{k}{\lambda^2} \quad , \end{aligned} \tag{3.3}$$

so choosing $\lambda = \sqrt{k}$, the curvature k can assume only the values $k = -1, 0, 1$. The function R(t) is usually normalized to its present value $a(t) = R(t)/R(0)$. and $a(t)$ is called **cosmic scale factor**.
Eq 3.2 is called the **Friedman-Lemaître-Robertson-Walker** metric (FLRW) and represents the most general homogeneous and isotropic space-time in four dimensions.
It interesting to look at the spatial geometry. If $k = 0$, space is flat and equivalent to a three-dimensional "plane". If $k = 1$, space is equivalent

[3]Mathematically, a maximally symmetric space M of dimension D is a space with a metric admitting D(D+1)/2 Killing vectors. Killing vectors form a vector field describing the infinitesimal isometric transformations in M.

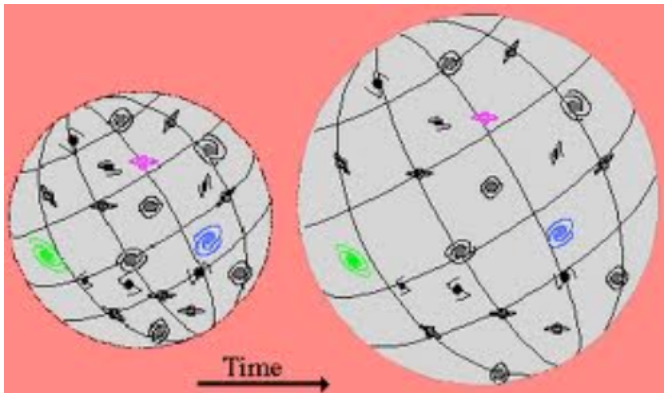

Figure 3.1: Comoving Coordinates

to the surface of a sphere with radius a(t). If $k = -1$, the space is hyperbolic. An important observation is that *the requirements of homogeneity and isotropy (the Cosmological Principle) allowed us to write the metric without solving or considering the Einstein Equations*.

3.3 Properties of the FLRW Universe

Considering the FLRW metric for an homogeneous and isotropic universe, we can directly calculate some relevant geometric quantities. In the $k = 1$ case, it is possible to calculate the spatial volume of the universe

$$^{(3)}V = \int \sqrt{|-^{(3)}g|}d^3x = a^3(t)\int_0^{2\pi} d\phi \int_0^{\pi} \sin\theta d\theta \int_o^{R_U} \frac{r^2 dr}{\sqrt{1-kr^2}} \quad , \tag{3.4}$$

where R_U is the "radius of the universe". R_U is finite only in the spherical $k = 1$ case, while in the other two cases $k = 0, -1$ it is infinite. Therefore, only in the $k = 1$ case we obtain a finite spatial volume $^{(3)}V = 2\pi^2 a^3(t)$ and $a(t)$ can be interpreted as a "radius". A $k = 1$ Universe is said to be **closed**, while the other two cases correspond to **open** universes.
Let's discuss now what the coordinates mean in the FLRW metric. These coordinates are called **comoving**, because the position of an observed does not change with respect to them. The idea is clearer looking at

Fig. 3.2: if the space-time is expanding (or contracting), the coordinates stretch according to the scale factor $a(t)$ and an object (say, a galaxy) keeps its position with respect to the axes.
An extremely simplified case is the one where $k = 0$ and $a(t)$=constant. Substituting the FLRW metric in the Einstein Equations gives $T_{\mu\nu} = 0$, since the components of the Ricci tensor $R_{\mu\nu}$ are zero (and therefore also the curvature scalar R). In this case, the equations of General Relativity describe an empty universe with a Lorentz (flat) metric. This case is trivial but it is a check that the Einstein Equations have an additional correct limiting case.

3.4 Friedmann Equations

Now it is time to use the FLRW metric in the Einstein equations. This will allow us to extract the exact form of the still unknown scale factor $a(t)$. The left side of the equation contains only the geometric quantities which can be calculated from the metric $g_{\mu\nu}$ which non-zero components are

$$\begin{aligned} g_{00} &= 1 \\ g_{11} &= -\frac{a^2(t)r^2}{1-kr^2} \\ g_{22} &= -a^2(t)r^2 \\ g_{33} &= -a^2(t)r^2\sin^2\theta \quad . \end{aligned} \tag{3.5}$$

From the metric tensor, we can directly calculate the Christoffel symbols: the non-zero ones are:

$$\begin{aligned} \Gamma^0_{11} = \frac{\dot{a}a}{1-kr^2} \quad ; \quad \Gamma^0_{22} = a\dot{a}r^2 \quad ; \quad \Gamma^0_{33} = a\dot{a}r^2\sin^2\theta \\ \Gamma^1_{01} = \Gamma^1_{10} = \Gamma^2_{02} = \Gamma^2_{20} = \Gamma^3_{03} = \Gamma^3_{30} = \frac{\dot{a}}{a} \\ \Gamma^1_{22} = -r(1-kr^2) \quad ; \quad \Gamma^1_{33} = -r(1-kr^2)\sin^2\theta \\ \Gamma^2_{12} = \Gamma^2_{21} = \Gamma^3_{13} = \Gamma^3_{31} = \frac{1}{r} \\ \Gamma^2_{33} = -\sin\theta\cos\theta \quad ; \quad \Gamma^3_{23} = \Gamma^3_{32} = \cot\theta \quad , \end{aligned} \tag{3.6}$$

and the Riemann tensor with its definition

$$R^{\mu}_{\beta\gamma\lambda} = \Gamma^{\nu}_{\lambda\beta}\Gamma^{\mu}_{\gamma\nu} - \frac{\partial\Gamma^{\mu}_{\gamma\beta}}{\partial x^{\lambda}} - \Gamma^{\nu}_{\gamma\beta}\Gamma^{\mu}_{\lambda\nu} + \frac{\partial\Gamma^{\mu}_{\lambda\beta}}{\partial x^{\gamma}} \quad . \tag{3.7}$$

Contracting the Riemann tensor we can calculate the Ricci tensor which non-zero components are

$$\begin{aligned} R_{00} &= -3\frac{\ddot{a}}{a} \\ R_{11} &= \frac{a\ddot{a} + 2\dot{a}^2 + 2k}{1 - kr^2} \\ R_{22} &= r^2(a\ddot{a} + 2\dot{a}^2 + 2kr) \\ R_{33} &= r^2(a\ddot{a} + 2\dot{a}^2 + 2kr)\sin^2\theta \quad , \end{aligned} \tag{3.8}$$

where the "dot" represents the total derivative with respect to the time ($\dot{x} = dx/dt$). Finally, contracting the Ricci tensor ($g^{\mu\nu}R_{\mu\nu}$) we obtain the curvature scalar

$$R = \frac{6}{a^2}(a\ddot{a} + 2\dot{a}^2 + k) \quad . \tag{3.9}$$

Now we have all the ingredients for calculating the left side of the Einstein equations and we just need $T_{\mu\nu}$. Again the Cosmological Principle can help us: an homogeneous and isotropic distribution of matter is the one corresponding to a perfect fluid with density ρ and pressure P:

$$T_{\mu\nu} = (\rho + P)v_{\mu}v_{\nu} - Pg_{\mu\nu} \quad , \tag{3.10}$$

where v is the four-velocity vector with components $v = (1, 0, 0, 0)$, since the "fluid" is at rest with respect to the comoving coordinates. Again, thinking at the fluid as made of point-like galaxies, they retain their place with respect to the coordinate axes: it is just the distance among them which changes through $a(t)$. Density and pressure can be time-dependent, but not space-dependent, otherwise this would be against the Cosmological Principle.
Consider now the energy-momentum conservation

$$\nabla_{\mu}T^{\mu}_{\nu} = \partial_{\mu}T^{\mu}_{\nu} + \Gamma^{\mu}_{\mu\beta}T^{\beta}_{\nu} - \Gamma^{\beta}_{\mu\nu}T^{\mu}_{\beta} = 0 \quad , \tag{3.11}$$

and the zero component (i.e. the energy component) of the above equation

$$\partial_0\rho(t) + 3\frac{\dot{a}(t)}{a(t)}(\rho(t) + P(t)) = 0 \quad . \tag{3.12}$$

This equation expresses **energy conservation** in the FLRW Universe. Notice that for obtaining Eq. 3.12 we had to use the space-time geometry through the covariant derivative and this brings us back to the complexity of the Einstein Equations, where curvature and energy/matter distribution are in general directly connected.
At his point we are stuck: we have the scale factor and other two unknowns in a single equation. The only way forward is to postulate a relationship between density and pressure, i.e. an **equation of state** for the energy/matter content of the universe. It can be showed that basically all the cosmologically relevant perfect fluids have an equation of state like $P = w\rho$ where w is a constant characteristic of the specific fluid. Substituting this generic equation of state in Eq. 3.12 we obtain

$$\frac{\dot{\rho}}{\rho} = -3(1+w)\frac{\dot{a}}{a} \quad , \tag{3.13}$$

which has solutions like

$$\rho(t) \propto a(t)^{-3(1+w)} \quad . \tag{3.14}$$

Now we have an equation that tells us how the density behaves while the universe expands or contracts. We still have to determine the dynamics of the scale factor.
Using the expressions for the Ricci tensor, the curvature scalar and the energy-momentum tensor, we can substitute them into the Einstein equations Eq. 2.18 finding (we leave $\Lambda = 0$ for the moment)

$$\begin{aligned} -3\frac{\ddot{a}}{a} &= 4\pi G(\rho + 3P) \quad \text{for} \quad (\mu,\nu) = (0,0) \\ \frac{\ddot{a}}{a} + 2\left(\frac{\dot{a}}{a}\right)^2 + 2\frac{k}{a^2} &= 4\pi G(\rho - P) \quad \text{for} \quad (\mu,\nu) = (i,j) \quad . \end{aligned} \tag{3.15}$$

For the spatial components $i, j = 1, 2, 3$ there is only one equation as it should be, given the requirement of isotropy. Substituting the second derivative of $a(t)$ from the first of the Eq. 3.15 into the second we obtain the **Friedmann Equations**

$$\begin{aligned} \frac{\ddot{a}}{a} &= -\frac{4\pi G}{3}(\rho + 3P) \\ \left(\frac{\dot{a}}{a}\right)^2 &= \frac{8\pi G}{3}\rho - \frac{k}{a^2} \quad . \end{aligned} \tag{3.16}$$

The Friedmann equations are basically the Einstein equations for an homogeneous and isotropic universe filled with a perfect fluid. For fully solve them and obtain the function $a(t)$, we need to specify the equation of state (or - almost equivalently - the parameter w).

3.5 The Cosmological Parameters

The expansion rate (how much a(t) changes in units of a(t) itself) is called the **Hubble Parameter**

$$H(t) = \frac{\dot{a}(t)}{a(t)} \quad . \tag{3.17}$$

The definition of H makes sense, since the scale of a itself is not important: in the ratio, we obtain a meaningful measurable quantity. The today's value of this parameter is called H_0.
It is also useful to rewrite the energy conservation equation in the FLRW Universe (Eq. 3.12) using the Hubble parameter as

$$\dot{\rho} + 3H(\rho + P) = 0 \quad . \tag{3.18}$$

Another relevant quantity is the **deceleration parameter**

$$q = -\frac{a\ddot{a}}{\dot{a}^2} \quad , \tag{3.19}$$

which quantifies the rate of change of H. Substituting the Hubble parameter in the second Friedmann equation

$$H^2 = \frac{8\pi G}{3}\rho - \frac{k}{a^2} \Rightarrow \frac{8\pi G}{3H^2}\rho - 1 = \frac{k}{H^2 a^2} \quad . \tag{3.20}$$

Defining the **critical density** $\rho_c = \frac{3H^2}{8\pi G}$ (today's value $\approx 10^{-29} g/cm^3 \sim 1.05 \times 10^{-4}\ eV/cm^3$) and the **density parameter** $\Omega = \rho/\rho_c$ we have

$$\Omega - 1 = \frac{k}{H^2 a^2} \quad . \tag{3.21}$$

The density parameter is quite important since it determines the geometry (through the curvature k) of the universe:

$$\begin{aligned} &\rho < \rho_c \iff \Omega < 1 \iff k = -1 && \text{(Open)} \\ &\rho = \rho_c \iff \Omega = 1 \iff k = 0 && \text{(Flat)} \\ &\rho > \rho_c \iff \Omega > 1 \iff k = 1 && \text{(Closed)} \end{aligned} \tag{3.22}$$

3.6 Cosmological Models

In order to treat all the possible cases, we will use the most general form of the Einstein equations, thus including the cosmological constant Λ. When the cosmological constant is taken into account, the Friedmann equations become

$$\begin{aligned} \frac{\ddot{a}}{a} = \dot{H} + H^2 = -\frac{4\pi G}{3}(\rho + 3P) + \frac{\Lambda}{3} \\ H^2 = \frac{8\pi G}{3}\rho - \frac{k}{a^2} + \frac{\Lambda}{3} \quad . \end{aligned} \tag{3.23}$$

Regarding the equation of state, the most relevant cases are

$$\begin{aligned} w = 0 \Rightarrow \rho \sim \frac{1}{a^3} \quad \text{"Dust"} \\ w = 1/3 \Rightarrow \rho \sim \frac{1}{a^4} \quad \text{"Radiation"} \\ w = -1 \Rightarrow \rho \sim const. \quad \text{"Vacuum"} \quad . \end{aligned} \tag{3.24}$$

In an universe filled with "dust", i.e. point-like massive particles, there is not interaction between them so the pressure is zero and therefore w=0. It is a standard physics result that for a volume filled with radiation only, $P = \rho/3$. The last case, where $P = -\rho$ (a sort of negative pressure) can arise in different models. It is called "vacuum energy" since this equation of state can arise from quantum field theory. We are now in the position to discuss some specific cosmological models.

3.6.1 The Einstein Universe

This cosmological model was first proposed by Einstein, who tried to obtain a static universe without expansion or contraction. This goal can be achieved only if $\Lambda \neq 0$. The static conditions are $\dot{a} = \ddot{a} = 0$ and from Eq. 3.23 we obtain

$$\begin{aligned} a = \sqrt{\frac{\Lambda}{k}} \Rightarrow k = 1 \\ \rho = \frac{\Lambda}{4\pi G} \quad . \end{aligned} \tag{3.25}$$

The previous equations describe a spherical universe with a constant radius (scale factor), a constant density and a non-zero cosmological constant. An unpleasant characteristic of this universe is its instability: a small perturbation would make it expand or contract. In this sense this model is not as static as its name may imply.

3.6.2 The Matter-dominated Universe

Suppose that the universe is uniformly filled only with non-interacting bodies. In this case, $P = 0$ (or $w = 0$), $\Lambda = 0$ and from Eq. 3.14 we have $\rho \cdot a(t)^3 = A$ with A =constant. The second of the Friedman equations Eq. 3.23 becomes

$$\dot{a}^2 = \frac{8\pi G}{3}\frac{A}{a} - k \quad . \tag{3.26}$$

Introducing the *conformal time* η instead of the time t such that $d\eta/dt = 1/a(t)$ the last equation becomes

$$a'^2 = \frac{8\pi G}{3}Aa - ka^2 \quad . \tag{3.27}$$

The apex in a' indicates differentiation with respect to the conformal time. The last equation can be easily integrated. For example, choosing as initial condition $a(0) = 0$ we have

$$\begin{aligned} k = 1 \Rightarrow a &= \frac{4\pi GA}{3}(1 - \cos\eta) \qquad ; \quad t = \frac{4\pi GA}{3}(\eta - \sin\eta) \\ k = 0 \Rightarrow a &= \frac{2\pi GA}{3}\eta^2 \qquad\qquad ; \quad t = \frac{2\pi GA}{9}\eta^3 \\ k = -1 \Rightarrow a &= \frac{4\pi GA}{3}(\cosh\eta - 1) \qquad ; \quad t = \frac{4\pi GA}{3}(\sinh\eta - \eta) \quad . \end{aligned} \tag{3.28}$$

In this model, a closed ($k = 1$) universe expands and eventually collapses again. Open universes ($k <= 1$) expand forever. In the boundary case $k = 0$, the expansion continues forever, but the expansion rate approaches zero for infinite times ($H \to 0$ when $t \to +\infty$).

3.6.3 The Radiation-dominated Universe

For radiation, we have already seen that $w = 1/3$, so $\rho = 3P$ and $\rho a^4 = A$ with A=constant. Setting $\Lambda = 0$, the second of the Friedman equations

Eq. 3.23 becomes

$$\dot{a}^2 = \frac{8\pi G}{3}\frac{A}{a^2} - k \quad . \tag{3.29}$$

Using the initial condition a(0)=0, the solutions are

$$\begin{aligned} k = 1 \Rightarrow a &= \sqrt{2\sqrt{\frac{8\pi GA}{3a^2}}t - t^2} \\ k = 0 \Rightarrow a &= \sqrt{2\sqrt{\frac{8\pi GA}{3a^2}}t} \\ k = -1 \Rightarrow a &= \sqrt{2\sqrt{\frac{8\pi GA}{3a^2}}t + t^2} \quad . \end{aligned} \tag{3.30}$$

As in the matter-dominated universe, the closed solution expands and then recollapses, while the other cases expand forever.

3.6.4 Vacuum-Dominated Universe

In the vacuum-dominated model, there is no matter present, so $P = \rho = 0$. In this case, only the cosmological constant plays a role ($\Lambda > 0$). A possible interpretation of this model comes from quantum field theory (QFT), where there are non-zero quantum fluctuations even in the vacuum where fields have zero average. QFT predicts a term analogous to the cosmological constant. In this case the second of the Friedman equations Eq. 3.23 reduces to

$$\dot{a}^2 = \frac{\Lambda a^2}{3} - k \quad , \tag{3.31}$$

and the solutions are

$$\begin{aligned} k = 1 \Rightarrow a &= \sqrt{\frac{3}{\Lambda}}\cosh\left(\sqrt{\frac{\Lambda}{3}}t\right) \\ k = 0 \Rightarrow a &= \sqrt{\frac{3}{\Lambda}}\exp\left(\sqrt{\frac{\Lambda}{3}}t\right) \\ k = -1 \Rightarrow a &= \sqrt{\frac{3}{\Lambda}}\sinh\left(\sqrt{\frac{\Lambda}{3}}t\right) \quad . \end{aligned} \tag{3.32}$$

The $k = 1$ case is also known as *deSitter Universe*.
The $k = 0$ case predicts an exponential growth of the Universe and as we will see later on, this solution has relevance in the framework of *inflationary models*. If we assume $\Lambda < 0$, there are no solutions for $k = 0, 1$, while for $k = -1$

$$a = \sqrt{-\frac{3}{\Lambda}} \cos\left(\sqrt{-\frac{\Lambda}{3}} t\right) \quad . \tag{3.33}$$

It can be verified that for $\Lambda = 0$ this model reduces to the flat spacetime case with $k = 0$ and $a =$constant.

3.6.5 Mixed Models

The models investigated so far contained only one type of matter/radiation. A more realistic model could contain different kinds of them in different proportions. In this case, the energy density will be the sum of the different components

$$\rho_{TOT}(a) = \sum_i \rho_i(a) = \rho_C \sum_i \Omega_i a^{-3(1+w_1)} \quad , \tag{3.34}$$

where ρ_c is the critical density and $\Omega_{TOT} = \rho_{TOT}/\rho_C$. Considering all the cases we treated so far and introducing the appropriate critical densities, the second Friedmann equation (Eq. 3.23) can be rewritten as

$$\frac{k}{a^2} = H^2(\Omega_{TOT} - 1) \quad . \tag{3.35}$$

Introducing in the last equations the density parameters observed today, together with the present Hubble parameter H_0 and the present scale a_0 we have

$$\frac{k}{a_0^2} = H_0(\Omega_m + \Omega_r + \Omega_\Lambda - 1) \quad , \tag{3.36}$$

where the density parameters describe pure matter (the "dust" universe), relativistic matter (radiation) and the effect of the cosmological constant.

3.7 Cosmological Red Shift

Most of the information we gather on earth about the cosmos comes in the form of electromagnetic radiation. Here we would like to investigate how

the universe's dynamics can affect a generic light signal of wavelength λ (or frequency $\nu = c/\lambda$). According to the Cosmological Principle, we can place the origin of our coordinate system where we would like to, so we choose $r = 0$ and for simplicity we forget about the angular coordinates θ and ϕ (equivalently, we can think of keeping them constant). An electromagnetic wave traveling from a distant star towards us (in the $-r$ direction) has the following equation of motion in an FLRW universe

$$d\tau^2 = dt^2 - a^2(t)\frac{dr^2}{1-kr^2} = 0 \quad . \tag{3.37}$$

If the wave (say, a certain crest of the wave) leaves the star at time t_1 and reaches our telescope at time t_0, integrating the last equation we have

$$\int_{t_1}^{t_0} \frac{dt}{a(t)} = \int_o^{r_1} \frac{dr}{\sqrt{1-kr^2}} = \begin{cases} \sin^{-1} r_1 & k = 1 \\ r_1 & k = 0 \\ \sinh^{-1} r_1 & k = -1 \end{cases} \quad . \tag{3.38}$$

If our star belongs to a galaxy (as basically always it is the case), it has fixed coordinates, so $\int_{t_1}^{t_0} \frac{dt}{a(t)}$ is a time-independent function, as it is clear from Eq. 3.38. This means that if we consider another crest of the electromagnetic wave leaving the star at a slight different time $t + \delta t$ we will find the same result as before for the integral $\int_{t_1+\delta t_1}^{t_0+\delta t_0} \frac{dt}{a(t)}$. Subtracting the two integrals and assuming that $a(t)$ does not vary much between the two crests,

$$\int_{t_1+\delta t_1}^{t_0+\delta t_0} \frac{dt}{a(t)} - \int_{t_1}^{t_0} \frac{dt}{a(t)} = \int_{\delta t_0}^{\delta t_1} \frac{dt}{a(t)} = 0 \Rightarrow \frac{\delta t_0}{a(t_0)} - \frac{\delta t_1}{a(t_1)} = 0 \tag{3.39}$$

and therefore

$$\frac{\delta t_0}{a(t_0)} = \frac{\delta t_1}{a(t_1)} \tag{3.40}$$

Frequencies and times are inversely proportional, so

$$\frac{\delta t_1}{\delta t_0} = \frac{a(t_1)}{a(t_0)} = \frac{\nu_0}{\nu_1} = \frac{\lambda_1}{\lambda_0} \quad . \tag{3.41}$$

We can now introduce the **red-shift parameter** and relate it to the scale factor

$$z = \frac{\lambda_0 - \lambda_1}{\lambda_1} = \frac{a(t_0)}{a(t_1)} - 1 \quad . \tag{3.42}$$

The wavelength λ_1 is the original one emitted from the star, as measured by a nearby observer, while λ_0 is what we will observe on the earth (at $r = 0$ of our coordinate system).
If $z > 0$, then $\lambda_0 > \lambda_1$: this is called **red-shift** and corresponds to an expanding universe.
If $z < 0$, then $\lambda_0 < \lambda_1$: this is called **blue-shift** and corresponds to a contracting universe.

3.8 Age of the Universe

We would like to use the Friedmann equations for determining how old the universe is as a function of the curvature and of the matter/energy content. The scale factor has no dimension and can be thought as the ratio of two lengths, or "radii": $R(t)$ at a time t, and $R(0)$ at $t = 0$ which is a reference time, for example "today". For $t = 0$ we have therefore a(0)=1. Multiplying and dividing the second Friedmann equation by the critical density $\rho_c = 3H_0^2/8\pi G$ (H_0 is the Hubble parameter's value today) we have

$$H^2 = \frac{8\pi G}{3}\rho_c \left[\sum_i \frac{\rho_i}{\rho_c} + \frac{\rho_k}{\rho_c}\right] \quad , \tag{3.43}$$

where we have defined $\rho_k = k/(a^2)$ which looks like a density due to the global curvature of the universe.
Strictly speaking, this is just a formal analogy, and we should not think at ρ_k as a contribution to the energy density: this definition just helps in writing the equations in a more appealing way.
Remembering how the different energy densities scale ($\rho(t) \propto a^{-3(1+w)}$) and introducing the present-day density factors $\Omega_x^0 = \rho_x^0/\rho_c$, Eq. 3.43 becomes

$$H^2 = H_0^2 \left[\frac{\Omega_m^0}{a^3} + \frac{\Omega_r^0}{a^4} + \frac{\Omega_k^0}{a^2} + \Omega_\Lambda^0\right] \quad . \tag{3.44}$$

For making better contact with measurements, we can introduce the red-shift parameter $z = a_0/a - 1$ ($a_0 = 1$ in our convention):

$$H^2 = H_0^2 \left[\Omega_m^0(1+z)^3 + \Omega_r^0(1+z)^4 + \Omega_k^0(1+z)^2 + \Omega_\Lambda^0\right] \quad . \tag{3.45}$$

The last equation can be further simplified with the following steps

- We can rewrite $H = \dot{a}/a$ using the red-shift parameter, obtaining $H = -\frac{1}{1+z}\frac{dz}{dt}$.
- Approximate $\Omega_r^0 \approx 0$ since the era when the universe was radiation-dominated was much shorter than the matter domination and vacuum-energy domination.
- Remember that the sum of all the density parameters is equal to 1 by definition, so we set $\Omega_k^0 = 1 - \Omega_m^0 - \Omega_\Lambda^0$.

obtaining after some algebra

$$\Delta t = \frac{1}{H_0}\int_0^z \frac{dz'}{1+z'}\frac{1}{\sqrt{(1+\Omega_m^0 z')(1+z')^2 - z'(2+z')\Omega_\Lambda^0}} \quad . \tag{3.46}$$

The integral over the red-shift factor extends from today ($z = 0$) to some era when the factor was equal to z. For obtaining the total age of the universe, we have to extend the integration to $z \to \infty$. Since the integral in Eq. 3.46 is of order one, a quick estimate of the age A of the universe is $A \sim 1/H_0 \approx 14$ Gyr.
The exact calculation can be carried out only numerically, but it is interesting to investigate the simple analytic result were the universe is flat ($k = 0 \Rightarrow \Omega_\Lambda^0 = 1 - \Omega_m^0$) and just dust-filled ($\Omega_\Lambda^0 = 0$):

$$A = \frac{1}{H_0}\int_0^\infty \frac{dz'}{(1+z')^{5/2}} = \frac{2}{3H_0} \sim 10 \text{ Gyr} \quad . \tag{3.47}$$

Chapter 4 | Elements of Nuclear Physics

Nuclei are at the core of every atom and are composed in general by Z protons and N neutrons. The number Z is also called *atomic number*, while the number A=Z+N is called *mass number*. An important concept is that of *binding energy* E_B of a nucleus: it is the minimal amount of energy needed for removing all the protons and neutrons from it and it is always a positive number.
The binding energy is given by the mass difference between the single nucleons and the nucleus:

$$E_B(Z,N) = \{Z \cdot m_p + N \cdot m_n - M(Z,N)\}c^2 \quad , \tag{4.1}$$

where M(Z,N) is the mass of the nucleus as a function of its proton and neutron content.

4.1 General Properties of Nuclei

In the following, we list some general aspects of nuclei which emerged after a century of theoretical and experimental efforts.

- Stable nuclei are found between Z=1 (hydrogen) and Z=82 (lead). These nuclei belong to the so-called valley of stability and this name comes from the binding energy chart as a function of Z and N (see figure).

- For every Z, there are different isotopes differing by the number of neutrons. The chemistry of an element is determined by the number

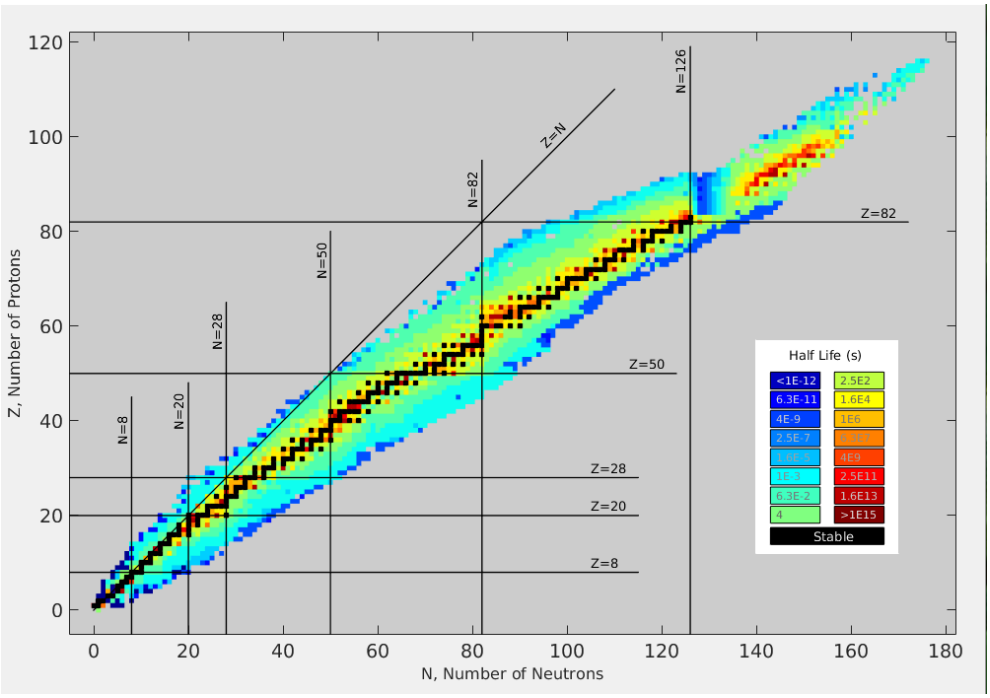

Figure 4.1: The nuclear valley of stability.

of electrons, which is equal to Z, therefore all the isotopes have the same chemical properties.

- Unstable nuclei (outside the "valley", see Fig. 4) decay after a certain time. Natural unstable isotopes are only the ones with half-lives comparable (or longer) to the lifetime of our solar system ($\sim 5 \times 10^9$ years). Unstable nuclei are created continuously in stars or artificially in laboratory.

- Roughly, stable nucley have the $Z = N$ property. This approximation becomes worse as Z increases. After a certain point, the Coulomb repulsion among protons is too high and only an increasing amount of neutrons is able to keep the nucleus together. In any case, a too big N with respect to Z (or the other way around) brings the nucleus farer away from the valley of stability.

- The lighter nucleus is hydrogen with just one proton. The next hydrogen isotope is called deuterium and it has une proton and

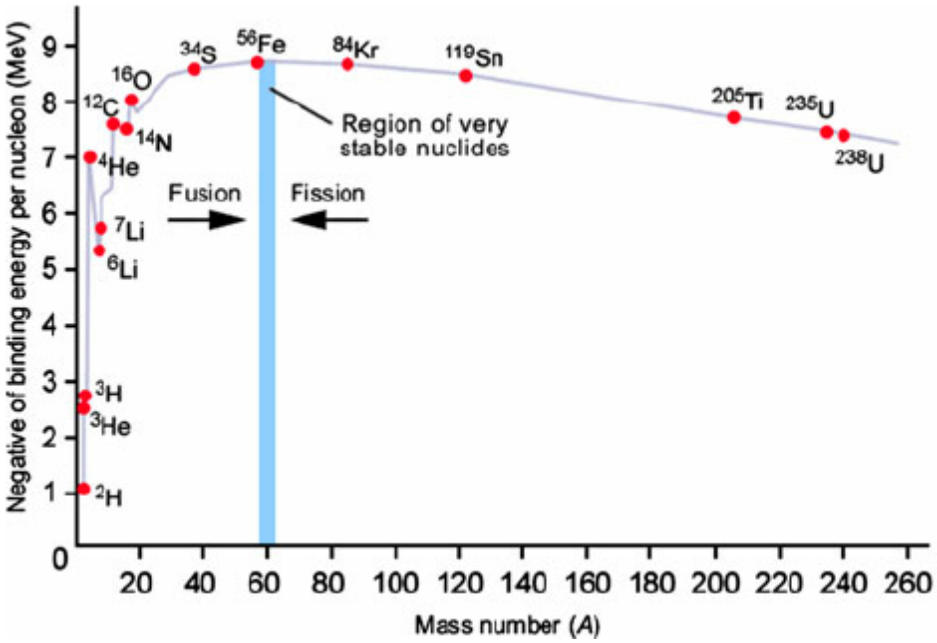

Figure 4.2: Binding energy per nucleon as a function of the mass number. The semi-empirical formula of Weiszäcker fits well the overall behaviour of E_B. Nuclear reactions releasing energy tend to produce nuclei which are more tightly bound than the initial ones: this means that fusion is favored for light nuclei, while heavier ones (beyond the iron peak) undergo fission.

one neutron. Nuclei with only two protons or two neutrons are not bound: this means that the n-p force is in general attractive but it is not the case for p-p or n-n.

- The rich variety of nuclei and their properties have roots in the nuclear force.

4.2 A simple nuclear model: Weizsäcker Semiempirical Mass Formula

The model takes its name from from the name of its proposer Carl von Weizsäcker (1912-2007). Experimentally, the binding energy $E_B(Z, N)$ of

a nucleus is approximately proportional to the number of nucleons A. This means that the binding energy is also proportional to the volume of the nucleus: this is why such a model is also referred as liquid drop model. The nucleus is thought as an incompressible liquid drop with a certain volume (proportional to the particles contained) and surface. In first approximation we can write

$$E(Z,N) = \alpha_1 A \quad , \tag{4.2}$$

The coefficient α_1 is called volume energy parameter. The last equation is very approximate and needs corrections since it tends to overestimate the binding energy as A grows. The first correction comes from surface effects: nucleons at the surface of the nucleus are less bound so the total binding energy should decrease with the number of them:

$$E(Z,N) = \alpha_1 A - \alpha_2 A^{2/3} \quad , \tag{4.3}$$

and α_2 is the surface energy parameter. Another corrections comes from the electric repulsion among protons which should diminish the total binding energy:

$$E(Z,N) = \alpha_1 A - \alpha_2 A^{2/3} - \alpha_3 \frac{Z^2}{A^{1/3}} \quad , \tag{4.4}$$

with α_3 the Coulomb energy parameter. In the third term, the formula of the Coulomb energy can be recognized. The $1/A^{1/3}$ factor comes from the fact that we are considering the nucleus a spherical object with constant density and therefore the radius is $R = r_0 A^{1/3}$. All the constants are factorized in the Coulomb energy parameter. According to this term, isobaric (same A) nuclei with less protons are more bound. Another correction comes from the following observed fact: nuclei with $Z \sim N$ are more bound. An imbalance among neutrons and protons corresponds to a less bound nucleus. This observation leads to the symmetry energy correction:

$$E(Z,N) = \alpha_1 A - \alpha_2 A^{2/3} - \alpha_3 \frac{Z^2}{A^{1/3}} - \alpha_4 \frac{(Z-N)^2}{A} \quad , \tag{4.5}$$

with α_4 the symmetry energy parameter. The presence of a factor A in the denominator compensates the growing number of neutrons present in

heavy nuclei. In heavy nuclei, the electric charge is so high that only more neutrons can compensate for it and keep the nucleus bound, therefore a larger asymmetry among nucleons is tolerated. The existence of the symmetry term already points to certain properties of the nuclear force. Another property is that even-Z/even-N nuclei (even-even for short) are more bound. This property is called pairing. For dealing with pairing force, we introduce another correction:

$$E(Z,N) = \alpha_1 A - \alpha_2 A^{2/3} - \alpha_3 \frac{Z^2}{A^{1/3}} - \alpha_4 \frac{(Z-N)^2}{A} + \Delta \quad , \tag{4.6}$$

where

$$D_{it} = \begin{cases} \delta & \text{for even-even nuclei} \\ 0 & \text{for odd-mass} \\ -\delta & \text{for odd-odd nuclei} \end{cases} \tag{4.7}$$

The last final form obtained is the Weizsäcker mass formula. Typical values for the constants (depending on the fitted dataset) are:

α_1 = 15.8 MeV
α_2 = 17.8 MeV
α_3 = 0.7 MeV
α_4 = 23.7 MeV
δ = 25/A MeV

The parameter δ is the less determined one since it varies significantly more than the others given the dataset considered. In Fig. 4.1 is shown the binding energy per nucleon as a function of the number of nucleons and a fit using the Weizsäcker mass formula. Note that E_B/A grows towards a maximum around the Fe nucleus (A $\sim$ 56) and then slowly decreases (because of Coulomb repulsion). This behavior explains why we can obtain energy by nuclear fusion with light elements or nuclear fission with heavy elements. If two light elements fuse together, the E_B/A will be higher for the resulting nucleus and the excess energy will be released. The opposite happens with heavy nuclei: for them it is more energetically convenient to fissionate and produce two daughter nuclei with higher E_B/A.

Chapter 5 | Early Universe Thermodynamics and Freeze-Out

During its expansion history, the Universe undewent periods of thermodynamic equilibrium and therfore for studying them we need the tools of (quantum) statistical mechanics.

5.1 Equilibrium

Before starting to discuss thermodynamic quantities, it is useful to recall some definitions about equilibrium.

- **Thermodynamic Equilibrium:** in this case, there are no net macroscopic flows of matter or of energy within a system. The entropy is maximized at thermodynamic equilibrium, while other relevant functions like the Helmholtz and Gibbs free energies are minimized. An isolated system out of equilibrium eveloves towards the equilibrium state.

- **Chemical Equilibrium:** if reactions are involved, at chemical equilibrium the concentrations of the reactants do not change. Reactions can still tranform one reactant into another, but the concentrations stay the same in case of dynamical equilibrium. A relevant quantity is the *chemical potential* μ, introduced originally by Gibbs, which gives the change in free energy as the number of particles in the system changes.

In chemical equilibrium, the reactions that create and destroy particles occur faster than the expansion and the chemical potential keep its equilibrium value determined by (for example)

$$\mu_i + \mu_j = \mu_k + \mu_l \quad , \tag{5.1}$$

if the reaction is binary: $i + j \leftrightarrow k + l$. In statistical equilibrium, the elastic scattering reactions that maintain the thermal energy distribution of particles occur faster than the expansion. A certain particle species can be in statistical equilibrium, but not in chemical equilibrium. Fully thermal equilibrium occurs when the particle species are in statistical and chemical equilibrium.
A small note about the *chemical potential*. Considering the Helmholtz free energy A

$$dA = -PdV - SdT + \mu dN \quad , \tag{5.2}$$

since it tends to reach its minimum, if the chemical potential μ is positive, the particle number N is driven to smaller numbers for minimizing A. This is why μ is called "potential". So at the end the chemical potential is the variation in energy when the number of particles changes (and V and T are kept constant).

5.2 Statistical Mechanics Recap

According to statistical mechanics, macroscopic thermodynamic quantities can be obtained as averages using specific probability distributions f over the phase space. The distribution for relativistic particles can be expressed as a function of the particle momenta: $f = f(\bar{k})$ where $E^2 - \bar{k}^2 = m^2$. By definition of f, its integral over the whole phase space is the particle density

$$n = \frac{g}{(2\pi)^3} \int f(\bar{k}) d^3k \quad , \tag{5.3}$$

where g is the number of degrees of freedom and the $(2\pi)^3$ factor represents the smallest volume of the phase space (here $\hbar = 1$).
Following statistical mechanics, the energy density ρ is

$$\rho = \frac{g}{(2\pi)^3} \int E(\bar{k}) f(\bar{k}) d^3k \quad , \tag{5.4}$$

and the pressure:

$$p = \frac{g}{(2\pi)^3} \int \frac{k^2}{3E(\bar{k})} f(\bar{k}) d^3k \quad . \tag{5.5}$$

Quantum particles can be either bosons (integer spin) or fermions (half-integer spin) and each class follows a different distribution function. In the following we give expressions for the number density, energy density, and pressure for bosons (characterized by the "-" sign) and fermions ("+")

$$n = \frac{g}{2\pi^2} \int_m^\infty \frac{(E^2 - m^2)^{1/2}}{e^{(E-\mu)/T} \pm 1} E dE \quad , \tag{5.6}$$

$$\rho = \frac{g}{2\pi^2} \int_m^\infty \frac{(E^2 - m^2)^{1/2}}{e^{(E-\mu)/T} \pm 1} E^2 dE \quad , \tag{5.7}$$

$$p = \frac{g}{6\pi^2} \int_m^\infty \frac{(E^2 - m^2)^{3/2}}{e^{(E-\mu)/T} \pm 1} dE \quad , \tag{5.8}$$

where the integral over three-momenta was changed to a one-dimensional integral over energy using the relativistic expression relating them and integrating over momenta in spherical coordinates.
The last integrals are not analytical but can be solved in physically relevant limiting cases summarized in the following table:

Bosons	Fermions	Bosons and Fermions
Limit: $T \gg \mu, m$	Limit: $T \gg \mu, m$	Limit: $T \ll \mu, m$
$n = \frac{\zeta(3)}{\pi^2} g T^3$	$n = \frac{3}{4} \frac{\zeta(3)}{\pi^2} g T^3$	$n = g \left(\frac{mT}{2\pi}\right)^{3/2} e^{-(m-\mu)/T}$
$\rho = \frac{\pi^2}{30} g T^4$	$\rho = \frac{7}{8} \frac{\pi^2}{30} g T^4$	$\rho = m \cdot n$
$p = \frac{\rho}{3}$	$p = \frac{\rho}{3}$	$p = n \cdot T \ll \rho$

5.3 Entropy and its Density

During the expansion of the Universe, there are phases where the reaction rate was much faster than the expansion rate and thus we can assume (local) thermal equilibrium (TE). It can be proved that in TE, the entropy per comoving volume element remains constant. The identification of a conserved quantity is important for successive calculations.
Remembering the second law of thermodynamics ($dS = \delta Q/T$, where Q is the heat, T the temperature) and rewriting the heat non-exact differential as $dU - dW$ where U is the energy and W the work, we have, rewriting the energy using the energy density ($U = \rho V$)

$$TdS = d(\rho V) + pdV \quad , \tag{5.9}$$

where we re-expressed the work as $dW = pdV$, with p and V being the pressure and volume of the system respectively. After expanding the differential $d(\rho V)$ we obtain

$$TdS = d[(p+\rho)V] - Vdp \quad . \tag{5.10}$$

The integrability condition

$$\frac{\partial^2 S}{\partial T \partial V} = \frac{\partial^2 S}{\partial V \partial T} \quad , \tag{5.11}$$

gives a direct relation between pressure and density:

$$T\frac{dp}{dT} = p + \rho \Longrightarrow dp = \frac{\rho + p}{T} dT \quad . \tag{5.12}$$

Substituting the last equation in Eq. 5.10, we obtain

$$dS = \frac{d[(p+\rho)V]}{T} - \frac{(p+\rho)VdT}{T^2} = d\left[\frac{(p+\rho)V}{T} + \text{const.}\right] \quad . \tag{5.13}$$

Eq. 5.13 gives an expression for the entropy per unit comoving volume ($V = a^3$): $S/V = S/a^3 = (p+\rho)/T$. Now we can show show that the entropy is a conserved quantity. Accoring to the first principle of thermodynamics (equivalent to energy conservation) we have

$$d[(p+\rho)V] = Vdp \tag{5.14}$$

and substituting into Eq. 5.12 we obtain

$$d\left[\frac{(p+\rho)V}{T}\right] = 0 \quad , \tag{5.15}$$

which proves that the entropy per unit comoving volume is conserved. We can now define the entropy density

$$s = \frac{S}{V} = \frac{p+\rho}{T} \quad , \tag{5.16}$$

as an useful quantity which stays constant during the expansion.
In the early Universe, the entropy density is dominated by relativistic particles, so considering the Bose and Fermi distributions in the relativistic limit the entropy density becomes

$$s = \frac{p+\rho}{T} = \frac{\rho/3+\rho}{T} = \frac{4}{3}\frac{\pi^2}{30}gT^3 = \frac{2}{45}\pi^2 gT^3 \quad . \tag{5.17}$$

If more relativistic particles are present, it is useful to introduce the effective number of degrees of freedom

$$g_* = \sum_B g_B \left(\frac{T_B}{T}\right)^4 + \frac{7}{8}\sum_F g_F \left(\frac{T_F}{T}\right)^4 \quad , \tag{5.18}$$

where the index B stands for bosons and F for fermions. The effective number of degrees of freedom g_* can be used instead of g in Eq. 5.17. The temperature T is the temperature of the photons, while $T_{B,F}$ are the temperatures of the additional relativistic bosons and fermions.
At high enough temperatures (T>200 GeV), all the Standard Model particles play a role and the number of effective degrees of freedom is

$$g_* = 28 + \frac{7}{8}90 \approx 106.72 \quad . \tag{5.19}$$

When the temperature is below ~ 1 GeV, there are no electroweak bosons and heavy quarks (b,t) and $g_* = 18 + (7/8)50 = 61.75$. For temperatures below ~ 100 MeV, the only relativistic particles left are electrons, positrons, photons, and neutrinos and thus $g_* = 2 + (7/8)10 = 10.75$.
The degrees of freedom carried by each particle of the Standard Model are summarized in Tab. 5.1.
The entropy density scales as $s \sim 1/a^3$ and therefore the following quantity remains constant as the Universe expands

$$g_* T^3 a^3 \sim \text{const.} \quad . \tag{5.20}$$

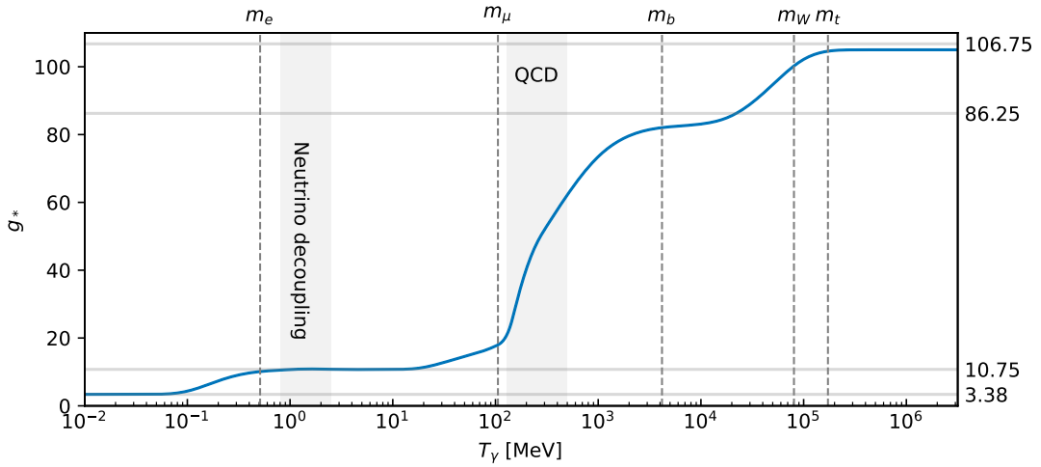

Figure 5.1: Change of the effective number of degrees of freedom as a function of the temperature. The QCD phase transition (confinement) and the neutrino decoupling events are marked by a grey band (figure from A. Lewis, U. Sussex, UK).

(anti)Particle(s)	Quantity	Spin	Other	g	g_{tot}
Quarks	6+6	1/2	Colors=3	2	$2 \cdot 2 \cdot 3 \cdot 6 = 72$
Gluons	8	1		2	$8 \cdot 2 = 16$
Massive Leptons	3+3	1/2		2	$2 \cdot 2 \cdot 3 = 12$
Massless Leptons (ν)	3	1/2		2	$2 \cdot 3 = 6$
EW bosons ($W^{\pm}$,Z)	3	1		3	$3 \cdot 3 = 9$
Photon	1	1		2	2
Higgs Boson	1	0		1	1
$\sum$Bosons	28				
$\sum$Fermions	90				

Table 5.1: Degrees of freedom of the Standard Model particles.

5.4 Thermal Decoupling

Until now, we assumed to be in thermal equilibrium, but now we have to understand better when we can consider to be in such condition. The idea is that if the reactions are fast enough with respect to the expansion rate, then thermodynamical equilibrium holds.

As the Universe expands, the temperature drops as

$$\frac{\dot{T}}{T} = -\frac{\dot{a}}{a} = -H \quad . \tag{5.21}$$

This can be seen using energy conservation $\dot{\rho}/\rho = -3(1+w)\dot{a}/a$ and remembering that in a radiation-domiated Universe $\rho \sim T^4$ and $w = 1/3$. We would like to compare H with the reaction rate Γ. To see how the balance between H and Γ determines if there is equilibrium or not, we can try to perform first a simplified calculation just for making the point. First, we can assume radiation domination and thus $H \sim T^2$, since $H^2 \sim \rho$ from Einstein equations for a Friedman Universe and $\rho_{rad} \sim T^4$. Second, we can assume that the reaction rate is proportional to some power of T: $\Gamma \sim T^n$, as it is usually the case. What we would like to calculated now is the number of reactions N happened from a certain time t onwards:

$$\begin{aligned} &N = \int_t^\infty \Gamma(t')dt' \sim \int_t^\infty T^n \frac{T^2}{T^2} dt' = \int_t^\infty T^{n-2} T^2 \sim \int_t^\infty T^{n-2}(-H)dt' = \\ &= \int_t^\infty T^{n-2} \frac{\dot{T}}{T} dt' = \int_t^\infty T^{n-3}\dot{T}dt' = \int_t^\infty \frac{d}{dt}\left(\frac{1}{n-2}T^{n-2}\right) = \quad . \\ &= \frac{1}{n-2}\frac{T^n}{T^2} \sim \frac{1}{n-2}\frac{\Gamma}{H} \end{aligned} \tag{5.22}$$

The last result

$$N = \int_t^\infty \Gamma(t')dt' \sim \frac{1}{n-2}\left(\frac{\Gamma}{H}\right)_t \quad . \tag{5.23}$$

shows that if $n > 2$, after $\Gamma \sim H$, a particle interacts less than one time and therefore it is decoupled: that particle will stay around without undergoing further interactions (on average). The last result shows the interplay between reaction rate and expansion: if the reactions cannot keep up the expansion and particles become too "diluted", than interactions stop and the particle species "freeze out" and their abundance will not change further.
The previous calculations were approximate for proving the point: in the next sections we will try to treat the problem in a more rigorous way.

5.5 The Boltzmann Equation

The correct method for treating the thermodynamics of the early Universe is using an equation which describes the evolution of the distribution

function for the various particles species. Such distribution over the phase space will depend in general from time, positions, and momenta of the particles: $f = f(t, x, p)$. If there are no interactions among particles which can modify f, we have $d/dt(f) = 0$ and therefore

$$\frac{\partial f}{\partial t} + \frac{dx}{dt}\nabla_x f + \frac{dp}{dt}\nabla_p f = 0 \quad . \tag{5.24}$$

and remembering the definition of velocity and force, can be rewritten as

$$\frac{\partial f}{\partial t} + v\nabla_x f + F\nabla_p f = 0 \quad . \tag{5.25}$$

The last equation is also known as Vlasov equation or collision-less Boltzmann equation, which can also be written as $L[f] = 0$. The operator L is called Liouville operator. The proper Boltzmann equation is

$$L[f] = C[f] \quad , \tag{5.26}$$

where $C[f]$ is a term accounting for particles collisions, or interactions. In the case of early cosmology, we have to consider the relativistic version of the Boltzmann equation

$$L[f] = p^\mu \frac{\partial f}{\partial x^\mu} - \Gamma^\mu_{\alpha\beta} p^\alpha p^\beta \frac{\partial f}{\partial p^\mu} \quad . \tag{5.27}$$

We would like now to write the last equation in the case of the Friedman metric, which is isotropic and homogeneous and therefore $f(t, x, p) \to f(t, |p|)$:

$$L[f] = E\frac{\partial f}{\partial t} - \frac{\dot{a}}{a}p^2\frac{\partial f}{\partial E} \quad . \tag{5.28}$$

By definition of f, we have

$$n(t) = \int \frac{d^3p}{(2\pi)^3} g f(|p|, t) \quad , \tag{5.29}$$

where g counts the spin degrees of freedom. Since we are interested in particle densities, we want to integrate out the momenta, obtaining

$$\int L[f] g \frac{d^3p}{(2\pi)^3} = \frac{dn}{dt} + 3Hn \quad . \tag{5.30}$$

In the following, we will show how the integral is calculated. Considering the collisionless case, we can divide L[f] by the energy E and integrate with spherical coordinates the mometum such that $d^3p \to 4\pi p^2 dp$. Dropping the overall factor $4\pi/(2\pi)^3$ factor we have

$$\int dp p^2 \frac{\partial f}{\partial t} - \frac{\dot{a}}{a}\frac{p^4}{E}\frac{\partial f}{\partial E} \quad . \tag{5.31}$$

The integral of the first term is exactly the particle density, while the second integral, using $E^2 - p^2 = m^2 \Rightarrow pdp = EdE$, $\dot{a}/a = H$, and integrating by parts becomes

$$-\int dp \frac{\dot{a}}{a}\frac{p^4}{E}\frac{\partial f}{\partial E} = -H\int dp p^3 \frac{\partial f}{\partial p} = 3Hn \quad . \tag{5.32}$$

We can also observe that

$$\dot{n} + 3Hn = 0 \Rightarrow \frac{d(a^3 n)}{dt} = 0 \quad , \tag{5.33}$$

which expresses the conservation of particle number per comoving volume in absence of interactions.
After having integrated over the phase space the Liouville operator L, we can do the same with the collision operator C[f]. We will not perform this (longer) calculation here but refer instead to the classic paper of P.Gondolo and G.Gelmini (Nucl.Phys. B360, 145-179 (1995)) and quote the main result of it. Considering the simplest process $1 + 2 \leftrightarrow 3 + 4$ where species 1 and 2 are in thermal equilibrium with 3 and 4 we have

$$g_1 \int C[f_1]\frac{d^3p}{(2\pi)^3} = -\langle \sigma v_M \rangle (n_1 n_2 - n_1^{eq} n_2^{eq}) \quad , \tag{5.34}$$

where n_i is the number density of the particle type i, n_i^{eq} are the corresponding number densities at equilibrium, and $\sigma = \sum_{fs} \sigma_{12 \to fs}$ is the invariant unpolarized cross section of the process $1 + 2 \to fs$ where fs are all the possible final states. The velocity v_M is called Møller velocity and is defined as

$$v_M = \sqrt{(v_1 - v_2)^2 - (v_1 \times v_2)^2} = \frac{\sqrt{(p_1 p_2)^2 - m_1^2 m_2^2}}{E_1 E_2} \quad , \tag{5.35}$$

where in the last expression v_M is written in explicity covariant form. The Møller velocity is a Lorentz invariant quantity and in the rest frame of e.g. particle 1 (or 2) it reduces to the relative velocity $v_{rel} = |v_1 - v_2|$. Thus, since all the quantities in the Boltzmann equation $L[f] = C[f]$ are invariant, the whole equation is invariant.
The product of the cross section times the velocity is in the $\langle .. \rangle$ operator which denotes the thermal average:

$$\langle \sigma v_M \rangle = \frac{\int dp_1^3 dp_2^3 \sigma v_M e^{-E_1/T} e^{-E_2/T}}{\int dp_1^3 dp_2^3 e^{-E_1/T} e^{-E_2/T}} \quad . \tag{5.36}$$

In the last equation, as an example (which works in many practical situations) we assumend a Maxwell-Boltzmann distribution instead of a Bose-Einstein or Fermi-Dirac one.
Summarizing the above results and considering a single particle type, we have the following Boltzmann equation for an expanding Friedman Universe

$$\dot{n} + 3Hn = \langle \sigma v \rangle \left(n^2 - n_{eq}^2 \right) \quad . \tag{5.37}$$

5.6 Freeze Out

We can now use the Boltzmann equation for better understanding thermal decoupling and its relation with expansion and reaction rates.
Starting from Eq. 5.37 and remembering that sa^3=const. (conservation of entropy), deriving both sides with respect to time we can easily discover that $\dot{s} = -3Hs$ (if g_* is constant). We can now define the new quantity $Y = n/s$: dividing the particle density by the entropy density, we obtain a new quantity which is proportional to the comoving number density. Further observing that

$$\frac{d}{dt} Y = \frac{d}{dt} \left(\frac{n}{s} \right) = \frac{1}{s} (\dot{n} + 3Hn) \tag{5.38}$$

and introducing the variable $x = m/T$ with time derivative

$$\frac{dx}{dt} = xH \quad , \tag{5.39}$$

Eq. 5.37 can be rewritten in the more suggestive form

$$\frac{x}{Y_{eq}}\frac{dY}{dx} = -\frac{\Gamma}{H(m)}\left(\frac{Y^2}{Y_{eq}^2} - 1\right) \quad . \tag{5.40}$$

where we defined $\Gamma = \langle\sigma v\rangle n_{eq}$. We used also the fact that since $H \propto T^2$ in a radiation-dominated phase, then $H \propto x^{-2}$ and

$$\frac{H(m)}{H(T)} = x^2 \quad . \tag{5.41}$$

Eq. 5.40 n clearly shows two distinct regimes controlled by the parameter Γ/H and divided by the value $\Gamma \sim H$ which defines the freeze-out temperature T_{fo}. If $\Gamma/H \ll 1$, the abundance Y stops changing and we have "freeze-out". If $\Gamma/H \gg 1$, Y is driven to its equilibrium value Y_{eq} and the particles are in thermal equilibrium (see Fig 5.2).

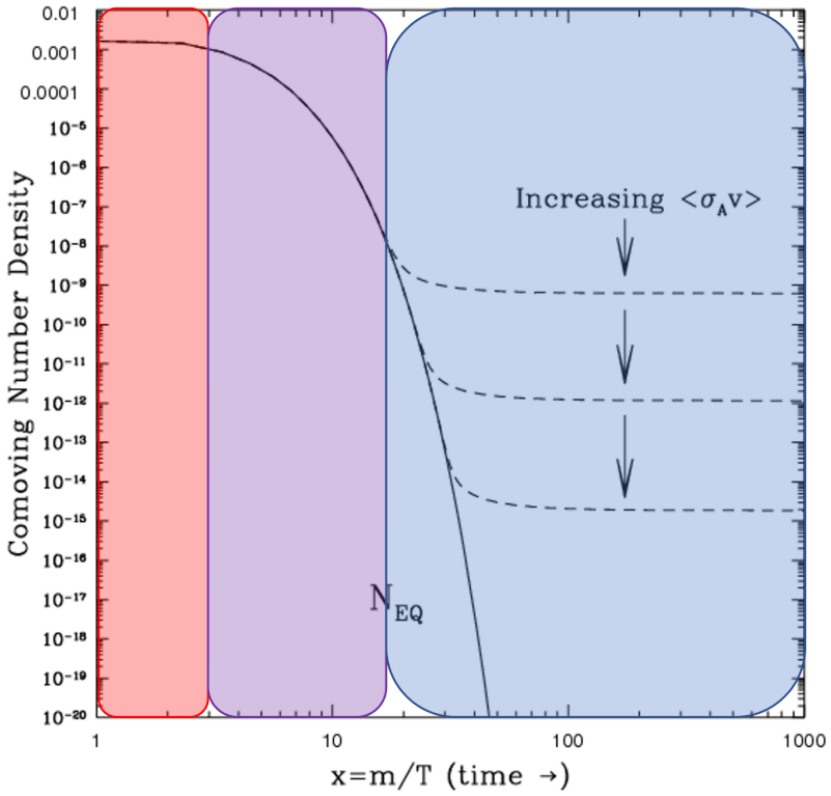

Figure 5.2: Graphical representation of Eq 5.40 (Figure from: https://www.particlebites.com/).

Chapter 6 | Nucleosynthesis

6.1 Introduction

One of the most strikingly correct predictions of the Big Bang model is the abundance of light elements present in the observed Universe. If we use the nuclear reaction rates measured in the laboratory in a calculation where we consider a plasma in an expanding Universe with the correct baryon density, we find the mass abundances of hydrogen ($\sim$ 75%) and helium ($\sim$ 25%) that we observe today, plus traces of deuterium and lithium (^{7}Li).
This primordial creation of the light nuclei is called "Big Bang Nucleosynthesis" (BBN). For creating nuclei, we need protons and neutrons: the proportion between them was fixed in the first second after the Big Bang, where the temperature was low enough for quarks to condense into hadrons. At that time, the universe was rather homogeneous and dominated by radiation. The sufficiently low temperature for nuclei to form was reached after about 10 seconds after the Big Bang. BBN created only light nuclei by fusion of protons and neutrons, and most of the neutrons ended up into ^{4}He nuclei.
Helium is special among light nuclei, since it has a quite high binding energy per nucleon. More massive nuclei can by even more tightly bound, but the freeze-out mechanism prevents reactions to form them in the early Universe: the expansion is faster than the reaction rates and almost only the helium nuclei have time to form.

6.2 Protons and Neutrons

After the formation of protons and neutrons, the balance between them was set by the electro-weak interaction through the following reactions

$$n \longleftrightarrow p + e^- + \bar{\nu}_e \quad , \tag{6.1}$$

$$\nu_e + n \longleftrightarrow p + e^- \quad , \tag{6.2}$$

$$e^+ + n \longleftrightarrow p + \bar{\nu}_e \quad . \tag{6.3}$$

The first equation is the β-decay of the free neutron, while the other two represent inverse β-decays for protons and neutrons. If $T \gg 1$ MeV, the rates of these reactions are faster with respect of the expansion rate set by the Hubble constant and therefore we can assume that chemical equilibrium holds:

$$\mu_n - \mu_p = \mu_{e^-} - \mu_{\mu_e} = \mu_{\bar{\nu}_e} - \mu_{e^+} \tag{6.4}$$

which implies that (detailed balance)

$$\frac{n_n}{n_p} = e^{-Q/T + (\mu_e - \mu_\nu)/T} \quad , \tag{6.5}$$

where $Q = m_n - m_p \approx 1.293$ MeV. Assuming charge neutrality in the Universe ($n_p = n_e$) and $T \gg m_e$:

$$\frac{\mu_e}{T} \sim \frac{n_e}{n_\gamma} = \frac{n_p}{n_\gamma} \sim \eta \sim 10^{-10} \quad , \tag{6.6}$$

where η is the baryon to photon ratio. A similar estimate can be carried out for neutrinos (μ_ν/T) but the relic neutrino background has not yet been detected and we can assume that, as for the baryon to photon ratio number η, also the equivalent quantity referred to leptons is small. In non-standard scenarios, such approximations are relaxed. Using here the approximations, we have in equilibrium

$$\frac{n_n}{n_p} = e^{-Q/T} \quad . \tag{6.7}$$

Now we have to consider the rates of the various electroweak processes. The neutron decay rate is

$$\Gamma_{n \to pe\nu} = \frac{1}{\tau_n} = \frac{G_F^2}{2\pi^3}(1 + 3g_A^2) m_e^5 \lambda_0 \quad , \tag{6.8}$$

where

$$\lambda_0 = \int_1^q d\epsilon\epsilon(\epsilon - q)^2\sqrt{\epsilon^2 - 1} \approx 1.6363 \quad , \tag{6.9}$$

is a phase-space factor, G_F the Fermi constant, and g_A the axial coupling constant. G_F and g_A can be measured with other electroweak processes and can be extracted for example from the measurement of the neutron lifetime $\tau_n \sim 15$ min and the neutron decay spectrum. The rate for proton/neutron conversion in a thermal bath at temperature T depends also from the neutron lifetime:

$$\Gamma_{pe\leftrightarrow n\nu} = \begin{cases} \frac{1}{\tau_n}\left(\frac{T}{m_e}\right)^3 e^{-Q/T} & T \ll Q, m_e \\ \frac{7\pi^4}{30\lambda_0\tau_n}\left(\frac{T}{m_e}\right)^5 \sim G_F^2 T^5 & T \gg Q, m_e \end{cases} \tag{6.10}$$

Plugging in the numbers, for $T \gg m_e$ we can find (remembering that $H \sim T^2$, i.e.: $H \sim 1.66\sqrt{g_*}T^2/M_{Pl}$)

$$\left(\frac{\Gamma}{H}\right) \sim \left(\frac{T}{0.8\text{ MeV}}\right)^3. \tag{6.11}$$

The last equation implies that if $T > 0.8$ MeV, we expect equilibrium among protons and neutrons, again because the reaction rates are larger than the expansion rate. At the same time, at $T = T_{f.o.} \sim 0.8$ MeV we have "freeze-out": after this point the relative amount of the two particles cannot change anymore significantly and

$$\left(\frac{n_n}{n_p}\right)_{f.o.} = e^{-Q/T_{f.o.}} \sim \frac{1}{6} \quad . \tag{6.12}$$

The last result gives the ratio between protons and neutrons as they emerge from the Big-Bang. As the temperature drops further (T = 0.3–0.1 MeV), neutrons and protons can start to combine forming nuclei.

6.3 Nuclear Reactions at Equilibrium

It is useful to introduce the following notation:

$$X_A = \frac{n_A A}{n_n + n_p + \sum_i (A n_A)_i} = \frac{n_A A}{n_N} \quad . \tag{6.13}$$

X_A represents the abundance fraction of the nucleus A with respect to all the free protons, free neutrons, and the other i nuclei $n_N = n_n + n_p + \sum_i (An_A)_i$. In the same way, we can consider the fraction of protons and neutrons (X_p, X_n) and thus the corresponding abundances ratio can also be written as $n_n/n_p = X_n/X_p$.
By definition of the abundance fraction, we have that

$$\sum_i X_i = 1 \quad . \tag{6.14}$$

Considering now a non-relativistic nuclear species with A nucleons, Z protons, and (A-Z) neutrons, in the case of kinetic equilibrium, the particle density is given by

$$n_A = g_A \frac{m_A T}{2\pi}^{3/2} e^{\frac{\mu_A - m_A}{T}} \quad , \tag{6.15}$$

where μ_A is the chemical potential. The same equation is in principle valid also for protons and neutrons. Chemical equilibrium is realized if the reaction producing the nucleus is fast with respect to the expansion rate. In this regime, the chemical potential of the nucleus is related to the one of the nucleons by

$$\mu_A = Z\mu_p + (A - Z)\mu_n \quad . \tag{6.16}$$

From Eq. 6.15 and Eq. 6.16, we can rewrite $e^{\mu_A/T}$ as

$$e^{\mu_A/T} = n_p^Z n_n^{A-Z} \left(\frac{2\pi}{m_N T}\right)^{3A/2} 2^{-A} e^{[Zm_p + (A-Z)m_n]/T} \quad . \tag{6.17}$$

Introducing in the last equation the definition of binding energy B_A

$$B_A = Zm_p + (A - Z)m_n - m_A \quad , \tag{6.18}$$

we can re-write Eq. 6.15 as

$$n_A = g_A A^{3/2} 2^{-A} n_p^Z n_n^{A-Z} \left(\frac{2\pi}{m_N T}\right)^{3(A-1)/2} e^{B_A/T} \quad . \tag{6.19}$$

We would like now to rewrite the last equation in terms of the fraction X_A. Considering the definition of abundance fraction (Eq. 6.13), the baryon

fraction $\eta = n_N/n_\gamma$, and the photon density of the relativistic Bose gas $n_\gamma = 2\zeta(3)T^3/\pi^2$, we can finally rewrite (after some algebra) Eq. 6.19 as

$$X_A = g_A \zeta(3)^{A-1} \pi^{\frac{1-A}{2}} 2^{\frac{3A-5}{2}} A^{\frac{5}{2}} \left(\frac{T}{m_N}\right)^{\frac{3(A-1)}{2}} \eta^{A-1} X_p^Z X_n^{A-Z} e^{\frac{B_A}{T}} \quad . \quad (6.20)$$

The last equation gives an expression for the fraction of a nucleus present at equilibrium given the fractions of protons and neutrons available.

6.4 Nucleosynthesis of the Light Elements

Using Eq. 6.20, it is possible to calculate the evolution of the fraction of a nucleus as a function of the temperature (which is equivalent to time, since the Universe is expanding lowering the temperature). For illustration, we can consider the evolution of protons, neutrons, hydrogen isotopes (A=1,2), and helium isotopes (A=3,4):

$$\begin{cases} X_n/X_p = e^{-Q/T} \\ X_2 = 16.3(T/m_N)^{3/2}\eta e^{B_2/T} X_n X_p \\ X_3 = 57.4(T/m_N)^{3}\eta^2 e^{B_3/T} X_n X_p^2 \\ X_4 = 113(T/m_N)^{9/2}\eta^3 e^{B_4/T} X_n^2 X_p^2 \\ 1 = X_n + X_p + X_2 + X_3 + X_4 \end{cases} , \quad (6.21)$$

where the numerical factors and the degrees of freedom g_A are already calculated. The method is completely analogous to the one used for tracking the time evolution of chemical reactions.
The binding energies per nucleon B_A are rather high, in the few-MeV range, but given the smallness of η (the entropy of the Universe is very large), the fraction of stable nuclei approaches values close to 1 only at much lower energies (temperatures). To see this, we can use Eq. 6.20 and solve it for the temperature T_A when $X_A \sim 1$ and $X_p \sim X_n \sim 1$:

$$T_A \sim \frac{B_A/(A-1)}{\log(1/\eta) + 1.5\log(m_N/T)} \quad . \quad (6.22)$$

From the last equation, we can calculate $T_A(^2\mathrm{H}) \sim$ 0.07 MeV, $T_A(^3\mathrm{He}) \sim$ 0.11 MeV, $T_A(^4\mathrm{He}) \sim$ 0.28 MeV. It is interesting to note that it is the large

entropy of the Universe (or $\eta \ll 1$) which prevents nuclei to form sooner during the Big Bang, and not the deuterium relatively small binding energy.
Let us see now in steps how the lightest elements were created. Starting in the radiation-dominated era at high temperature (T=10 MeV, $t = 10^{-2}$s), the only relativistic species we can have are electrons, positrons, photons, and neutrinos, adding up to an effective number of degrees of freedom $g_* = 10.75$ (if the neutrinos are three and there is no "new physics"). The electroweak reaction rates at this time are larger than the expansion rate, so at equilibrium we have $X_n = X_p = 1/2$. The light nuclei were in nuclear statistical equilibrium and the abundances can be calculated with the system of equations 6.21 and $\eta \sim 10^{-9}$

$$\begin{cases} X_n = X_p = 1/2 \\ X_2 \sim 6 \times 10^{-12} \\ X_3 \sim 2 \times 10^{-23} \\ X_4 \sim 2 \times 10^{-34} \end{cases} , \tag{6.23}$$

which shows how difficult was at that time to find nuclei in the primordial plasma. As the Universe expands and cools, we can consider an epoch where T=1 MeV ($t \sim 1s$): at this time neutrinos decouple from the plasma, positrons and electrons start to annihilate into photons, and the $p \leftrightarrow n$ reactions freeze out ($\Gamma \ll H$), fixing their ratio $n_n/n_p \sim 1/6$, as calculated before (Eq. 6.12). Using the last ratio and T=1 MeV:

$$\begin{cases} X_n = 1/7 \\ x_P = 6/7 \\ X_2 \sim 6 \times 10^{-12} \\ X_3 \sim 2 \times 10^{-23} \\ X_4 \sim 2 \times 10^{-28} \end{cases} . \tag{6.24}$$

Considering now temperatures low enough for nuclei to form ($T \sim 0.3 - 0.1$ MeV, t=3 min), the number of effective degrees of freedom becomes similar to the today's one: $g_* = 3.36$. Reactions forming ^{4}He are initially too slow and nuclear electromagnetic repulsion forces nuclei to be formed via tunnel effect, further slowing down ^{4}He formation. When finally the temperature reached ~ 0.1 MeV, the helium fraction started to grow significanly. Almost all the neutrons ended up in helium and therfore we

can estimate its fraction as

$$X_4 = \frac{4n_4}{n_N} = \frac{4(n_n/2)}{n_n + n_p} = \frac{2(n_n/n_p)}{1 + (n_n/n_p)} \sim 25\% \quad . \tag{6.25}$$

The ratio $n_n/n_p \sim 1/6$ is now a bit lower due to occasional residual electroweak interactions until ^{4}He really starts to form, so we considered it $\sim 1/7$.
The large Coulomb barrier for reactions like ^{4}He(^{3}H,γ)^{7}Li and ^{4}He(^{3}He,γ)^{7}Be, and the absence of stable nuclei with $A = 5$ and $A = 8$ strongly limits the production of heavier elements after the Big Bang. There is the possibility to create ^{12}C with the triple-alpha reaction, but the nucleon density is too low for a significant rate.
The heavier nucleus which could be produced in a non-negligible amount is ^{7}Li from the direct reaction mentioned before, or by decay of ^{7}Be.
The abundance of ^{7}Li over hydrogen is of the order of $10^{-10} - 10^{-9}$. There is also some ^{3}He left over, with an abundance over hydrogen of $10^{-5} - 10^{-4}$. For a complete overview of the nuclear reactions relevant for BBN, see Fig. 6.2.

6.5 Predictions of Big Bang Nucleosynthesis

G. Gamow was the first proposing the idea of nucleosynthesis after the Big Bang in 1946. Gamow's original idea was that all the elements were created during the Big Bang through successive neutron capture followed by beta-decay.
F. Hoyle and others proved that this was not possible and only the lightest elements could have been created cosmologically. Gamow's theory still predicted correctly the relative abundances of hydrogen and helium which form the bulk of the cosmologically produced nuclei.
After him and his collaborator's work, computer codes implementing the full reaction network similar to the small one sketched in the previous section were developed. With the advances in computer hardware and the development of better computer codes, today we can solve the reaction network with high numerical accuracy (see Fig. 6.3).
Since the numerical error is not a problem, we have to focus on the errors in the input parameters of the calculation, like nuclear cross sections and the neutron lifetime. The final results of the calculation are quite robust

against errors in the cross sections, while the neutron lifetime traditionally represented a rather large uncertainty, which improved with time (besides some systematic uncertainty problems). The current PDG value (2019) is $\tau_n = 879.4 \pm 0.6$ s but still it represent the major influencing factor on the ^{4}He abundance. This happens because the neutron lifetime influences all the electroweak reactions ($\Gamma \propto 1/\tau_n$) and an increase in its value would slow down the $p \leftrightarrow n$ rates leading to a n/p freeze-out at a higher temperature ($T_{f.o} \propto \tau_n^{1/3}$). From Eq. 6.12 and Eq. 6.25 an increase in the neutron lifetime will lead to an increase in the helium abundance prediction. Since the helium abundance is known with good precision, the neutron lifetime precision is also very important as a test for the Big Bang nucleosynthesis model.

The Origin of Chemical Elements

R. A. ALPHER*
Applied Physics Laboratory, The Johns Hopkins University, Silver Spring, Maryland

AND

H. BETHE
Cornell University, Ithaca, New York

AND

G. GAMOW
The George Washington University, Washington, D. C.
February 18, 1948

Figure 6.1: The famous "$\alpha\beta\gamma$" paper about big bang nucleosynthesis.

6.6 Observations

The measurement of the abundances of the various elements is a complex problem. The first issue is the fact that we would like to know the abundance of the elements of cosmic origin, which is different from today's abundance: the latter can be different due to further reactions happened e.g. in stars. In the following, we briefly review the experimental methods and issues in determining the abundances of the light elements produced during the Big Bang nucleosynthesis.

- **Deuterium (^{2}H)**
  A good source of information about cosmologically-created elements

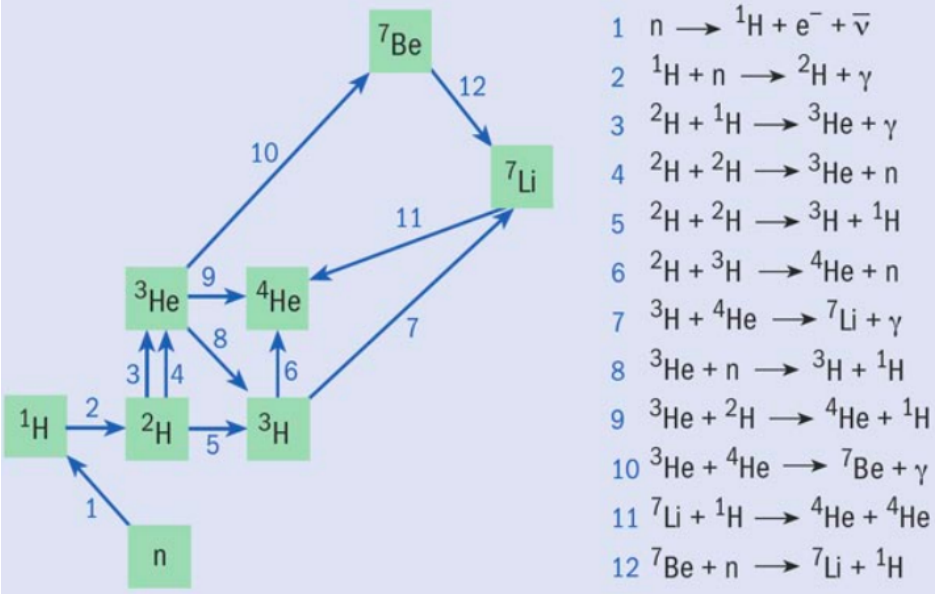

Figure 6.2: Reaction network for the creation of the light elements in the Big Bang.

is spectroscopy of the interstellar medium. From such measurements the deuterium abundance is estimated to be $\sim 10^{-5}$ with respect to hydrogen. Since deuterium is a weakly-bound nucleus, it is easy to break (temperatures of $\sim 0.5 \times 10^{6}$ K are sufficient) and it is not easily synthesized astrophysically. This means that the deuterium we measure is a good representative of the cosmological one and thus gives us a lower bound on its abundance.

- **Helium-3 (^{3}He)**
  The abundance of this nuclide is also of the order of $\sim 10^{-5}$ and has been measured for example with galactic spectroscopy, rocks/meteorites analysis, and lunar soil. In our solar system, deuterium was converted in ^{3}He by the Sun and therefore local measurements of ^{3}He represent the local abundances of ^{2}H+^{3}He.

- **Helimu-4 (^{4}He)** This nuclide is copiously produced in stars and thus counting of the cosmologically-produced one is a primary issue in the determination of its abundance. The latter observation points towards measurements outside the solar system or in extra-galactic

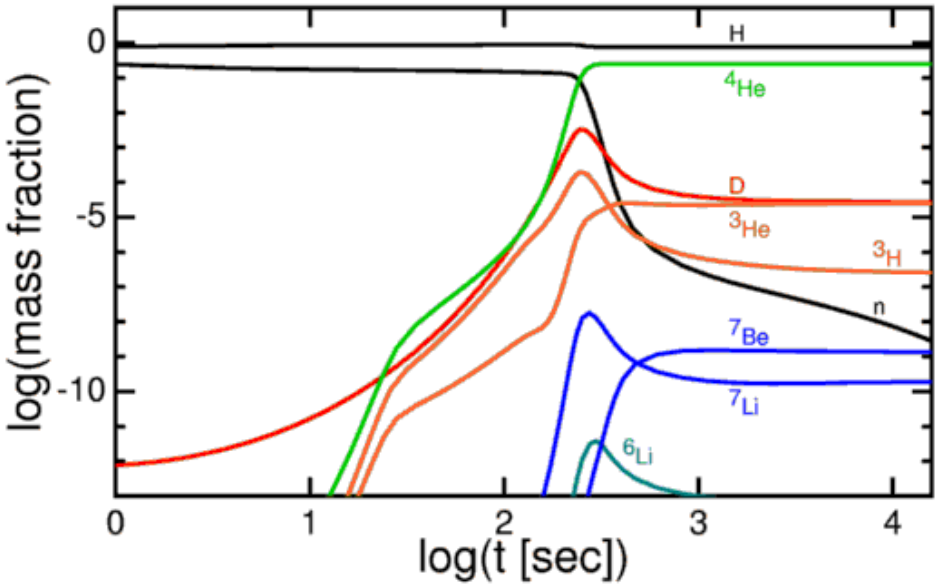

Figure 6.3: Evolution of the baryon fractions during Big Bang Nucleosynthesis (figure from www.astro.ucla.edu/~wright/BBNS.html).

regions.

- **Lithium-7 (^{7}Li)** This is the heaviest nuclide created during BBN and its very low abundance is also the most difficult to precisely assess. This is because ^{7}Li has a low binding energy and is easily destroyed in stellar environments, while it can be created also by cosmic rays interactions. The abundance can be measured for example in the athmosphere of low-metallicity stars and values of the order of 10^{-10} are found, roughly consistent with the abundances of the other light elements according to BBN calculations. The correct abundance of this nuclide is still at the center of a theoretical and experimental debate.

The BBN model can explain the relative abundances with the same value of η (the barion-to-photon ratio) and this can be regarded as another success of this model.

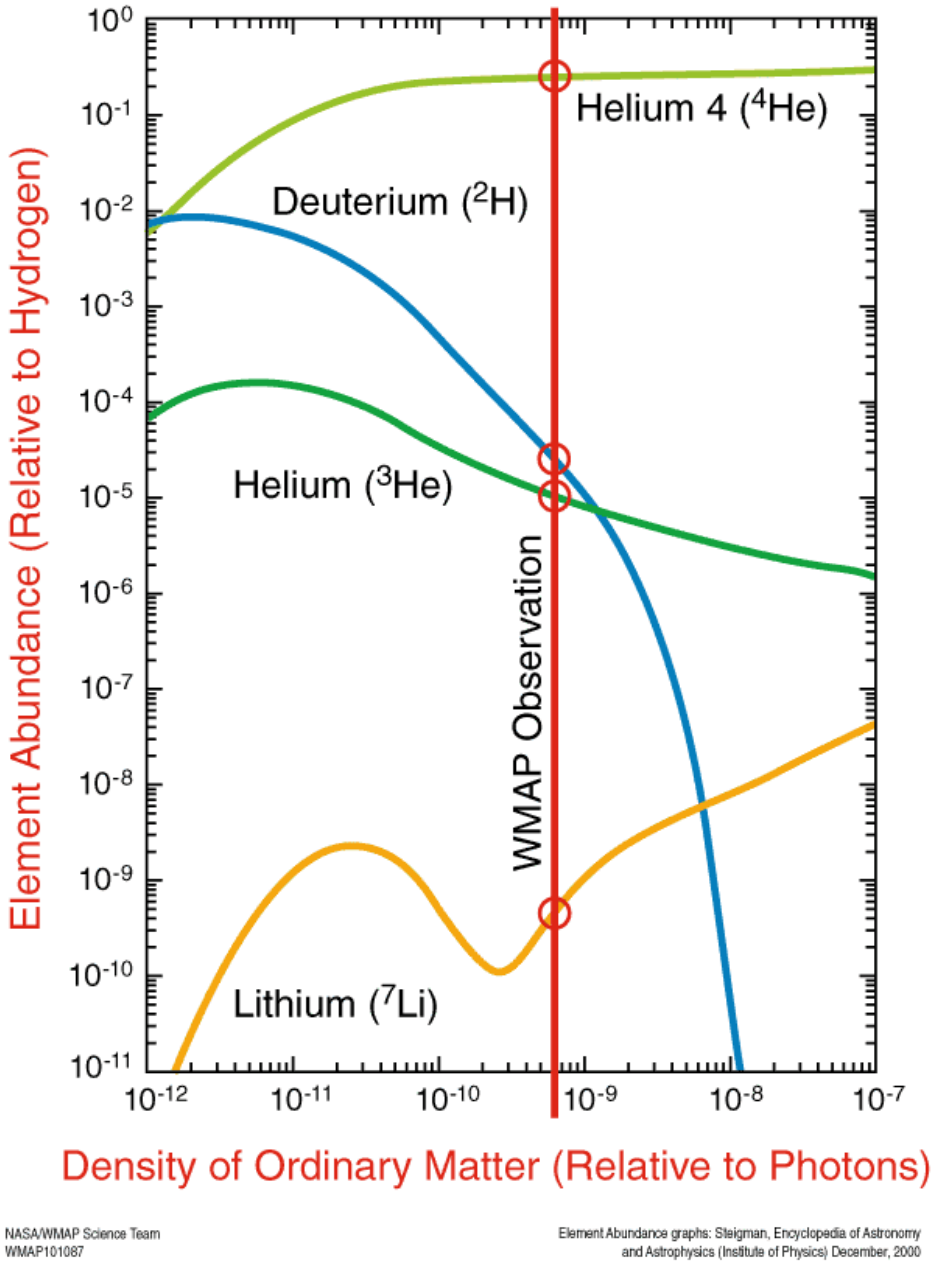

Figure 6.4: Evolution of the nuclear fractions as a function of the baryon-to-photon ratio η, which can be measured with high accuracy with the CMB. (figure from WMAP Collaboration)

Chapter 7 | Cosmic Rays

7.1 Introduction

Cosmic rays are particles of different species arriving on earth from the cosmos. Usually cosmic rays (CR) are divided in **primary** and **secondary**. Primary cosmic rays are fully ionized nuclei, protons or other particles accelerated by some astrophysical sources and sent around in the Universe and thus also in the direction of the Earth. Secondary CRs are produced by primary CRs entering the atmosphere and interacting with atoms and molecules.
The discovery of CRs is attributed to the austrian physicist Victor Hess in 1912. It was known that a kind of natural radioactivity existed also when radioisotopes were not close to detectors. Hess, with a series of balloon flights at altitudes beyond 5000 m showed that such radioactivity was increasing, thus demonstrating its cosmic nature. Later, the discovery was confirmed showing that CRs had a latitude dependence and detectors put in time-coincidence and separated by more than 200 m were detecting large showers caused by a primary CR.
The study of CRs allowed also the discovery of new subatomic particles (*e.g.* pions and muons) and opened a new window on our Universe, beyond optical observations. In principle, CRs comprehend also neutrinos but they will be treated separately in the next chapter.

7.2 Cosmic Ray Flux

An important quantity for characterizing cosmic rays is the flux, defined as

$$\Phi(E) = \frac{d^2\Phi}{dEd\Omega}(E) = \frac{dN}{A \cdot T \cdot d\Omega dE} \left[\frac{\text{\# particles}}{\text{cm}^2 \text{ sr s GeV}}\right] \quad , \tag{7.1}$$

which is the differential intensity of incoming particles per solid angle and per energy. Cosmic rays arrive approximately isotropically on Earth and in some cases it can be useful to integrate over all the angles considering the flux through a sphere: $d^2\Phi/dEd\Omega \rightarrow 4\pi\ d\Phi/dE$.
An experimentally interesting case is the one where cosmic rays from one hemisphere reach a detection plane

$$\Phi_{pl}(E) = \int \frac{d^2\Phi}{dEd\Omega} \cos\theta d\Omega \left[\frac{\text{\# particles}}{\text{cm}^2 \text{ s GeV}}\right] \quad . \tag{7.2}$$

The angle θ is the angle between the vertical to the detector plane and the direction of the incoming cosmic ray. If the cosmic rays have an isotropic distribution, we can integrate over all the angles

$$\Phi_{Pl} = \frac{d\Phi}{dE} \int_0^{2\pi} d\phi \int_0^{\pi/2} d\theta \sin\theta \cos\theta = \pi \frac{d\Phi}{dE} \quad . \tag{7.3}$$

7.3 Primary Cosmic Rays

Scientists study CRs since a century and this has lead to a rather precise measurement of the energy spectrum of the primary CRs. The spectrum extends from few MeV to the extremely high energy of about 10^{20} eV = 10^8 TeV. To make a comparison, the highest energies we realize in laboratory on Earth is of the order of 10 TeV. To give an idea about how CRs are distributed in energy, we can consider the energy-integrated spectrum

$$F(E_{CR} > E) = \pi \int_E^{\infty} dE \Phi_{Pl} \left[\frac{\text{\# particles}}{\text{cm}^2 \text{ s}}\right] \quad , \tag{7.4}$$

where we integrate all the cosmic rays from a certain energy E_{CR} onwards. What we obtain is the number of particles per surface and per time. What

it is observed is approximately

$$\begin{array}{lcl} F(E > 1\text{GeV} = 10^9 \text{ eV}) & \sim & 1000 \text{ particles/s/m}^2 \\ F(E > 1\text{PeV} = 10^{15} \text{ eV}) & \sim & 1 \text{ particle/year/m}^2 \\ F(E > 100 \text{ EeV} = 10^{20} \text{ eV}) & \sim & 1 \text{ particle/century/km}^2 \end{array} \quad (7.5)$$

The CRs spectrum is rather smooth with two main features: the so-called "knee" and "ankle". At those points, the energy spectrum changes slope in a logarithmic plot (see Fig. 7.3).
In general, the energy spectrum can be decribed by a power-law

$$\Phi(E) = KE^{-\alpha} \quad , \quad (7.6)$$

where the parameter α is the *differential spectral index* and K a normalization constant. From a fit of the experimental data from the few-GeV to the knee range, we have

$$K \sim 3.01 \quad ; \quad \alpha \sim 2.7 \quad . \quad (7.7)$$

Different fits give slightly different numbers but the values are approximately the ones reported above and the data includes protons and also heavier nuclei.
After the knee, the spectrum becomes steeper with $\alpha \sim 3.1$, while after the ankle the spectrum flattens again. After the ankle, CRs are believed to have an extra-galactic origin.
Often, the cosmic ray spectrum is presented as $E^{2.6}\Phi$ for flattening the first part and make the knee/ankle features more evident.
Concerning the low-energy region, below $\sim$4 GeV the largest source of CRs is the Sun where they are produced by solar flares and are composed mainly of protons, electrons and heavier nuclei. The solar activity is usually measured with neutron monitors. These detectors measure neutrons produced in the atmosphere by solar CRs: the advantage is that neutrons are not deviated by the Earth's magnetic field and thus even low-energy CRs can be detected. Neutron monitors clarly show the 11-year cycle of solar activity which is thus correlated to CRs emission.

7.4 Secondary Cosmic Rays and Showers

Cosmic rays interact with the Earth's atmosphere creating the so-called extensive air showers (EAS). If we would like to detect these secondary

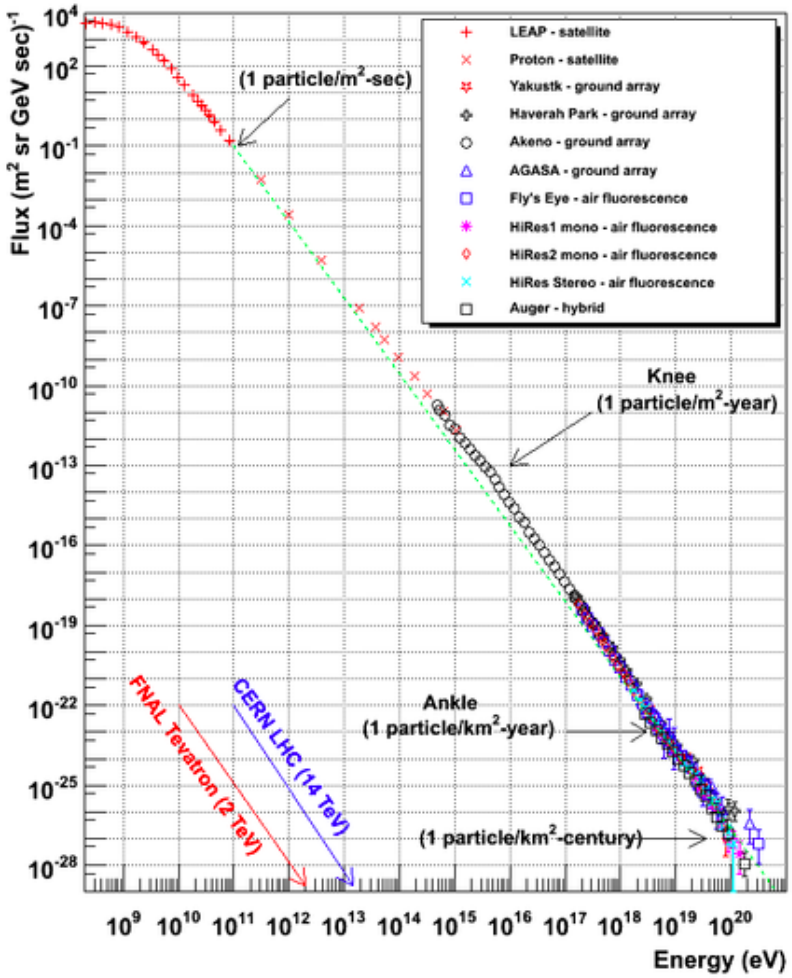

Figure 7.1: Energy spectrum of the primary cosmic rays measured by various experiments. The two points where the slope changes are conventionally called "knee" and "ankle". For reference, the maximum energies of the two most powerful proton accelerators are reported (Tevatron and LHC). (Figure from W. Hanlon, U. Utah).

rays, we are effectively using the atmosphere as a calorimeter. In general, EAS have electromagnetic and hadronic components. If the primary CR is a photon, the shower is almost purely electromagnetic, so it is useful to characterize the two types of showers separately.

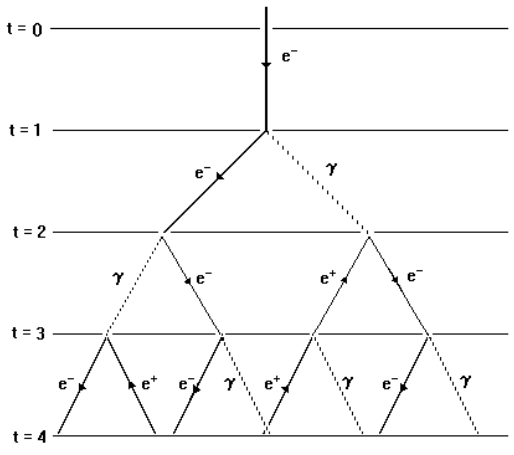

Figure 7.2: Evolution of an electromagnetic shower according to the approximate Heitler model. In this model, the evolution proceeds only through bremstrahlung and pair creation at each step.

Electromagnetic Showers

These showers are entirely composed by photons, electrons and positrons. The main processes multiplying the particles are bremsstrahlung and pair production. The main features of the EM showers can be understood with a simple model due to Heitler (1944), where the shower is divided in steps where at each step a photon creates an e^+e^- pair or an electron radiates a photon via bremsstrahlung. The whole process can be tought as a binary tree and therefore it will have an exponential character. Until photons have energies higher than about twice the electron mass ($\sim$ 1 MeV), the multiplication process continues.

In general, in an EM cascade, there are excitation/ionization (described by a function K(E)) and bremstrahlung ($\sim E/X_0$) components and the change in energy is described by

$$-\frac{dE}{dX} \sim K(E) + \frac{E}{X_0} \quad , \tag{7.8}$$

where X is measured in g·cm^{-2} and X_0 is the so-called *radiation lenght* and it is dependent from the material where the cascade develops. In an electromagnetic EAS we can neglect the ionization part ($K \sim 0$) such that the solution of Eq. 7.8 becomes

$$E(X) = E_0 e^{-X/X_0} \quad , \tag{7.9}$$

which describes the energy of the single electrons. Since after each bremsstrahlung/pair creation step we assume approximately that the energy drops its value by one half,

$$\frac{E(X=d)}{E_0} = e^{\frac{-X_0 \ln 2}{X_0}} = \frac{1}{2} \quad , \tag{7.10}$$

and the single steps have a radiation length of $d = X_0 \cdot \ln 2$. Following this model, after k steps, we have $N = 2^k$ particles with energy $E_0/2^k$ and the process continues until the critical energy E_C is reached after $k = k^*$ steps. The critical energy is the energy at which excitation/ionization processes have the same rate as radiation processes. The so-called *shower maximum*, where the maximum of particles is produced, is reached at

$$N_{max} = 2^{k^*} \sim \frac{E_0}{E_c} \tag{7.11}$$

In air we have $X_0 \sim 37$ g·cm^{-2} and $E_C \sim 86$ MeV. For example, using the previous approximate formulas, a 10 TeV photon entering the atmosphere would create on average about 10^5 electrons.
We can now calculate at which depth in the atmosphere (in g·cm^{-2}) X_{max} the shower maximum occurs. Defining X_i the depth at which the shower starts we have

$$X_{max} = X_i + k^* \cdot d = X_i + k^* X_0 \cdot \ln 2 = X_i + X_0 \left(\frac{E_0}{E_C} \right) \quad . \tag{7.12}$$

The shower development is usually simulated using Monte Carlo simulations, which roughly confirm the simplified Heitler model. One of the main differences is that the Heitler model overpredict the number of particles, assuming that the electron/photon ratio is 2, while in reality is closer to 1/6. The discrepancy is explaning by the fact that during bremstrahlung more than one photon is emitted on average.

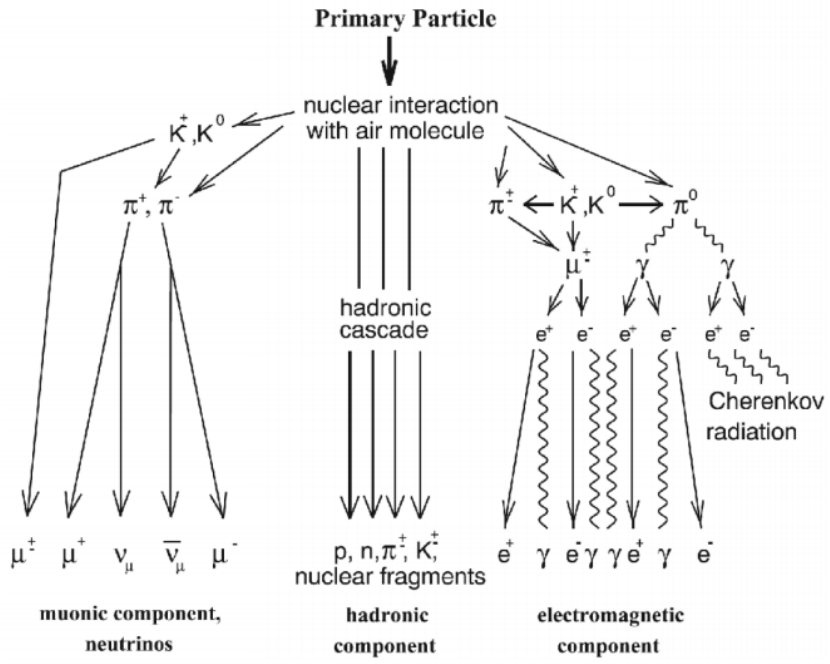

Figure 7.3: Schematic evolution of an hadronic shower.

Hadronic Showers

CRs initiated by protons or heavy nuclei create *hadronic shower* in the atmosphere. The number of charged particles in such a shower with initial energy E_0 can be approximated by

$$n \propto E_0^{0.2} \quad . \tag{7.13}$$

The evolution of an hadronic shower is more complex than that of an EM shower, at least because they can *contain* EM showers. Protons (or nuclei) entering the atmosphere and colliding with nuclei create mainly charged and neutral pions $\pi^{\pm}$, π^0. The main decay mode of the neutral pion is $\pi \rightarrow \gamma\gamma$ and the produced γ-rays can start sub-electromagnetic showers. Charged pions decay mainly into muons: $\pi \rightarrow \mu\nu$. If the energy is sufficient, also kaons can be created, which produce further pions and muons. Fig. 7.3 shows schematically how an hadronc shower develops. The balance between hadronic and electromagnetic components in terms of total hadronic energy E_h and electromagnetic energy E_{EM} after k steps

is given approximately by

$$E_h = \left(\frac{2}{3}\right)^k E_0 \quad ; \quad E_{EM} = E_0 - E_h \quad . \tag{7.14}$$

Hadronic showes induced by nuclei can be approximately treated with a superposition model, where a nucleus with mass number A is treated as A incoming protons.
Extended showers in the atmosphere have to be ultimately treated with simulations, given their complexity of the large amount of particles of different types, decays, interactions, and wide energy range involved.

7.5 Diffusion

After the production of CRs at astrophysical sites which are also responsible for their acceleration, CRs diffuse throughout the galaxy (disregarding for now extragalactic CRs). As CRs travel through the galaxy, they are bent by the galactic magnetic field and interact with the interstellar medium: these physics effects determine the property of the CRs which we measure on Earth. For example, the galactic magnetic field is responsible for "randomizing" the CRs such that we measure an isotropic distribution for their incoming direction.
Information about the diffusion of CRs in the galaxy can be gathered studying their interaction with the interstellar medium. The medium is mainly constituted by hydrogen and nuclei present in the CRs can interact with it. These nuclear reactions can give rise to light nuclei like B, Be, and Li. These light nuclei are poorly present in our solar system while they are more abundant in CRs: why?
Heavy nuclei are created by reactions in the stellar environment up to the Fe nucleus. Stars cannot create nuclei heavier than Fe by fusion since it is not anymore energetically convenient. Nuclei heavier than Fe are believed to be created by supernova explosions (or, as recently discovered, by neutron star mergers). These highly energetic events project heavy nuclei through the galaxy and they interact with the interstellar medium producing light nuclei. These light nuclei are not particularly present in the solar system, since they act as catalyzers in stellar reactions and are not directly produced, thus their abundance does not grow due to star

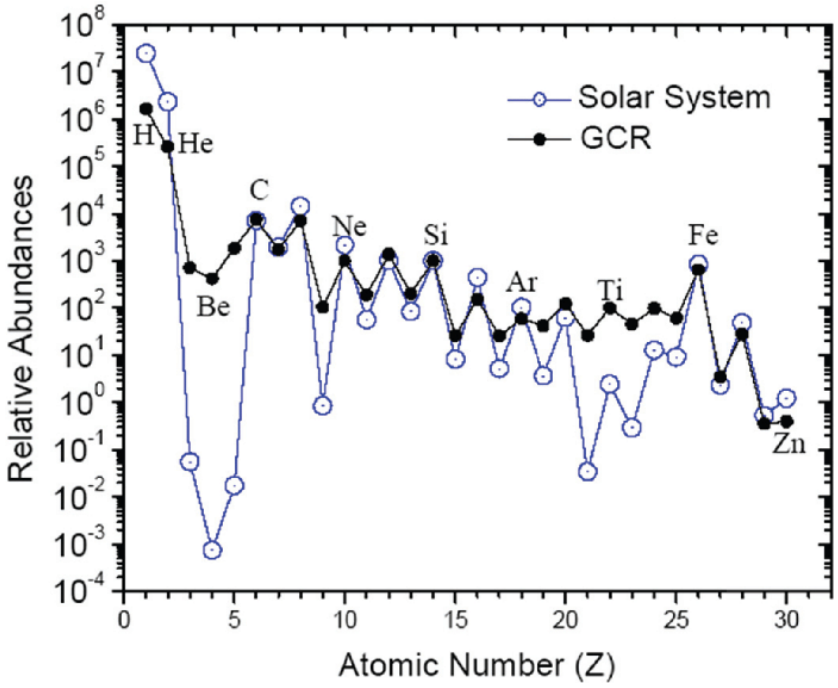

Figure 7.4: Galactic cosmic rays elemental abundance compared to the solar system's one. Note the drop in abundance for the light elements. Stellar processes do not produce them, while they are produced by fragmentation of heavier nuclei in the interstellar medium (Figure from: A. Pacini, Rev. Bras. Ensino Fis. 39, 1, (2017)).

burning.
What is possible to do, is to measure the B, Be, and Li abundances in our planetary system and look at their ratio with respect to CRs. From this number we can deduce interesting informations about the propagation of CRs in the galaxy.
Summarizing: light elements are created by the fragmentation of heavier elements present in CRs. The heavy elements are present in CRs because they were produced e.g. in supernova explosions or other astrophysical sites. The light elements are not produced in stars since there they act just as catalyzers. Measuring the abundance of light elements in CRs and in the Solar system we can infer properties about CRs.

In Fig. 7.5 the abundance of nuclear species in galactic cosmic rays and in the solar system are compared.

In order to study how CRs diffuse and create an excess of light elements, we have to introduce few concepts.
The probability of a nuclear reaction to occur is characterized by its cross section σ (in units of cm^2). If one projectile goes through a medium, its mean free path λ (the path in cm travelled until an interaction occurs) is

$$\lambda = \frac{1}{n\sigma} \quad , \tag{7.15}$$

where n is the volume density (in units of particles/cm^3). Since the number density n depends on the density ρ of the medium, the relevant quantity is the *nuclear interaction length* (in units of g/cm^2)

$$\lambda_I = \frac{\rho}{n\sigma} \approx \frac{Am_p}{\sigma} \tag{7.16}$$

where m_p is the proton mass and A the nucleus mass number. The simplest model of the nuclear cross section is a rough estimation of the nucleus' cross section area considering it a sphere with radius R: $\sigma = \pi R^2$. If the volume is proportinal to the number of nucleons A, then $R \sim rA^{1/3}$ where $r \sim 1.2 \times 10^{-13}$ cm is the radius of one nucleon.
CRs are composed mainly by protons and medium-mass nuclei. We introduce now the labels L for quantities relative to light nuclei (B, Be, and Li) and M for medium-mass nuclei (mainly C,N,O). The reaction we are interested in is

$$M + p \rightarrow L + X \quad , \tag{7.17}$$

where p is a proton and X are other nuclear fragments. The relevant variable in these interactions is the path length ξ

$$\xi = \rho_{ISM} \cdot x \quad , \tag{7.18}$$

where ρ_{ISM} is the density of the interstellar medium and x the path travelled by the CR. From experimental measurements, we can calculate the average cross sections for the light and medium-mass nuclei against protons: $\sigma_M \sim 280$ mb and $\sigma_L \sim 200$ mb.
Now we can write an equation describing how the number of nuclei M changes in time (due to interactions with the medium)

$$\frac{dN_M}{d\xi} = -\frac{1}{\lambda_M} N_M(\xi) \quad , \tag{7.19}$$

where λ_M is the interaction length defined in Eq. 7.16. The number of light nuclei varies instead according to

$$\frac{dN_L}{d\xi} = \frac{P_{LM}}{\lambda_M} N_M - \frac{1}{\lambda_L} N_L(\xi) \quad , \tag{7.20}$$

where $P_{LM} \sim 0.28$ is the average probability that M fragments into N. The average is calculated from the average nuclear cross sections of B, Be, Li, C, N, and O. From the cross sections we have also $\lambda_M \sim 6$ g cm^{-2} and $\lambda_L \sim 8.4$ g cm^{-2}.
The right-hand side of the last equation has two terms. The first one is a source term describing how N are created, while the second term is an attenuation term, describing how L can be destroyed by further interactions. The Eqs. 7.19 and 7.20 represent a coupled system of differential equations that we have to solve. Eq. 7.19 gives directly the solution $N_M(\xi) = N_M^0 e^{-\xi/\lambda_M}$. Replacing this solution in Eq. 7.20 and multiplying by e^{ξ/λ_L} one can recognize a derivative of the product of two functions:

$$\frac{d}{d\xi}\left(N_L \cdot e^{\xi/\lambda_L}\right) = \frac{P_{LM}}{\lambda_M} N_M^0 e^{\xi/\lambda_L - \xi/\lambda_M} \quad . \tag{7.21}$$

Using as *ansatz* the form $e^{-\xi/\lambda_L - \xi/\lambda_M}$ one finds the solution

$$N_L(\xi) = N_M^0 \cdot \frac{P_{LM}}{\lambda_M} \frac{\lambda_M \lambda_L}{\lambda_L - \lambda_M} e^{-\xi/\lambda_L - \xi/\lambda_M} \quad . \tag{7.22}$$

Looking at the evolution of N_L and N_M as a function of ξ, we can calculate the point $\xi = \xi_{esc}$ where the experimental value $N_L/N_M = 0.25$ is reproduced (looking at this ratio, the value of N_M^0 is not relevant). The value ξ_{esc} is called *average escape length* and it is linked to the distance x_{esc} a CR can travel before exiting our galaxy:

$$x_{esc} = \frac{\xi_{esc}}{\rho_{ISM}} \frac{5\ g/\text{cm}^2}{1.6 \times 10^{-24} g\ \text{cm}^{-3}} = 10^{25}\ \text{cm} \sim 3\ \text{Mpc} \quad . \tag{7.23}$$

Our galaxy has a radius of ∼15 kpc and a thicknes of ∼300 pc: this means that the CR can travel really a large distance circling in the galaxy (due to the galactic magnetic fields) before exiting it. Assuming a CR travelling at the speed of light, we can also calculate an average escape time:

$$t_{esc} = \frac{x_{esc}}{c} \sim 3 \times 10^{14}\text{s} = 10^7\text{y} \quad . \tag{7.24}$$

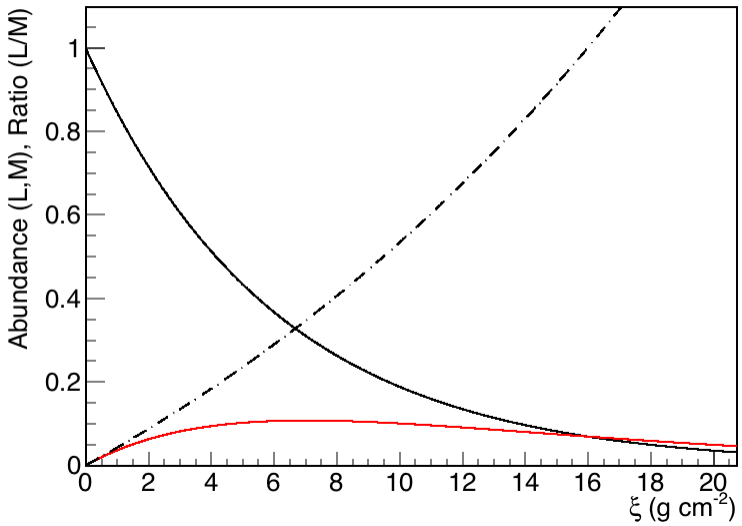

Figure 7.5: Evolution of the medium-mass (black line) and light mass nuclei (red line) abundances and their ratio (dashed black line) as a function of $\xi = x \cdot \rho_{ISM}$. The initial medium-mass abundance is set arbitrarily to 1 and decreases due to the interactions with the interstellar medium (ISM). The light-mass abundance increases due to fragmentation of heavier nuclei agaist the hydrogen of the ISM. The measured ratio of about 0.25 corresponds to $\xi \sim 5$ g/cm^2.

From the above numbers, we see that the galaxy is rather efficient in keeping the CRs confined in its volume and their motion can be seen as a kind of random walk. Since the propagation time is so long with respect to their creation time, these observations justify a separate treatment of propagation and creation of the CRs.

7.6 Acceleration Mechanisms

CRs have a non-thermal distribution, so they cannot be considered as particles escaped from a thermal astrophysical environment: CRs should have undergone a process of acceleration. A theory for CR acceleration must explain a multitude of features: the E^{-a} dependence of the flux, the

value $a \sim 2.7$ for protons and nuclei before the knee, $a \sim 3$ above the knee, the CR composition, and the flattening after the ankle. The first ideas about possible acceleration mechanisms were proposed by Fermi, which imagined the particles accelerated by their interactions with gas clouds moving at high speed because of an (maybe explosive) astrophysical event. Before looking at the acceleration mechanisms, we have to investigate what can "reflect" a charged particle: it turns out that a non-uniform magnetic field (as fields present in the vicinity of astrophysical objects) can indeed act as a "mirror".

7.6.1 Magnetic Mirrors

If a magnetic field is spacially not homogeneous, an electric field arises, as known from Faraday's law

$$\nabla \times E = -\frac{1}{c}\frac{\partial B}{\partial t} \quad . \tag{7.25}$$

The electric field can modify the energy K associated to the radial motion of the particle:

$$\Delta K = \Delta\left(\frac{1}{2}mv_\perp^2\right) = \oint qE \cdot dl = q\oint \nabla \times E \cdot dS = -\frac{q}{c}\oint -\frac{\partial B}{\partial t} \cdot dS \quad , \tag{7.26}$$

where the surface integral (on the surface S) is performed on the approximate circular orbit of radius r the particle induced by the magnetic field. Considering the Larmor period $T_L = 2\pi/\omega$ ($\omega = qB/mc$ is the Larmor frequency) the time derivative of the magnetic field can be approximated by

$$\frac{\partial B}{\partial t} \sim \frac{\Delta B}{T_L} \quad . \tag{7.27}$$

Reinserting in Eq. 7.26 we have

$$\Delta K = \frac{q}{c}\Delta B\frac{\omega}{2\pi}(\pi r^2) = \left(\frac{1}{2}mv_\perp^2\right)\frac{\Delta B}{B} = K\frac{\Delta B}{B} \quad . \tag{7.28}$$

Rearranging the first and last terms of the last equation

$$\frac{\Delta K}{K} = \frac{\Delta B}{B} \quad \Rightarrow \quad \Delta\left[\ln\left(\frac{K}{B}\right)\right] \quad \Rightarrow \quad \frac{K}{B} = \text{const.} \quad . \tag{7.29}$$

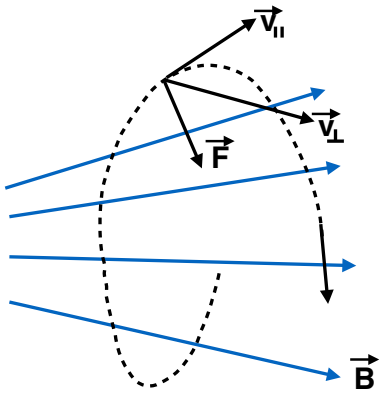

Figure 7.6: Schematic representation of a magnetic mirror. A spacially inhomogeneous magnetic field B can reflect the motion of a particle through the force of an induced electric field.

The last result proves that changes in B induce changes in K. Because of conservation of energy, if the transverse energy K changes, also the energy associated to the parallel component of the motion must change. For example, if B increases, also K increases, and therefore, the energy in the parallel component must decrease: this effect in in opposition to the particle motion. Actually, if the field B increases enough, the particle can even be "reflected" and we have an effective *magnetic mirror*.
Another way to see this is the following. Defining θ as the angle between the particle velocity and the magnetic field we have $v_{\perp} = v \sin\theta$. Since v is assumed constant, from Eq. 7.29 we can conclude that

$$\frac{\sin^2\theta}{B} = \text{const.} \quad \Rightarrow \quad \sin\theta = \sin\theta_0 \sqrt{\frac{B}{B_0}} \quad , \tag{7.30}$$

which says that the angle can increase up to $\pi/2$: after that, the particle must reverse its motion. A similar mechanism traps charged particles in the van Allen radiation belts around the Earth.

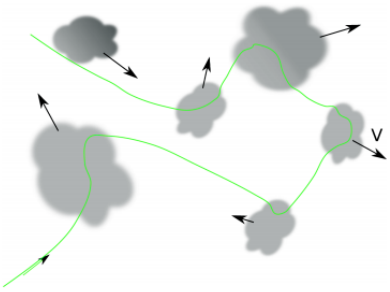

Figure 7.7: Schematic representation of the second order (stochastic) CR acceleration mechanism (Figure from N. Murphy, Harvard-Smithsonian Center for Astrophysics).

7.6.2 Second Order Fermi Acceleration

This is the (historically) first acceleration mechanism devised by Fermi in 1949 and why it is called "second order" will be clear towards the end of the discussion. Fermi imagined that a particle with velocity v could collide with a gas cloud moving with speed U and being reflected for example through the magnetic mirror mechanism. Modeling the scattering as elastic, the new velocity of the particle after the collision is

$$v' = \frac{(m-M)v + 2mM}{m+M} \quad , \tag{7.31}$$

where m and M are the masses of the particle and the cloud, respectively. Assuming $M \gg m$, the last formula reduces to $v' \approx -v \pm 2U$. If the cloud and the particle move towards each other, $v' = -v - 2U$, while if the particle and the cloud are moving in the same direction we have $v' = -v + 2U$. In both cases, the particle reverses its motion. The kinetic energies E and E′ before and after the collisions are

$$E = \frac{1}{2}mv^2 \qquad ; \qquad E' = \frac{1}{2}m(-v \pm 2|U|)^2 \quad . \tag{7.32}$$

The kinetic energy variation $\Delta E = E' - E$ at first order in U/v is

$$\Delta E \approx \pm 4\frac{U}{v}E \quad , \tag{7.33}$$

where the approximation is justified by assuming $v \gg U$. This acceleration mechanism is "stochastic" in the sense that we assume that clouds

are present in both directions of the particle and after one collision, more of them happen against different clouds (see Fig 7.7). With such random distribution of clouds, we can estimate an average collision rate f

$$f_1 = \frac{v+U}{l} \qquad ; \qquad \frac{v-U}{l} \quad , \tag{7.34}$$

where the indices 1,2 refer to the two collision cases (cloud moving agaist or away from the particle) and l is the mean free path travelled by the particle before a collision. We can now estimate the average change of kinetic energy with time

$$\frac{\Delta E}{\Delta t} = f_1 \Delta E_1 + f_2 \Delta E_2 = \left(\frac{8U^2}{lv}\right) E \quad . \tag{7.35}$$

From the last equation, we can identify a characteristic time $\tau = lv/(8U^2)$ The fact that the cloud velocity U appears at second order gives the name "second order acceleration" to this process. The coefficient 8 stems from having considered an unidimensional problem. The full 3-dimensional treatment reduces the factor to 2.
The described collisions with interstellar clouds for accelerating CRs is quite inefficient, as soon realized by Fermi himself. Since interstellar clouds velocities in our galaxy are estimated to be small, of the order of $U \sim 10^6$ cm/s, and $l \sim 0.1$ pc, as estimated by the size of typical magnetic inhomogeneities in the interstellar medium, we have as typical time

$$t \sim \frac{l}{c} = \frac{3 \times 10^{17}\text{cm}}{3 \times 10^{10}\text{cm/s}} = 10^7\text{s} \quad , \tag{7.36}$$

which implies only few collisions per year. The time constant τ in Eq. 7.35

$$\tau = \frac{lv}{8U^2} \quad , \tag{7.37}$$

is estimated to be $\tau \approx 10^9$ years: this means that an appreciable CR acceleration can be achieved only on cosmological scales. The latter considerations lead Fermi to devise a different mechanism, described in the next section.

7.6.3 First Order Fermi Acceleration

In 1954 Fermi devised a more efficient mechanism for obtaining particle acceleration, which is based on the presence of shock waves in astrophysical environments.
Shock waves have typically magnetic inhomogeneities both preceding and following them. If a charged particle travels through the shock wave it encounters a moving change in the magnetic field: this can reflect it back through the shock front at increased velocity. A similar process occurs on the other side of the shock front and the particle will gain energy again. These multiple reflections between the upstream and downstream parts of the shock wave can effectively increase the particle's energy.
Let us consider the 4-momentum of the particle (head-on collision in the direction x with a front of velocity U) in the observer's reference frame (E, p_x) and the the wave's reference frame (E', p'_x) where through the Lorentz transformations we have

$$E' = \gamma(E + Up_x) \qquad ; \qquad p'_x = \gamma(p_x + \frac{U}{c}E) \quad . \tag{7.38}$$

If the collision is elastic, the y and z components are conserved and $E \to E'$, $p_x \to -p_x$.
In the reference frame of the observer, the energy is obtained by inverting Eq. 7.38: $E = \gamma(E' - Up'_x)$ and in the same frame, after the collision, the energy is

$$E^* = \gamma[E' - U(-p'_x)] = \gamma\left[\gamma(E + Up_x) + U\gamma(p_x + \frac{U}{c^2}E)\right] \quad . \tag{7.39}$$

Condidering polar coordinates, $p_x = mv\gamma\cos\theta$ and using $E = mc^2\gamma$

$$\frac{p_x}{E} = \frac{v}{c^2}\cos\theta \quad . \tag{7.40}$$

Using the last expression in Eq. 7.39 we have

$$E^* = \gamma^2 E\left[1 + 2U\frac{v\cos\theta}{c^2} + \frac{U^2}{c^2}\right] \quad . \tag{7.41}$$

Using now the approximation $\gamma^2 = 1/[1 - (U/c)^2] \approx 1 + (U/c)^2$, up to second order the energy is

$$E^* \approx E\left[1 + 2U\frac{v\cos\theta}{c^2} + 2\frac{U^2}{c^2}\right] \quad . \tag{7.42}$$

The energy gain is $\Delta E = E^* - E$. When averaging over all the directions, the $\cos\theta$ term is zero, since energy is gained with head-on collisions $\cos\theta > 0$ and lost in the other case with $\cos\theta < 0$. In this averaged case, $\Delta E \approx 2E(U/c)^2$, which is a second-order effect in agreement with the Fermi acceleration of the previous section. In the shock-wave case, we have to consider only head-on collisions. Assuming further $U/c \ll 1$ and $v \sim c$:

$$\Delta E = 2E\frac{U\cos\theta}{c} \quad ; \quad E^* = E + 2E\frac{U}{c}\cos\theta \quad . \tag{7.43}$$

Remembering that the average of a quantity x distributed like $f(x)$ is $\langle x\rangle = \int xf(x)dx / \int f(x)dx$, assuming only head-on collisions ($\cos\theta > 0$) and integrating over all the angles $d\Omega = \cos\theta d\theta d\phi$ with $f(x)$ given by Eq. 7.43

$$\langle\cos\theta\rangle = \frac{\int \cos^3\theta d\theta d\phi}{\int \cos\theta d\theta d\phi} = \frac{2}{3} \quad , \tag{7.44}$$

and therefore

$$\Delta E = \frac{4E}{3}\frac{U\cos\theta}{c} \quad . \tag{7.45}$$

In this case, the cloud velocity appears at first order: this is the difference between a stochastic mechanism like the second-order one, and a head-on collisions only mechanism, which is more efficient.
It is interesting to note, that the first-order acceleration mechanism can also be obtained considering only "f_1"-type collisions in the second order mechanism (see Eq. 7.35):

$$\frac{\Delta E}{\Delta t} = f_1\Delta E_1 = 4\frac{U}{v}E\frac{U+v}{l} \approx 4\frac{U}{l}E = \frac{E}{\tau_{F1}} \quad , \tag{7.46}$$

where we used $v \sim c \gg U$ and we define τ_{F1} as the characteristic time of the first order acceleration mechanism. By comparison with the time obtained for the second-order mechanism, that we call now τ_{F2} we have the relation

$$\tau_{F1} = \frac{l}{4U} = \frac{2U}{c}\tau_{F2} \quad . \tag{7.47}$$

The really interesting feature of the first-order Fermi mechanism, is its ability to reproduce the correct spectral index for the CR spectrum.

7.7 Supernovae as Sources of Shock Waves

Very massive stars (with masses exceeding about 8 solar masses) undergo a *core collapse*, becoming Type II supernovae. Nuclear fusion can counteract the gravitational force up to the systhesis of iron. After that, no more exothermic fusion reactions are energetically allowed and the star collapses. The compression induced by the collapse forces electrons to combine with protons producing neutrons and neutrinos. The infalling material in the outer layers of the stars, when reaching the neutron core bounches back, producing a shock wave (the supernova explosion). About 99% of the energy is emitted as neutrinos, while 1% is contained in the shock wave and composed by other material. A 10-solar masses supernova (M_{SN}) weights about 2×10^{34} g which translate in a gravitational energy of $\sim 2 \times 10^{53}$ erg. Considering 1% of the gravitational energy, the the kinetic energy of a shock wave would be $K \sim 2 \times 10^{51}$ erg. With the last number, we can estimate the speed of the wave

$$U \approx \sqrt{\frac{2K}{M_{SN}}} = \sqrt{\frac{4 \times 10^{51}}{2 \times 10^{34}}} \approx 5 \times 10^{8} \text{ cm/s} \Rightarrow \frac{U}{c} \approx 2 \times 10^{-2} \quad . \tag{7.48}$$

The last result shows that the wave is non-relativistic, but the velocity is still much larger than typical velocities of the interstellar medium.
As the wave expands roughly spherically, its density ρ_W diminishes: the wave will stop when its density will be comparable to the interstellar medium one $\rho_{ISM} \sim 1.6 \times 10^{-24}$ g/cm^3 (about 1 proton per cm^3):

$$\rho_W = \frac{M_{SN}}{\frac{4}{3}\pi R_W^3} = \rho_{ISM} \tag{7.49}$$

From the last condition, we can extract the radius of the shock wave R_W

$$R_W = \left(\frac{3 \times M_{SN}}{4\pi\rho_{ISM}}\right)^{1/3} = \left(\frac{6 \times 10^{34}}{4\pi \cdot 1.6 \times 10^{-24}}\right)^{1/3} \approx 1.4 \times 10^{19}\text{cm} = 5 \text{ pc} \quad . \tag{7.50}$$

Wave maximum radius and velocity (assuming it constant) allow the estimation of the time T_W during which particles can be accelerated

$$T_W = \frac{R_W}{U} = \frac{1.4 \times 10^{19}\text{cm}}{3 \times 10^{8}\text{cm/s}} \approx 3 \times 10^{10}\text{s} \approx 10^3 \ y \quad . \tag{7.51}$$

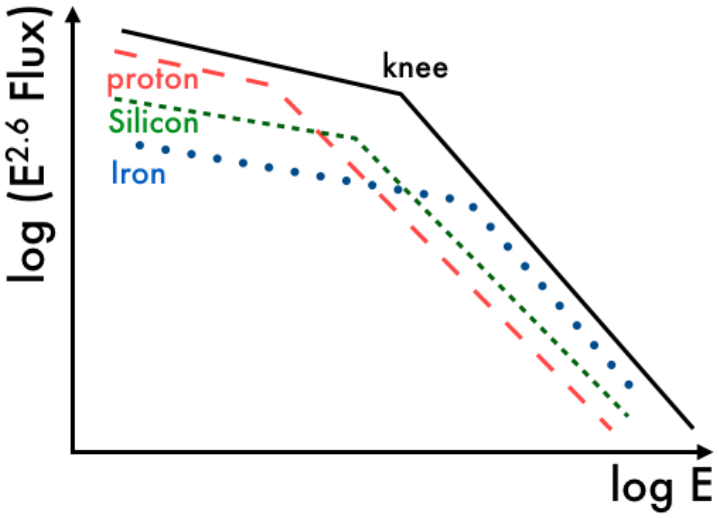

Figure 7.8: Correlation between Z and the cosmic ray energy and how it contributes to the creation of the knee effect in the CR flux.

A supernova can accelerate particles during a period of the order of 1000 years, while, as calculated before, CRs have a galactic escape time of the order of ten million years: this means that supernova explosions actively fill the galaxy with CRs.
As a side-note, it is worth noting that the average distance between stars in the galaxy is of the order O(1 pc), which fits with the estimated maximum radius of supernova explosions.

7.8 The Knee

The origin of the knee is still debated but there are some observations which can explain it. We start estimating the gyroradius of a proton in the magnetic field B of the galaxy. Equating magnetic force to centripetal force

$$qBv = m\frac{v^2}{R} \Rightarrow R = \frac{mv}{qB} \quad . \tag{7.52}$$

The same quantity, taking into account relativity is

$$R = \frac{mv\gamma}{qB} = \frac{\gamma mc^2 \frac{v}{c}}{qB} = 3.3 \frac{\frac{\gamma mc^2}{\text{GeV}} \frac{v}{c}}{\frac{q}{e} \frac{B}{\text{T}}} \quad . \tag{7.53}$$

The last expression in GeV/Tesla units is very common in accelerator physics and v is the orthogonal component of the velocity with respect to the motion.
Considering a mean galactic magnetic field of 10^{-10} T, we can evaluate the gyroradius at the knee energy $\sim 10^{15}$ eV for a proton with $v \sim c$, obtaining

$$R \sim 10^{16} \text{ m} \quad , \tag{7.54}$$

which is of the same order of our galactic spiral arm. Energetic events after the knee can thus be due to some powerful sources near us.
Another explanation can be the inefficiency of the galaxy (due to its magnetic field) to confine CRs with energies larger than the knee one.
Another explanation for the knee, or at least, a contribution to it, is the correlation between energy and nuclear charge. To see this, we have first to estimate the maximum CR energy achievable by the acceleration mechanisms. Recalling the result of the first order Fermi mechanism $\langle \Delta E \rangle = 4U/(3c)\langle E \rangle = \eta E$, we can estimate

$$\frac{dE}{dt} \approx \frac{\eta E}{T_{acc}} \quad , \tag{7.55}$$

where T_{acc} is the typical time between two successive accelerations, which we have to estimate. The typical size of the confinement region around the shock wave is given by the Larmor radius $r_L = E/(ZeB)$. If we consider the shock velocity U, we have $T_{acc} \approx r_L/U$. Inserting in Eq. 7.55, we have

$$\frac{dE}{dt} \approx \eta ZeBU \quad . \tag{7.56}$$

In the following we approximate further $\eta \approx U/c$. The maximum energy a particle can obtain is dE/dt times the acceleration time T_W we estimated before in Eq. 7.51:

$$E_{max} \approx \frac{dE}{dt} T_W = \eta ZeBR_W \approx \frac{ZeBR_W U}{c} \quad . \tag{7.57}$$

For a proton and a galactic magnetic field of 4×10^{-6} G we can roughly estimate

$$\begin{aligned} &E_{max} = \\ &(e = 4.8 \times 10^{-10}) \cdot (B = 4 \times 10^{-6}) \cdot (\tfrac{U}{c} = 2 \times 10^{-2}) \cdot (1.4 \times 10^{19}) \cdot Z \\ &\approx Z \cdot 300 \text{ TeV} \quad . \end{aligned} \tag{7.58}$$

We showed that the maximum energy depends from the the CR particle charge: a nucleus can obtain a higher energy than a proton. There is some evidence that indeed higher energy CRs have higher mass. The correlation between E and Z in forming the knee is sketched in Fig 7.8.

7.9 After the Knee

If we would like to say something about CRs after the knee, we have to find stronger acceleration mechanisms (or stronger astrophysical sources). Let's try first to understand what is the maximum energy of a particle in the proximity of an astrophysical object with a very strong rotating magnetic field, like a pulsar, for example.
Let's start with estimating the power P (energy per unit time) needed for keeping the present level of CRs above an energy E_{CR} in the galaxy

$$P(> E_{CR}) = \frac{\rho_{CR} \cdot V_G}{\tau_{esc}(> E_{CR})} \quad , \tag{7.59}$$

where V_G is the galactic volume, τ_{esc} is the escape time (or the time the CR remains in the galaxy), and ρ_{CR} is the CR energy density in the galaxy. The energy density can be estimated using the integral of the CR spectrum above the knee, which is approximately given by

$$\Phi(> E) \approx 2.2 \times 10^{-10} \left(\frac{E}{1 \text{ PeV}}\right)^{-2.06} \frac{\text{parts.}}{\text{cm}^2 \text{ s sr}} \quad , \tag{7.60}$$

integrating the experimental data: $\rho_{CR} = (4\pi/c) \int \Phi(> E) dE$. The escape time is estimated to be

$$\begin{aligned} &\tau \sim 2.5 \times 10^5 \left(\tfrac{E}{1 \text{ TeV}}\right)^{-0.13} y \quad \text{for} \quad 1 < E < 5 \times 10^3 \text{ TeV} \\ &\tau \sim 0.8 \times 10^5 \left(\tfrac{E}{5 \text{ PeV}}\right)^{-0.53} y \quad \text{for} \quad E > 5 \times 10^3 \text{ TeV} \quad . \end{aligned} \tag{7.61}$$

Taking now a galactic volume $V \sim 6 \times 10^{66}$ cm^3, Eq. 7.60, and Eq. 7.61 we can estimate

$$P(> E_{CR}) \approx \begin{array}{lll} 2 \times 10^{39} \text{ erg.s} & \text{for} & E > 100 \text{ TeV} \\ 2 \times 10^{38} \text{ erg.s} & \text{for} & E > 1 \text{ PeV} \\ 5 \times 10^{37} \text{ erg.s} & \text{for} & E > 10 \text{ PeV} \end{array} \quad . \tag{7.62}$$

The conclusion is that the power needed for accelerating particles at energies above the knee is about 3 orders of magnitude smaller than the power contained in the whole CR spectrum. This means that even few very powerful sources within our galaxy can be relevant in explaining these high-energy CRs: the problem is to find them!

7.10 Can be a (binary) pulsar a candidate source for high-energy cosmic rays?

A pulsar, with its rapidly rotating intense magnetic field, can be a good candidate for CRs beyond the knee. We can try to estimate what is the maximum energy a particle can obtain if accelerated by a typical pulsar. The magnetic field B of a pulsar is not aligned with its angular momentum vector thus the rapid rotation of the magnetic field vector produces an electric field $\mathcal{E}$, which can be estimated from Faraday's law

$$\frac{\mathcal{E}}{L} = \frac{1}{c}\frac{dB}{dt} \quad , \tag{7.63}$$

where the line integral is approximated with the typical lenght L. In order to estimate the maximum energy E_{max}, we can take $L = R_P$ where R_P is the pulsar radius

$$E_{max} = \int eZ\mathcal{E}dx = \int eZ\frac{L}{c}\frac{dB}{dt}dx = \frac{e}{c}ZR_P B\omega_P R_P \quad , \tag{7.64}$$

where ω_P is the rotation angular velocity. Considering a typical radius of 10 km, a magnetic field of 10^{11} Gauss, and a proton as accelerated particle near the surface of the pulsar rotating at the angular velocity of the Crab nebula one ($\omega \sim 60\pi$/s) we obtain

$$E_{max} \approx 3 \times 10^3 \text{ PeV} \quad . \tag{7.65}$$

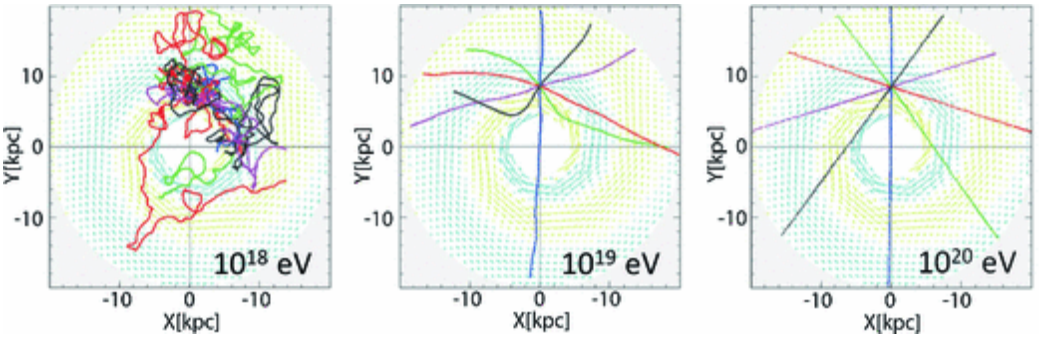

Figure 7.9: Simulation of the propagation of CRs through the galactic magnetic fields for different CR energies. In the rightmost panel, particles above 10^{20} eV propagate almost on straight paths (from T. Ebisuzaki).

The obtained energy is very high, and hints towards the possibility that pulsars are good candidate sources of very high-energy cosmic rays beyond the knee.
Pulsars, neutron stars or balck holes can be present in binary systems. These compact objects attract material from the companion star: this material spirals towards the compact object and emits electromagnetic radiation and particles. Also in such systems, an estimate similar to the one we performed above leads to accelerations up to O(10^3) PeV, therefore they are other candidates for high-energy CRs.

7.11 Ultra-High Energy Cosmic Rays

CRs above $\sim 10^{18}$ eV = 10^3 PeV are usually called Ultra-High Energy Cosmic Rays (UHECR). Looking at the CR spectrum, UHECRs form the *ankle* energy region. In the previous section we have seen that CRs up to the ankle can in priciple be created by compact astrophysical objects with intense rotating magnetic fields. CRs with even high energies must have extra-galactic origin, since their Larmor radius is very large and we do not measure any anisotropy in their distribution.
Expressing the Larmor radius in "galactic" units we have

$$r_L = 110 \text{ kpc } \frac{1}{Z}\left(\frac{\mu G}{B}\right) \cdot \left(\frac{E}{10^{20}\text{eV}}\right) \quad , \tag{7.66}$$

from which we can calculate the approximate angular deflection for a particle after travelling a distance d

$$\theta \approx \frac{d}{r_L} \approx 0.5^\circ Z \left(\frac{10^{20}\text{eV}}{E}\right) \cdot \left(\frac{d}{\text{kpc}}\right) \cdot \left(\frac{B}{\mu G}\right) \quad . \tag{7.67}$$

The last formula shows that for an UHECR proton (Z=1), the deviation is within few degrees. This estimation is made more concrete in Fig. 7.9, where simulated CR trajectories for different energies are shown: if UHECR were produced within the galaxy from powerful sources, we should have detected an anisotropy in their distribution. Since the anisotropy is not present in the data, UHECRs should come from extra-galactic sources.
The latter considerations move our attention to extra-galactic magnetic fields. These fields are poorly known: the current data comes from Faraday rotation measurements in galaxy clusters where synchrotron radiation is emitted. These measuremets place extra-galactic magnetic fields in the 0.1–1 μG region.

7.12 The GZK Effect

In 1966 K. Greisen, V. Kuzmin, and G. Zatsepin independently studied a new effect UHECRs should undergo. This effect was named "GZK effect" after them and it has to do with the interaction of UHECRs with the cosmic microwave background (CMB).
The prediction of GZK is that proton CRs will be strongly attenuated after an energy

$$E_{GZK} \sim 5 \times 10^{19} \text{ eV} = 5 \times 10^4 \text{ PeV} \quad , \tag{7.68}$$

while nuclei with mass A will be attenuated after an energy $A \cdot E_{GZK}$.
This cut-off energy arises because of the interaction of CRs with the CMB photons:

$$p^+\gamma \to \Delta^+ \to \pi^+ n \text{ (or } \pi^0 p \text{)} \quad . \tag{7.69}$$

Neutral pions futher decay as $\pi^0 \to \gamma\gamma$, charged pions as $\pi^\pm \to \mu^\pm \nu_\mu(\bar{\nu}_\mu)$, and neutrons as $n \to pe^-\bar{\nu}_e$.
In the final state of the GZK reaction there is always a proton, although it lost part of its energy. Another result of the process is the production of

high-energy photons and neutrinos.
The Δ-resonance has mass $m_\Delta = 1232\ MeV$. If the initial four-vectors of the proton and the photon are $p_p = (E_p, p_p)$ and $p_\gamma = (E_\gamma, p_\gamma)$, in order to excite the resonance the condition is

$$s = (p_p + p_\gamma)^2 = m_\Delta^2 \quad \Rightarrow \quad m_p^2 + 2E_pE_\gamma - 2p_p \cdot p_\gamma = m_\Delta \quad . \tag{7.70}$$

For a photon $|p_\gamma| = E_\gamma$ (c=1) and at high energy $|p_p| \approx E_p$ and the last equation becomes

$$E_p = \frac{m_\Delta^2 - m_p^2}{2E_\gamma(1 - \cos\theta)} \quad . \tag{7.71}$$

Considering the minimum possible value of E_p, which happens at $\theta = \pi$ and taking the average CMB photon energy $E_\gamma \sim 1.2 \cdot 10^{-3}$ eV we have the estimate

$$E_p = 1.2 \times 10^{20} \text{ eV} \quad . \tag{7.72}$$

The GZK effect starts to become significant at the slightly lower energy quoted at the beginning of the section, but the estimate is quite close: this happens because protons start to interact already with the high-energy tail of the CMB spectrum.
The energy loss of the protons per interaction can be estimated noting that there is a pion in all the final states and thus

$$y = \frac{\Delta E_p}{E} \sim \frac{m_\pi}{m_p} \sim 0.1 \quad . \tag{7.73}$$

The last result tells us that protons loose about 10% of their energy after each interaction.
We can now try to calculate the *energy loss length* $\lambda = 1/(y \cdot \sigma \cdot n)$, where $\sigma = 250\mu b$ is the $p\gamma$ cross section and $n \sim 400/\text{cm}^3$ is the CMB photon density:

$$\lambda = \frac{1}{0.1 \cdot 250 \times 10^{-30} \cdot 400} = 10^{26} \text{ cm} = 30 \text{ Mpc} \quad . \tag{7.74}$$

The last result tells us that protons produced at distances larger than about 30 Mpc should arrive on Earth with an energy $E < E_{GZK} \sim 10^{20}$ eV. The obtained distance corresponds roughly to the closest galaxy cluster (the Virgo cluster) and we cannot receive information through CRs from

sources which are farer than that.
As last comment, in the case of nuclei with mass number A and energy E, the photon interacts with a proton inside them: if we consider therefore the proton energy $E_p = E/A$ we arrive at a GZK cutoff which is higher by a factor A.

Chapter 8 | The Gamma Ray Sky

Gamma rays are an important tool for looking at the sky. Since they are neutral, they are not deviated by magnetic fields and thus observing them we can "point" directly to their sources. The latter advantage is shared also by neutrinos.
Gamma rays are produced by a large variety of astrophysical sources and by interactions of CRs with the interstellar medium.
After initial experiments on earth, real fundamental advancement in this field came with the launch of satellites like Swift (2004), AGILE (2007), and the latest Fermi-LAT mission (2008). The measurement of high-energy gamma rays implies the use of particle physics technology for the detectors mounted on the satellites.
Satellites can observe the sky in the multi-GeV range but since they are limited in weight, it is not possible to mount detectors able to go to higher energies. A new method for observing the gamma ray sky in the TeV range is to use ground-based experimens and optical techniques which are able to see Cherenkov light induced by high-energy gamma rays.

8.1 Hadronic Sources

The presence of high-energy protons can lead to gamma-ray production through hadronic mechanisms. In particular, proton-proton collisions can produce a variety of hadrons: $p + p \rightarrow p, n, \pi^{\pm}, \pi^0, K^{\pm}, K^0, ...$
The decay of neutral kaons then produces gamma rays, like for example $\pi^0 \rightarrow \gamma\gamma$. A second mechanism is photoproduction (like in the GZK effect case): $p + \gamma \rightarrow \Delta^+ \rightarrow \pi^+(\pi^0) + n(p)$.
The $p + p$ process cross section is about 100 times larger than photoproduction, thus it is also the relevant gamma production mechanism.

We can now estimate one of the most relevant components of gamma production: the neutral pion decay. From $\pi^0 \to \gamma\gamma$, the energy of the photons in the center of mass (*) is

$$E^*_\gamma = \frac{1}{2} m_\pi c^2 = 67.5 \text{ MeV} \quad , \tag{8.1}$$

and the momenta have opposite directions. Since the pion has spin zero, the angular gamma distribution is uniform and $dN/d\Omega^* = 1/4\pi$.
Moving now to the laboratory system, the pion has a boost described by $\beta = |p_\pi|/E_\pi$ and $\Gamma = E_\pi/m_\pi$:

$$E_\gamma = \Gamma E^*_\gamma + \beta\Gamma p^*_\gamma \cos\theta^* \Rightarrow E_\gamma = \frac{E_\pi}{2}(1 + \beta\cos\theta^*) \quad , \tag{8.2}$$

where we used $p^*_\gamma = E^*_\gamma$ and $E^*_\gamma = m_\pi/2$. Differentiating the last equation

$$dE_\gamma = \beta\Gamma p^*_\gamma d\cos\theta^* \Rightarrow \frac{d\cos\theta^*}{dE_\gamma} = \frac{1}{\beta\Gamma E^*_\gamma} \quad . \tag{8.3}$$

We can now calculate the differential cross section in energy

$$\frac{dN}{dE_\gamma} = \frac{dN}{d\cos\theta^*}\frac{d\cos\theta^*}{dE_\gamma} = \frac{1}{2}\frac{1}{\beta\Gamma p^*_\gamma} \quad . \tag{8.4}$$

Depending on the emission angle, E_γ can range from $E_{min} = \frac{E_\pi}{2}(1-\beta)$ to $E_{max} = \frac{E_\pi}{2}(1+\beta)$: in this range the photon emission probability with energy E_γ is the same, since the cross section is constant.
Since the emission probability is constant and the spectrum of accelerated protons scales as $1/E^2$, if we represent photon emission in a plot of $E^2_\gamma dN_\gamma/dE_\gamma$ as a function of the energy, we should see a flat distribution. This is indeed what is observed: a steep rise at about $E_\gamma = 200$ MeV and then a flat distribution. This feature in gamma spectra is known as the "pion bump" (see Fig. 8.1).

8.2 Leptonic Sources

The model of photon emission through electrons/positrons is called SSC, or Self-Synchrotron Compton mechanism. The idea is that electrons in

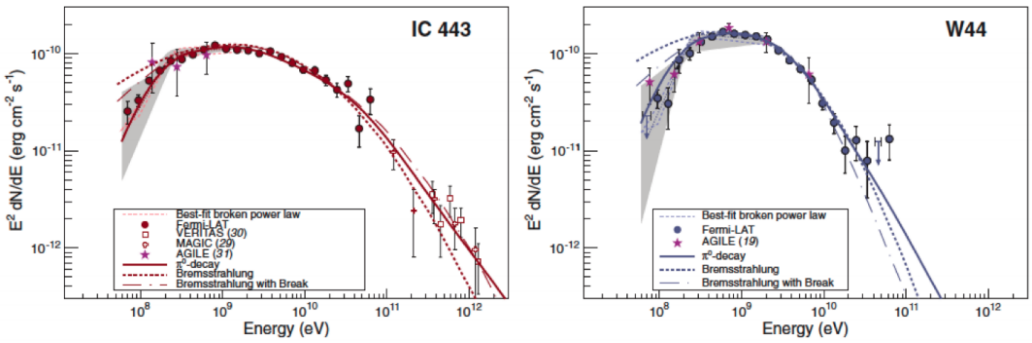

Figure 8.1: Pion bump detected by the Fermi-LAT satellite in the direction of two different supernova remnants.

strong magnetic fields emit synchrotron radiation. This radiation is usually in the infrared up to the X-ray band (see Fig. 8.2). The energy loss rate due to synchrotron radiation is described by

$$-\frac{dE}{dt} = \frac{4}{3}\sigma_T c \rho_B \Gamma^2 \quad , \tag{8.5}$$

where $\rho_B = B^2/8\pi$ is the magnetic energy density, $\Gamma = E_e/m_e$ the electron boost factor, and

$$\sigma_T = \frac{8\pi r_e^2}{3} = \frac{8\pi e^2}{3 m_e^2 c^4} \approx 0.66 \cdot 10^{-24}\text{cm}^2 \quad , \tag{8.6}$$

is the Thomson cross section which was re-expressed using the classical electron radius $r_e = e^2/(m_e c^2)$. The Thomas cross-section describes the scattering of photons on charged particles and can be viewed as an approximation to the Compton cross section.
Further electrons can hit the synchrotron photons and through inverse-Compton scattering they can be pushed into the gamma band.
The energy loss of inverse Compton scattering electrons against a "cloud" of photons can be described by

$$-\frac{dE}{dt} \sim \frac{4}{3}\sigma_T c \rho_{rad} \Gamma^2 \quad , \tag{8.7}$$

where ρ_{rad} is the energy density of the photon field and the approximation $\Gamma\epsilon \ll m_e c^2$ was used (ϵ is the average photon energy). Note the

formal similarity between Eq. 8.5 and Eq. 8.7: it stems from the similarity of the two processes which are based on an energy loss due to the presence of an energy density. In one case it is due to photons, and in the other one is a magnetic field.
The inverse Compton scattering energy spectrum is instead

$$E_\gamma^2 \frac{dN_\gamma}{dE_\gamma} \sim E_\gamma \quad , \tag{8.8}$$

which is consistent with observations (see Fig. 8.2).
For having an idea about how much photons can gain energy through this mechanism, calculations show that IR photons (galaxies produce a large quantity of them) can be pushed into the optical (eV) frequency range, while optical photons can be pushed into the X-ray band (keV energy range) up to the gamma band (MeV range).
Synchrotron radiation and inverse Compton scattering are strongly correlated, since e.g. if one process increases, also the other one increases. Using Eqs. 8.5 and Eq. 8.7 we can write

$$\frac{(dE/dt)_{iCS}}{(dE/dt)_{sync}} = \frac{\rho_{rad}}{\rho_B} \quad . \tag{8.9}$$

The last formula shows that with X-ray/Gamma-ray observations we can infer informations about the magnetic fields and the photon density. In practice, numerical simulations are used for describing the measured photon spectrum. An example of observations carried out with the gamma-ray satellite Fermi-LAT is showed in Fig. 8.3.

8.3 The 511 keV Line

A very important gamma line in astrophysical spectroscopy is the 511 keV line resulting from the annihilation process

$$e^+e^- \rightarrow \gamma\gamma \quad , \tag{8.10}$$

where two photons are produced, each with an energy equal to the rest-mass of the electron (or positron) $m_e = 0.511$ MeV.
A strong 511 line can be emitted for example in the surroundings of a

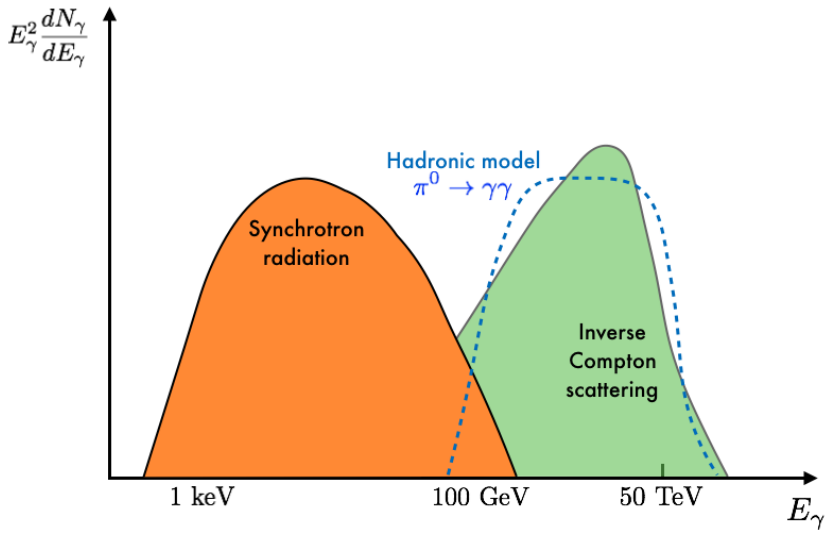

Figure 8.2: Schematic representation of the main characteristics of the gamma spectrum. Synchrotron emission starts at very low energies producing photons at the astrophysical site (organce shaded spectrum). Proton interactions generate mesons which decay into photons: the spectrum for these processes is dominated by the "pion bump" (dashed blue line). Synchrotron photons constitute targets for high-energy electrons, which by inverse Compton scattering produce high-energy photons (green shaded spectrum).

black hole, where an accretion disk is present. For example, the galactic center is a strong 511 emitter and we think that a super-massive black hole is responsible for this signal. Indeed, an intense radio-source accompanied by 511 emission in its surroundings was identifyed very close to the galactic center: Sagittarius A* (Sgt A*).
Sgt A* is a super-massive black hole (millions of solar masses) with many stars orbiting it.
The Doppler effect can broaden the 511 line giving information about the speed of the emitting object (e.g. gas clouds) around the astrophysical site. 511 gamma rays emitted from the interstellar medium have quite sharp lines.
Another interesting object is $1E1740.7 - 2942$, also called the "Great Annihilator", which is a microquasar located near the center center of our

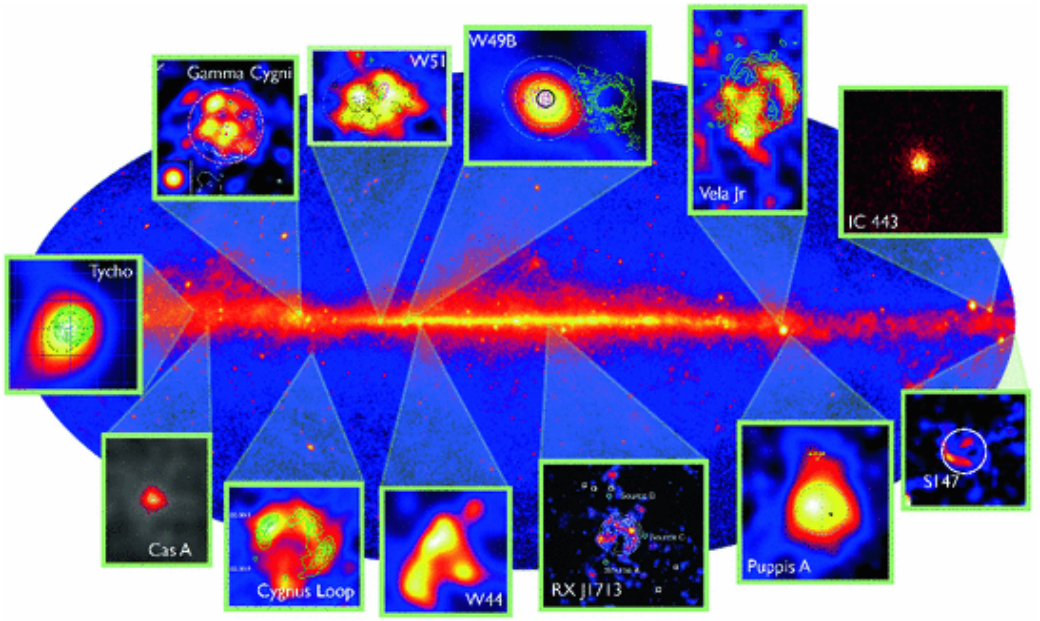

Figure 8.3: Position of supernova remnants from observations of the gamma-ray sky by the Fermi-LAT satellite. The long bright central region corresponds to the galactic plane.

galaxy. The great annihilator is a binary system composed by a black hole and a companion star. It is one of the brightest X-ray sources in the region around the galactic center and also a strong 511 emitter. The emitted 511 gamma flux has strong time variability.

8.4 The Crab Nebula

In 1054 chinese astronomers noted the appearence of what today we know it was a supernova. Today, in the place of the explosion we observe a nebula (the Crab nebula) formed by the ejected material from the supernova. At the center of the nebula, there is a pulsar (PSR 0531+21) with rotation period 0.0332 s. This pulsar is also the first discovered pulsar ever and we observe it at various wavelenghts bands, one of which is the gamma one (see also Fig. 8.4).

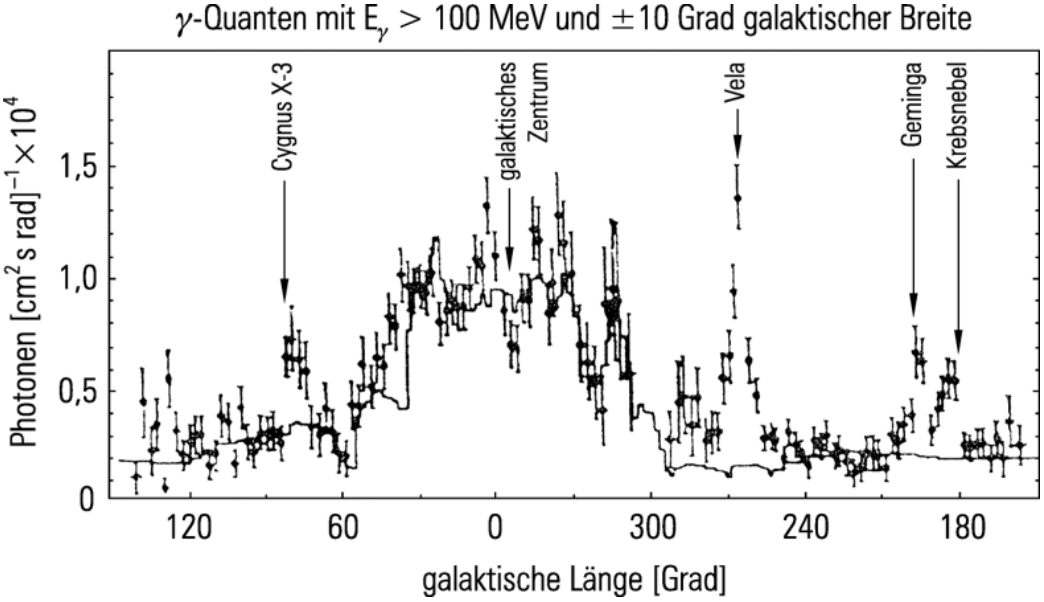

Figure 8.4: Strong gamma sources in our Galaxy. The photon flux is histogrammed as a function of the galactic plane coordinate.

8.5 An interesting gamma source: Geminga

Geminga, or Gemini-Gamma-Ray, is one of the first strong gamma sources identified (Fig. 8.4). The discovery happened in 1975 by the satellite mission SAS-2.
The clarification of the nature of this object came only in 1991: Geminga is a pulsar with rotation period of 0.237 s. Its identification was difficult, since pulsars are intense radio-sources, while Geminga is radio-quiet, having instead strong emission in the X and gamma bands.
This pulsar is "only" 800 ly away from us and it is believed to contribute significantly to the positron CR flux we measure from Earth (or its orbit with satellites like AMS-02).

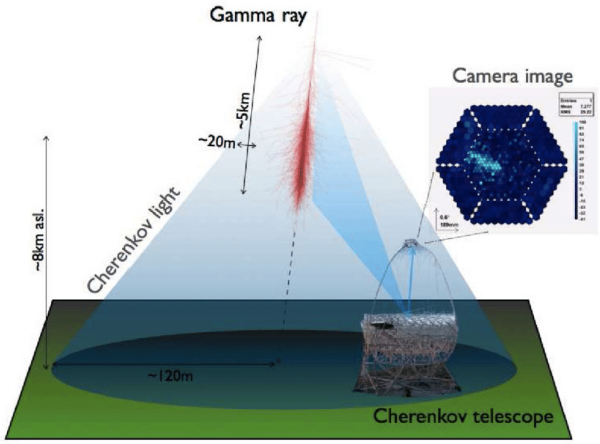

Figure 8.5: Working principle of the Imaging Atmospheric Cherenkov Telescope (IACT) (Figure from: N. Sidro)

8.6 Gamma ray bursts

A quite new observed phenomenon is the appearance of gamma-ray bursts (GRBs). GRBs are very bright gamma-ray emissions which last for about 10 ms to 100 s in the 10 keV-100 MeV energy range with an intensity following approximately

$$I(>E) \sim 7 \cdot \frac{E^{-1.25}}{\text{MeV}} \text{cm}^{-2}\text{s}^{-1} \quad . \tag{8.11}$$

GRBs are observed in distant galaxies and are the brightest (but short in time) sources of gamma rays. The emission is concentrated in time, followed by a characteristic "after-glow" of increasing wavelenght.
The origin of these high-energy events is still not known but the most probable explanation are the birth of a black-hole or neutron star, or neutron-star mergers. GRBs are very bright, even if billions of ly far away: estimates point toward an emitted energy in few seconds comparable to the total energy emitted by the Sun in its entire life.
No GRBs within our galaxy were observed yet.

8.7 The "TeV Sky"

Satellites are very effective in detecting gamma rays, avoiding atmospheric absorption. However, they can cover a limited acceptance, given the weight limits set by current launch vehicles. This is an issue in the case we would like to detect very high-energy events, which are also more rare. For example, the most recent satellite mission, Fermi-LAT, has a surface of the order of ~ 6 m^2 and it is quite effective in the ~ 100 GeV range. For observing photons in the TeV range, a different technique has to be developed.
The idea is to build ground-based experiments, which can be much larger than satellite ones and use the fact that such high-energy photons can enter the atmosphere inducing extended showers. In fact, these experiments will use the atmosphere as detection medium.
The technique is based on Imaging Atmospheric Cherenkov Telescopes (IACTs). More IACTs work together realizing a stereoscopic reconstruction using the Cherenkov light produced by the high-energy shower. A IACT is composed by a large reflector (~ 10 m^2) which concentrates the light on a light sensor (a pixelized camera, like an array of photomultipliers). Such arrangements are sensitive to energies on the O(10 TeV) range. The energy threshold for a IACT is

$$E_{th} = \frac{\sqrt{\Phi \Omega \tau}}{\epsilon A} \quad , \tag{8.12}$$

where Φ is the photon flux, Ω the solid angle, τ the energy integration time, ϵ the efficiency, and A the mirror surface.
The light collected by IACTs is very dim: that's why observations can be made only with clear skies and not during the day: IACTs are installed in areas where th weather allows such conditions for a large part of the year.
The speed of light in atmosphere is

$$c = \frac{c_0}{c} = 299710637 \text{ m/s} \tag{8.13}$$

where c_0 is the speed of light in vacuum and $n = 1.000273$ is the air refraction index at standard conditions (temperature T=20°, pressure 1 atm).

Such speed is obtained by an electron with kinetic energy

$$E_{kin} = E_{tot} - m_0c^2 = \gamma m_0c^2 - m_0c^2 = \left(\frac{n}{\sqrt{n^2-1}}\right) - 1 \approx 21.36 \text{ MeV} \quad . \tag{8.14}$$

The obtained energy is the threshold energy for an electron in atmosphere for emitting Cherenkov light. The Cherenkov light is emitted in a cone with opening angle

$$\theta = \frac{1}{n\beta} \quad , \tag{8.15}$$

and for a multi-GeV energy photon this means $\theta \sim 1^\circ$.

Chapter 9 | Neutrino Astronomy

9.1 Neutrino Basics

Neutrinos are embedded in the SM as massless particles with a definite helicity state. However, the discovery of neutrino oscillations implies that at least two of them must have a non-zero mass. Massive neutrinos imply that the flavour $\nu_{e,\mu,\tau}$ and mass eigenstates $\nu_{1,2,3}$ are different, like in the case of quarks. These states are related by a unitary mixing matrix: the Pontecorvo-Maki-Nakagawa-Sakata Matrix (PMNS), see Fig. 9.1) U:

$$\begin{pmatrix} \nu_e \\ \nu_\mu \\ \nu_\tau \end{pmatrix} = \begin{pmatrix} U_{e1} & U_{e2} & U_{e3} \\ U_{\mu 1} & U_{\mu 2} & U_{\mu 3} \\ U_{\tau 1} & U_{\tau 2} & U_{\tau 3} \end{pmatrix} \begin{pmatrix} \nu_1 \\ \nu_2 \\ \nu_3 \end{pmatrix} \quad . \tag{9.1}$$

Neutrino mixing gives rise to the neutrino oscillation phenomenon, which has been observed experimentally. The probability of the oscillation from a flavour $\alpha = (e, \mu, \tau)$ to a flavour $\beta = (e, \mu, \tau)$ is described by

$$\begin{aligned} &P(\nu_\alpha \to \nu_\beta) = \delta_{\alpha\beta} \\ &-4 \sum_{i>j} \Re(U^*_{\alpha i} U_{\beta i} U_{\alpha j} U^*_{\beta j}) \sin^2[1.27 \cdot \Delta m^2_{ij}(L/E)] \\ &+2 \sum_{i>j} \Im(U^*_{\alpha i} U_{\beta i} U_{\alpha j} U^*_{\beta j}) \sin[2.54 \cdot \Delta m^2_{ij}(L/E)] \quad , \end{aligned} \tag{9.2}$$

where i,j=(1,2,3) label the mass eigenstates, L is the distance in km traveled by the neutrino, and E is its energy in GeV [1].
From the measurement of the oscillation probabilities, the difference of

[1]The km/GeV convention is particularly useful for designing neutrino oscillation experiments. For example, if the neutrino energy is of the order of 1 GeV, $\sin^2 2\theta \sim 0.8$ (assuming only one oscillation parameter in a simplified two-flavour model), and the neutrino mass difference is $\Delta m^2 \sim 3 \cdot 10^{-3}\text{eV}^2$, the maximum oscillation probability will be located at $L \sim 400$ km.

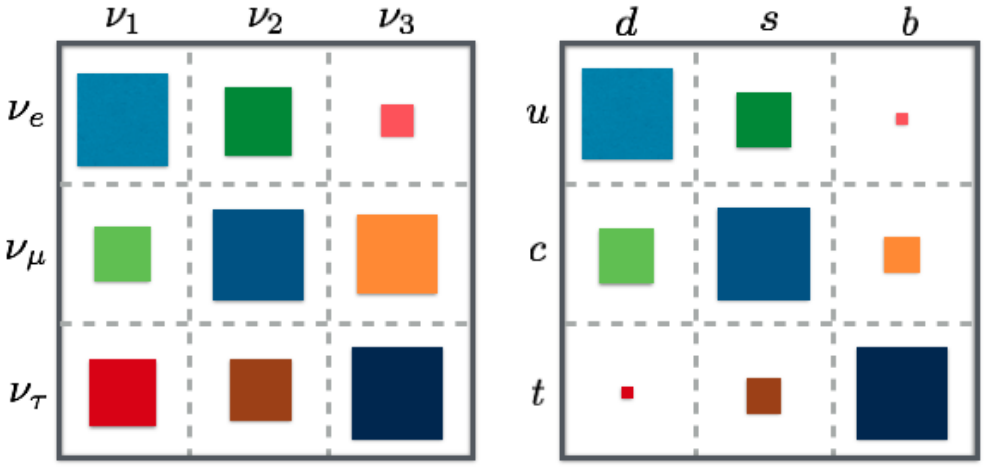

Figure 9.1: **Left:** neutrino mixing matrix elements, **Right:** quark mixing matrix elements. The surface of the squares represents the absolute value of the relative magnitudes of the matrix elements. In the quark CKM matrix a hierarchical pattern can be seen, in contrast to the present knowledge of the neutrino PMNS matrix.

the squared neutrino masses $\Delta m^2_{ij} = m^2_i - m^2_j$ and the mixing angles can be extracted. Oscillation experiments are sensitive to different mixing angles depending on the employed neutrino source. Neutrinos from the sun, the atmosphere, fission reactors or spallation sources at accelerators have been used for investigating neutrino properties.

The PMNS matrix can be conveniently parameterized with three angles $\theta_{12}, \theta_{13}, \theta_{23}$ (defined in the first quadrant $[0, \pi/2]$):

$$U = \underbrace{\begin{pmatrix} c_{12} & s_{12} & 0 \\ -s_{12} & c_{12} & 0 \\ 0 & 0 & 1 \end{pmatrix}}_{\text{Solar Neutrinos}} \underbrace{\begin{pmatrix} c_{13} & 0 & s_{13}e^{-i\delta} \\ 0 & 1 & 0 \\ -s_{13}e^{-i\delta} & 0 & c_{13} \end{pmatrix}}_{\text{Reactor Neutrinos}} \underbrace{\begin{pmatrix} 1 & 0 & 0 \\ 0 & c_{23} & s_{23} \\ 0 & -s_{23} & c_{23} \end{pmatrix}}_{\text{Atmospheric/Accel. Neutrinos}} \underbrace{\begin{pmatrix} 1 & 0 & 0 \\ 0 & e^{i\alpha_1/2} & 0 \\ 0 & 0 & e^{i\alpha_2/2} \end{pmatrix}}_{\text{Majorana Phases}} , \tag{9.3}$$

where $s_{ij} = \sin\theta_{ij}$, $c_{ij} = \cos\theta_{ij}$. For example, in this parameterization, $U_{e1} = \cos\theta_{12}\cos\theta_{13}$ (compare with Eq. 9.1). The most sensitive experiments to the different angles are highlighted under the matrices[2]. Besides

[2]Accelerator experiments can also access the CP phase δ comparing data produced

the angles, there are also three phases δ and $\alpha_{1,2}$ related to the Dirac or Majorana nature of neutrinos.

If neutrinos ψ have Dirac nature, their mass will be described by a term like $m\psi\psi = m(\bar{\psi}_L\psi_R + \bar{\psi}_R\psi_L)$ in the SM lagrangian and the "Dirac phase" δ will describe CP violation in the lepton sector (in analogy with the CKM matrix).
Neutrinos admit another possibility for constructing their mass term. Unlike the other SM fermions, neutrinos carry no electric charge. They still carry lepton and flavour number but these can be violated by BSM physics. If the neutrino does not have conserved quantum numbers, it can be its own antiparticle. In this case neutrinos must be described by Majorana fermions and the only difference between ν and $\bar{\nu}$ is a spin flip. Mathematically, a Majorana neutrino is described by a two-component Weyl spinor instead of a 4-component Dirac spinor. In the case of Majorana neutrinos, two additional phases have to be present: α_1 and α_2 [3]. For Majorana neutrinos, a different mass term is allowed:

$$\mathcal{L}_M = \underbrace{m_D\bar{\nu_L}\nu_R}_{\text{Dirac term}} + \underbrace{\frac{1}{2}m_L\nu_L^T\nu_L + \frac{1}{2}m_R\nu_R^T\nu_R}_{\text{Majorana terms}} + h.c. \quad . \tag{9.4}$$

In the case of a charged lepton (e.g. an electron), the fields e_R and e_L have the same mass, as showed by the Dirac term in Eq. 9.4. For a neutrino, all three terms in Eq. 9.4 are instead in principle allowed. The interesting feature of the two additional Majorana terms is that they induce lepton number violation (LNV). LNV gives rise to new phenomena , like neutrinoless double beta decay of nuclei ($0\nu\beta\beta$, *e.g.* for ^{130}Te, ^{76}Ge, ^{136}Xe) and SM-forbidden $\Delta L = 2$ decays like $B_c^- \to \pi^+\mu^-\mu^+$ or $K^+ \to \pi^+e^-\mu^+$.

Majorana neutrinos have the interesting feature of providing a possible explanation for the smallness of the neutrino mass. Rewriting Eq. 9.4 as

$$\mathcal{L}_M = \frac{1}{2}(\nu_L, \nu_R)\begin{pmatrix} m_L & m_D \\ m_D & m_R \end{pmatrix}\begin{pmatrix} \nu_L \\ \nu_R \end{pmatrix} + h.c. \quad , \tag{9.5}$$

and supposing that ν_R is a very heavy *sterile* neutrino (*i.e.* does not couple to SM forces), diagonalizing the mass matrix we obtain the effective

with neutrino and antineutrino beams.

[3] In the Dirac case, these phases vanish. Neutrino oscillations are influenced only by a linear combination of Majorana phases.

masses

$$\begin{array}{c} M_H \approx m_R \\ M_L \approx m_L - \frac{m_D^2}{m_R} \end{array} \quad , \tag{9.6}$$

where M_H and M_L are the masses of a "heavy" and a "light" state respectively. If $m_L \ll m_D \ll m_R$, then if $m_D \approx 200$ GeV and $m_R \approx 10^{15}$ then $M_L \approx 0.04$ eV, which is close to the mass scale observed for neutrinos. This is the so-called *seesaw mechanism*: if m_R is large, M_H is pushed at high masses while M_L becomes small.
In conclusion, if neutrinos are Majorana particles, there is a possible explanation for their small mass if a very heavy right-handed sterile neutrino is introduced.

9.2 Neutrino Sources and the Waxman-Bahcall Bound

Neutrinos produced at astrophysical sites are produced through hadronic interactions: neutrinos come mainly from meson and muon decays. The observation of a point neutrino source would be an unambiguous proof of the acceleration of hadrons (protons). Neutrinos share the same advantage of photons: they are not sensitive to magnetic fields and thus allow an exact pointing to the source.
A significant high-energy neutrino flux is generically expected from all the high-energy sources like gamma-ray bursts and active galactic nuclei: these sources should be responsible for a diffuse extragalactic neutrino flux.
We would like to calculate now an upper bound to the neutrino flux.
From the data, considering ultra-high energy cosmic rays ($E > 10^{19} eV$), we can calculate the energy density over time

$$E_p^2 \frac{\dot{N}}{dE_p} \sim 10^{44} \frac{\text{erg}}{\text{Mpc}^3 \text{ yr}} \quad . \tag{9.7}$$

We use the factor E_p^2 as it eliminates the dependence of the proton energy spectrum from the Fermi acceleration mechanism, which scales as E^{-2}.
At these energies, neutrino production comes from the interaction of protons with the CMB photons and thus neutrinos come from π^0 decays and

meson/muon decays. Comparing the proton flux with the neutrino flux, we can obtain an upper bound

$$E^2_{\nu_\mu}\frac{dN}{dE_{\mu_\mu}} \approx \frac{1}{4}\epsilon\frac{1}{H_0}E_p^2\frac{\dot{N}}{dE_p} \quad . \tag{9.8}$$

$H_0 \sim 10^{10}$ yrs is the inverse of the Hubble constant and thus a measure of the Universe's age, while ϵ is the fraction of the initial energy going into meson production (through the Δ excitation mechanism). The Hubble constant term is the result of an approximate time integration over the age of the Universe and in the following we assume $\epsilon = 1$ for simplicity. The factor $1/4$ comes from the following two observations:

- The proton energy is about equally split between π^0 and $\pi^\pm$ production.
- In the decay chain $\pi^+ \to \mu^+\nu_\mu \to e^+\bar{\nu}_\mu\nu_e$, there are only two muon neutrinos and here we are considering only the muon neutrino flux.

Substituting the numbers

$$E^2_{\nu_\mu}\frac{dN}{dE_{\mu_\mu}} \sim 1.5\cdot 10^{-8}\frac{\text{GeV}}{\text{cm}^2\cdot s\cdot \text{sr}} \quad . \tag{9.9}$$

The last result constitutes the *Waxman-Bahcall bound*.

9.3 Short Digression: Neutrino freeze-out

We can use what we learned before about early cosmology thermodynamics and freeze-out for determining the freeze-out temperature T_ν of neutrinos during the Universe expansion.
The freeze-out condition is

$$n_\nu\cdot\sigma_\nu = H \quad . \tag{9.10}$$

We can think about the neutrino reactions as $\nu + \bar{\nu} \leftrightarrow f + \bar{f}$ where f is a generic charged fermion. Converting energies in temperatures, electroweak cross sections scale as $\sigma \sim G_F^2T^2$ ($G_F \sim 10^{-5}$ GeV^{-2}). Remembering that in a radiation-dominated Universe $H \sim T^2/M_P$ and $n \sim T^3$:

$$T_\nu^3 G_F^2 T_\nu^2 = \frac{T_\nu^2}{M_P} \Rightarrow T_\nu = \frac{1}{(G_F^2M_P)^{1/3}} \approx 1\text{MeV} \quad . \tag{9.11}$$

The assumption $n \sim T^3$ is valid only relativistically if $T_\nu \gg m_\nu$, which we can now verify *a posteriori*. We also notice that neutrinos from the early Universe are *hot relics*, in the sense that they freeze-out as relativistic particles.

9.4 Solar Neutrinos

Neutrinos coming from the Sun are produced in nuclear reactions. The primary nuclar reactions powering the Sun are together called the *pp-chain* and make up to 98.4% of the produced energy.
The p-p fusion goes mainly through (99.75%)

$$p + p \rightarrow^2 \mathrm{H} + e^+ + \nu_e \quad , \tag{9.12}$$

where the neutrino has an energy < 0.42 MeV. A 0.25% contribution comes from

$$p + p + e^+ \rightarrow^2 \mathrm{H} + \nu_e \quad . \tag{9.13}$$

with a neutrino energy of 1.44 MeV.
The lightest helium isotope is created without neutrino emission:

$$^2\mathrm{H} + p \rightarrow^3 \mathrm{He} + \gamma + 5.49 \text{ MeV} \quad . \tag{9.14}$$

With 86% probability, ^{4}He is created by the following reaction (also without neutrinos)

$$^3\mathrm{H} +^3 \mathrm{He} \rightarrow^4 \mathrm{He} + 2p + 12.86 \text{ MeV} \quad . \tag{9.15}$$

With negligible probability ($\sim 10^{-5}$), a third neutrio could come also from

$$^3\mathrm{He} + p \rightarrow^4 \mathrm{He} + e^+ + \nu_e + 18.77 \text{ MeV} \quad . \tag{9.16}$$

In total, since we need two reactions described by Eq. 9.12 for having two 3^He to fuse, two electron neutrinos are produced up to this point. Neutrinos from Eq. 9.16 are highly energetic, up to 18.77 MeV, although their flux is very small.
The next step is the creation of beryllium

$$^3\mathrm{He} +^4 \mathrm{He} \rightarrow^7 \mathrm{Be} + \gamma + 1.59 \text{ MeV} \quad . \tag{9.17}$$

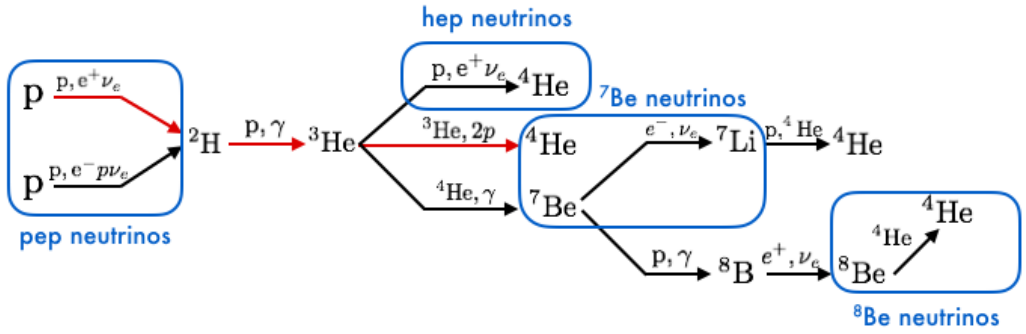

Figure 9.2: The pp-chain reaction which describes the reaction path following proton-proton fusion. The red arrows indicate the most probable reaction path. The blue boxes indicate the important neutrino emission reactions. The ^7Be reaction box is responsible for two neutrino emission lines, depending on the produced nuclear state.

The last reaction branches in two different reactions (the complete picture can be seen in Fig. 9.2):

$$\begin{aligned} &^7\mathrm{Be} + e^- \rightarrow ^7\mathrm{Li} + \nu_e \quad E_\nu = 0.862 \text{ MeV or } 0.384 \text{ MeV} \quad , \\ &^7\mathrm{Be} + p \rightarrow ^8\mathrm{B} + \gamma + 0.14 \text{ MeV} \end{aligned} \tag{9.18}$$

The first reaction can generate neutrinos with two different energies, since ^7Li can be produced in an excited state (10% branching ratio). The second reaction generates another high-energy neutrino with the decay

$$^8\mathrm{B} \rightarrow ^8\mathrm{Be}^* + e^+ + \nu_e \quad E_\nu < 14.06 \text{ MeV} \quad . \tag{9.19}$$

The excited beryllium state decays through $^8Be^* \rightarrow ^4He + ^4He$, closing the "cycle".
The second relevant fusion cycle is the CNO-cycle, which is responsible for the remaining 1.6% solar energy production:

$$\begin{aligned} ^{12}\mathrm{C{+}p} &\rightarrow ^{13}\mathrm{N} + \gamma \\ ^{13}\mathrm{N} &\rightarrow ^{13}\mathrm{C} + e^+ + \nu_e \quad E_\nu < 1.2 \text{ MeV} \\ ^{13}\mathrm{C{+}p} &\rightarrow ^{14}\mathrm{N} + \gamma \\ ^{14}\mathrm{N{+}p} &\rightarrow ^{15}\mathrm{O} + \gamma \\ ^{15}\mathrm{O} &\rightarrow ^{15}\mathrm{N} + e^+ + \nu_e \quad E_\nu < 1.73 \text{ MeV} \\ ^{15}\mathrm{N{+}p} &\rightarrow ^{12}\mathrm{C} + ^4\mathrm{He} \end{aligned} \tag{9.20}$$

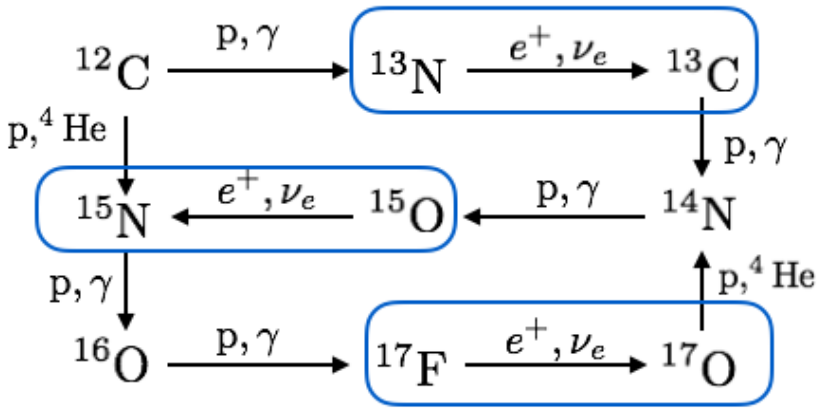

Figure 9.3: The CNO cycle. The blue boxes indicate the reactions where neutrino emission is implied: the β-decay of ^{15}O, ^{13}N, and ^{17}F.

The full CNO cycle is represented in Fig. 9.4.

9.5 Solar Neutrino Spectrum

The nuclear reactions we have seen in the previous section are one of the ingredients one needs for calculating the neutrino enegy spectrum from the Sun. The other ingredients are quantities describing the stellar environment, namely: gravity and thermodynamics.
A star is a complex system and the equations describing it can be fully solved only numerically. These equations are:

Density equation

$$\frac{dr}{dm} = \frac{1}{4\pi r^2 \rho} \quad , \tag{9.21}$$

Pressure equation:

$$\frac{dP}{dm} = -\frac{Gm}{4\pi r^4} \quad , \tag{9.22}$$

Luminosity equation

$$\frac{dL}{dm} = \epsilon - \left[\frac{d}{dt}\left(\frac{u}{\rho}\right) - \frac{P}{\rho^2}\frac{d\rho}{dt}\right] \quad , \tag{9.23}$$

Source	**Flux** (10^{10} cm^{-2} s^{-1})
pp	6
pep	$41.4 \cdot 10^{-2}$
^{7}Be	$4.5 \cdot 10^{-1}$
^{8}Be	$5 \cdot 10^{-4}$
^{13}N	$5 \cdot 10^{-2}$
^{15}O	$4 \cdot 10^{-2}$
^{17}F	$4.5 \cdot 10^{-4}$
Target	**SNU**
$\sum(\Phi\sigma)_{\mathrm{Cl}}$	7 ± 1
$\sum(\Phi\sigma)_{\mathrm{Ga}}$	127 ± 7

Table 9.1: Approximate neutrino fluxes on Earth from the various nuclear reaction processes in the Sun. The expected flux$\times$ cross section for Clorine and Germanium detectors is also indicated below in SNU (Solar Neutrino Units: 1 SNU = 10^{-36} captures per atom, per second).

Energy transport equation

$$\frac{dT}{dm} = \begin{cases} -\frac{3\kappa}{4acT^3}\frac{L}{16\pi r^4} & \text{radiative e. transport} \\ \frac{\Gamma_2 - 1}{\Gamma_2}\frac{T}{P}\frac{dP}{dm} & \text{convective e. transport} \end{cases} \tag{9.24}$$

Hydrogen abundance equation

$$\frac{dX}{dt} = r_X \quad . \tag{9.25}$$

r_X is the hydrogen burning rate and it is calculated as a sum over the different reactions which can consume hydrogen. In general, all the possible nuclear reactions should have thier own equation.
ϵ is the energy production rate, κ the opacity (absorption coefficient), Γ_i are the adiabatic coefficients ($\Gamma_1 = \partial(\ln P)/\partial(\ln \rho)$, $\Gamma_2/(\Gamma_2 - 1) = \partial(\ln P)/\partial(\ln T)$, $\Gamma_3 - 1 = \partial(\ln T)/\partial(\ln \rho)$), $a = 7.5 \cdot 10^{-15}$ erg cm^{-3} K^{-4} is radiation density constant ($u_{rad} = aT^4$).
Solving the latter system of equations, one can estimate the neutrino flux coming from each reaction. The result is showed in Fig. 9.4 and in Tab. 9.1.

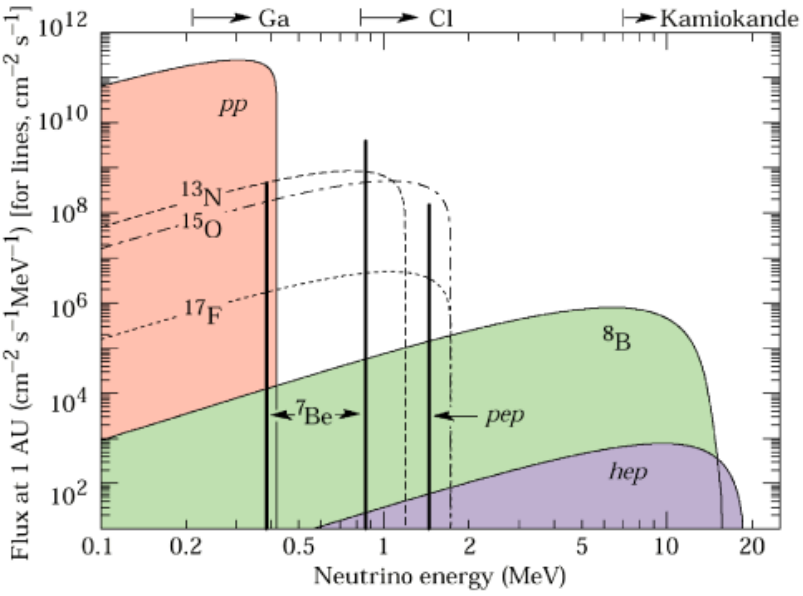

Figure 9.4: The CNO cycle. The blue boxes indicate the reactions where neutrino emission is implied: the β-decay of ^{15}O, ^{13}N, and ^{17}F.

9.6 The Solar Neutrino Problem

The Solar neutrino problem can be summarized in the following table, presenting the approximate results of experiments and theory values:

Experiment	**Result**	**Theory**
Homestake	2.56 ± 0.22 SNU	8 SNU
Kamiokande	$2.9 \pm 0.22 \pm 0.35 \cdot 10^{-36}$ cm^{-2}s^{-1}	5 cm^{-2}s^{-1}
GALLEX	69.7 ± 7 SNU	132 SNU
SAGE	69 ± 10 SNU	120 SNU

Different experiments using different techniques and targets were consistently measuring a lower neutrino count (or flux). This mismatch between experiments and theory represented the so-called solar neutrino problem, which was interpreted as due to neutrino oscillations and experimentally confirmed with new experimental techniques.

9.7 How to detect Solar Neutrios

Solar (electron) neutrinos have relatively low energies and in the few-MeV regime they mostly interact quasi-elastically with nucleons

$$\nu_e + n \rightarrow p + e^- \quad . \tag{9.26}$$

or elastically ($\nu_e + n \rightarrow \nu_e + n$)/
Since a free-neutron target does not exist, we have to consider neutrons embedded in nuclei X

$$\nu_e + {}^A_Z X \rightarrow {}^A_{Z+1} Y + e^- \quad . \tag{9.27}$$

where Y is the resulting nucleus after the neutrino interaction.
The last reaction could be used for detecting solar neutrinos, if it is possible to separate the new few Y elements from the (way more) abundant X. Chemical techniques are based on exposing a large quantity of an element X to a neutrino flux and later on nuclei Y are searched for with chemical separation techniques.
Another technique is based on the in real-time detection of reactions like Eq. 9.26 or $\nu_e + e^- \rightarrow \nu_e e^-$.

9.8 Radiochemical Experiments

Chlorine Experiment
The first reaction for detecting solar neutrinos was suggested by B. Pontecorvo already in 1946

$$\nu_e + {}^{37}_{17}\mathrm{Cl} \rightarrow {}^{37}_{18}\mathrm{Ar} + e^- \quad . \tag{9.28}$$

R. Davis (Nobel Prize 2002) was the first developing working detectors based on clorine, and later building a 390.000l tank filled with C_2Cl_4 in the Homestake mine (South Dakota) in 1965. Measurements continued until 2002.
Chlorine is a good nucleus for such measurements since the threshold energy for neutrino interactions is 0.814 MeV. The resulting argon is chemically inert and thus could be extracted with 95% efficiency from the detector. ^{37}Ar is radioactive with a lifetime of 35 days: the decay proceeds

via the capture of one of the orbital electrons returning to chlorine with the inverse Eq. 9.28 reaction. The resulting ^{37}Cl nucleus is formed in an excited state which decays emitting a 2.82 keV X-ray. Davis developed detectors for detecting these X-rays and thus count the number of neutrino interactions. The resulting rate was about 25 counts per year.

Gallium Experiment

Another reaction which was exploited for example in the SAGE[4] and GALLEX detectors is

$$\nu_e + {}^{71}_{31}\mathrm{Ga} \rightarrow {}^{71}_{32}\mathrm{Ge} + e^- \quad . \tag{9.29}$$

SAGE (Caucasus mountains) used 50 tons of liquid gallium kept at 30°C (1989-), while GALLEX (Gran Sasso) used 30 tons of $GaCl_3$ solution (1991-1997). The resulting germanium isotope has a half-time of 11.4 days, while its extraction is chemically more complex as for argon. The reaction thershold is 233 keV. An important feature of the gallium-based experiments was the possibility to use an external electron neutrino source of known activity for calibrating the detectors The source was based on ^{51}Cr with an intensity of about 0.5 MCi, emitting electron neutrinos by electron capture (half-life 27.7 days).

9.9 Real-time Experiments

The real-time experiments measured directly the neutrino interactions as they happen, without the need of a later-phase chemical separation process.

Super Kamiokande

This experiment based in Japan employed a 2.2 kton water tank for detecting the

$$\nu_e + e^- \rightarrow \nu_e + e^- \quad , \tag{9.30}$$

with the Cherenkov effect. This method is sensitive only to the highest energy neutrinos coming from ^{8}B. The scattered electrons create Cherenkov "rings" which are detected by 948 20-inch photomultipliers.

Also Super Kamiokande, like radiochemical experiments, confired the deficit in solar neutrinos.

[4]later renamed GNO: Gallium Neutrino Observatory

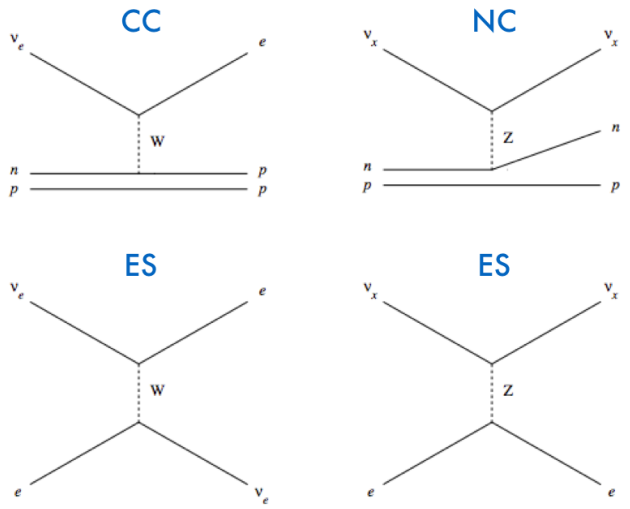

Figure 9.5: Reactions in the SNO detector, allowing the simulataneous measurement of the total and the electron neutrino fluxes.
[!t]

SNO: Sudbury Neutrino Observatory
SNO was active in the period 1999-2006 and detected neutrinos by Cherenkov light using a 12-m diameter spherical acrylic vessel viewed by 9500 20-cm photomultipliers. The detection medium was 1000tons heavy water (D_2O) in an inner volume surrounded by 1500 tons of normal water for screening.
The relevant neutrino interactions in the detector were (see also Fig. 9.5)

1. Elastic scattering (ES) $\nu_e + e^- \rightarrow \nu_e e^-$. This reaction is in principle sensitive to all neutrino flavours, but
$$\sigma(\nu_e + e^- \rightarrow \nu_e e^-) \approx 6 \times \sigma(\nu_{\mu,\tau} + e^- \rightarrow \nu_{\mu,\tau} + e^-) \quad . \tag{9.31}$$

2. Charged-current interaction (CC), which happens only for electron neutrinos ($W^{\pm}$ exchange)
$$\nu_e + d \rightarrow e^- + p + p \quad , \tag{9.32}$$

The deuterium break-up reaction is 1.44 MeV and almost all the energy is carried out by the electron and thus this reaction can be detected by Cherenkov effect.

3. Deuterium break-up by Z^0 exchange neutral current interaction (NC)

$$\nu_f + d \rightarrow \nu_f + p + n \quad , \tag{9.33}$$

where $f = e, \mu, \tau$. The reaction emits a 2.2 MeV gamma (this energy is the deuteron binding energy).

The data collected by SNO contain all the three reactions listed above. In principle, the last reaction cannot produce Cherenkov light, but the emitted neutron can be recaptured by deuterium releasing a 6.25 MeV gamma ray. This gamma can further produce through Compton scattering an electron above Cherenkov threshold.
In a first phase (**SNO-1**), the detector took data only with heavy water. In a second phase (**SNO-2**), 2 tons of salt (NaCl) were added. The salt helped in increasing the neutron capture rate (third reaction)

$$n + {}^{35}\mathrm{Cl} \rightarrow {}^{35}\mathrm{Cl}^* \rightarrow {}^{35}\mathrm{Cl} + \gamma \quad . \tag{9.34}$$

In a third phase (**SNO-3**), the salt was removed and special proportional counters (^{3}He/CF_4) installed in the detector volume for directly count the neutrons from the third reaction. The neutron detection proceeded through the reaction $n + {}^3\mathrm{He} \rightarrow p + {}^3\mathrm{H}$. The three experimental phases delivered consistent results. The measured fluxes (in $10^6 \times \mathrm{cm}^{-2}\mathrm{s}^{-1}$) were

$$\begin{aligned} \Phi^{NC} &= \Phi_{\nu_f} = 5.25 \pm 0.16 \pm 0.13 \\ \Phi^{CC} &= \Phi_{\nu_e} = 1.68 \pm 0.06 \pm 0.09 \\ \Phi^{ES} &\sim \Phi_{\nu_e} + \tfrac{1}{6}\Phi_{\nu_\mu + \nu_\tau} = 2.35 \pm 0.22 \pm 0.15 \end{aligned} \tag{9.35}$$

where the first error is statistical and the second systematic.
The results clearly show that

$$\Phi_{\nu_\mu + \nu_\tau} = \Phi_{\nu_f} - \Phi_{\nu_e} \neq 0 \quad , \tag{9.36}$$

and this finally demonstrates that 2/3 of the ^{8}B electron neutrinos change their flavour on their way from the Sun to the Earth. Moreover, the total neutrino flux measured by the NC reaction is finally consistent with the solar neutrino model (Fig. 9.6). A.B. McDonald was awarded the 2015 Noble prize in physics for leading the SNO experiment (together with T. Kajita for SuperKamiokande.

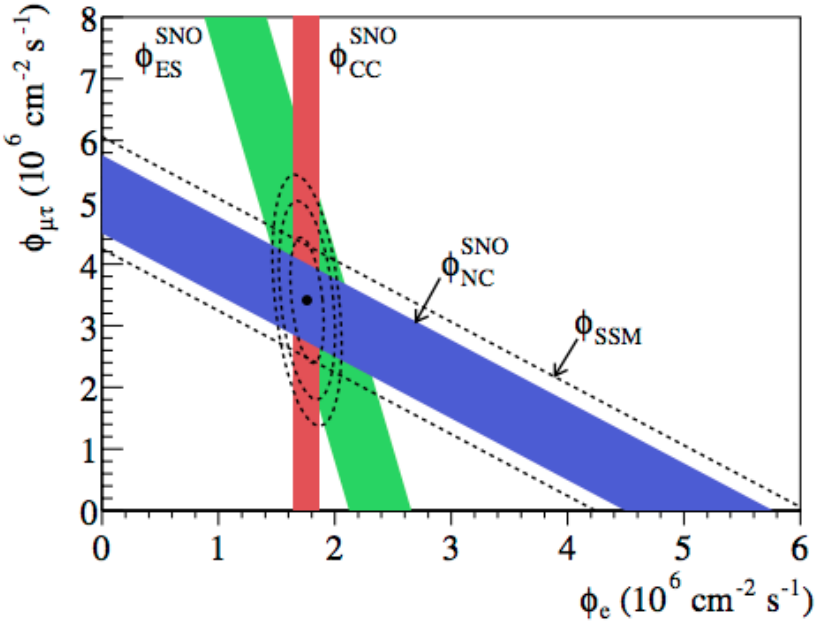

Figure 9.6: Results of the SNO experiment.

9.10 Supernova Neutrinos

Stars heavier than 8 solar masses can reach high enough temperatures to sythesize iron. Once this point is reached, they cannot sustain their weight through further nuclear reactions. At this stage, the star has developed an "onion-like" structure where the heavier nuclei fuse only in the deepest layers. Starting from the outermost layer, the ongoing reactions are

$H \rightarrow He$
$He \rightarrow {}^{12}C, {}^{16}O, {}^{22}Ne$
${}^{12}C \rightarrow {}^{20}Ne, {}^{24}Mg$
${}^{20}Ne \rightarrow {}^{16}O, {}^{24}Mg$
${}^{16}O \rightarrow {}^{28}Si$
${}^{28}Si \rightarrow Fe, Ni$

After the exaustion of the iron reactions, if the star iron core has a mass

larger than the *Chandrasekhar mass*

$$M_C = 5.72 \cdot Y_e^2 \cdot M_{\text{Sun}} \quad , \tag{9.37}$$

(Y_e is the electron-to-nucleon ratio) an irreversible collapse begins.
A typical value for the Chandrasekhar mass for a 15-solar masses progenitor star is $\sim M_c = 1.5$ solar masses with a central temperature of $\sim 8 \cdot 10^9$ K, density of $3.7 \cdot 10^9$ g/cm^3, and $Y_e \sim 0.42$. During the collapse, photodisintegration of the iron-group elements takes place:

$$^{56}\text{Fe} \rightarrow 13\,^4\text{He} + 4\text{n} \quad (\text{- 124 MeV}) \quad . \tag{9.38}$$

These reactions revert to helium all what thousands of years of nuclear fusion turned into iron. Further photodisintregration of helium frees protons and neutrons. A rapid "neutronization" phase of the core of the star is then expected, through the reactions

$$p + e^- \rightarrow n + \nu_e \quad , \tag{9.39}$$

$$^Z\text{A} + e^- \rightarrow ^{Z-1}\text{A} + \nu_e \quad , \tag{9.40}$$

thus with a strong emission of electron neutrinos with a duration of $\mathcal{O}$(10 ms).
Using computer simulations, it was realized that the collapse followed by a shock wave and neutrino emission was not sufficent for explaining supernova explosions. The reason is that the shock wave energy will quickly slow down since its energy will go into the dissociation of nuclei in the outer crusts of the collapsing star.
At the core of the collapsing star, the density is so high to trap neutrinos. This region is called *neutrinosphere*.
In the central region, the temperature is very high ($\sim$ 10 MeV) and electron pairs can create neutrinos of all flavours (see also Fig. 9.7):

$$e^+ + e^- \rightarrow \nu_f + \bar{\nu}_f \quad . \tag{9.41}$$

This reaction stops when the in-falling material pushes the density so high to start the inverse reaction, reaching eventually thermal equilibrium.

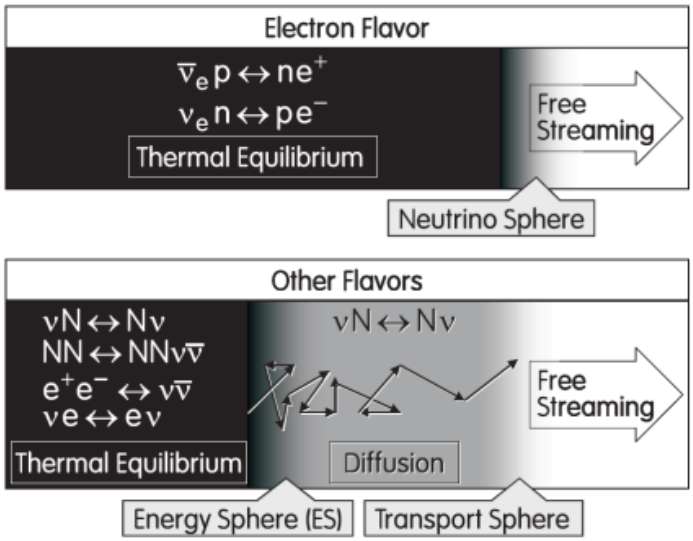

Figure 9.7: Neutrino production in a supernova. **(Top):** in the core, electron neutrinos are produced by electron capture by protons. **(Bottom):** other electroweak reactions in the dense parts of the collapsing star produce neutrinos of every flavour.

The produced neutrinos carry the bulk of the gravitational collapse energy and can deposit part of their energy in the region between the forming neutron star and the stalled first shock wave through the reactions

$$\begin{aligned} \nu_e + n &\rightarrow e^- + p \\ \bar{\nu}_e + p &\rightarrow e^+ + n \end{aligned} \tag{9.42}$$

and neutral-current interactions involving also the other flavours (Fig. 9.7). These reactions increase the temperature of the stellar matter behind the first shock wave. When the pressure inside the first shock becomes higher than the one after it, the star explodes and the neutrinos are released. About 99% of the energy of the collapse is converted into neutrinos.
The general characteristic of the neutrino species average energies are

$$\langle E_{\nu_e} \rangle < \langle E_{\bar{\nu}_e} \rangle < \langle E_{\nu_x} \rangle \quad , \tag{9.43}$$

where ν_x represents all the other (anti)neutrino flavours (Fig. 9.8).
The ordering is the consequence of neutrino interactions with matter:

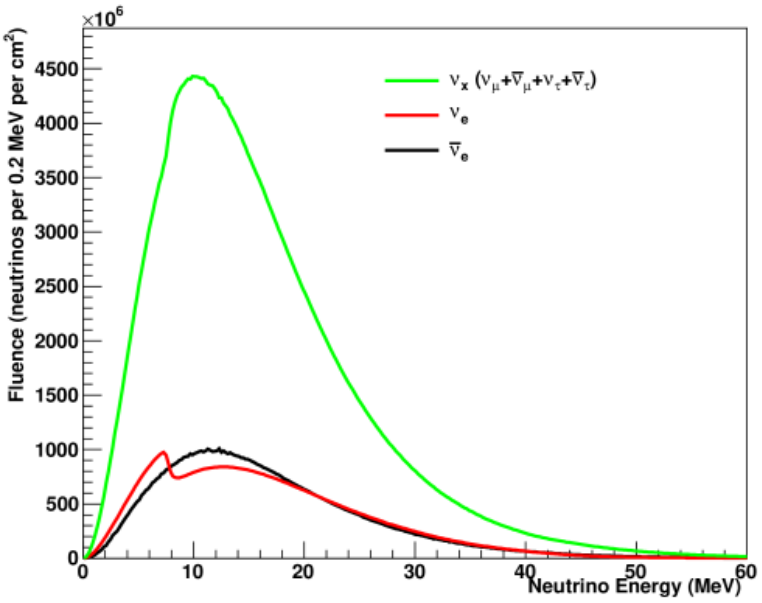

Figure 9.8: Neutrino fluence from the GKVM (Gava-Kneller-Volpe-McLaughlin) model. The structure in the ν_e spectrum is caused by collective effects (a "gas" of neutrinos can undergo collective flavour changes).

electron neutrinos undergo more interactions than anti-electron neutrinos, since in the core there are more neutrons than protons. Muon- and tau-neutrinos have larger energies since they can interact mostly only through neutral currents.
The energy of neutrinos emitted by a supernova is in the $\sim$ 10-20 MeV range. The flux can be parameterized by

$$\Phi(E_\nu) = N \left(\frac{E_\nu}{\langle E_\nu \rangle} \right)^\alpha \exp \left[-(\alpha+1) \frac{E_\nu}{\langle E_\nu \rangle} \right] \quad , \tag{9.44}$$

where the normalization constant is

$$N = \frac{(\alpha+1)^{\alpha+1}}{\langle E_\nu \rangle \Gamma(\alpha+1)} \quad . \tag{9.45}$$

9.11 How to detect supernova neutrinos

The expected number N of supernova neutrinos a detector on earth can detect scales with the supernova distance D as $N \sim 1/D^2$. Approximately, if the detector has mass M, then $N \sim M$. Given the typical energy of supernova neutrinos, a threshold of few MeV would be sufficient.
Given the relatively high energy of the supernova neutrinos, radioactive backgrounds should not be a problem, since they are all at energies < 10 MeV. The supernova burst lasts about 10 s and also this helps in suppressing backgrounds, which, in an underground detector accumulate over long times. The underground location helps also in suppressing cosmics-induced backgrounds.
Since detectors contain mainly protons (many of them are based on water or scintillators which are basically C_nH_{2n} chains), they are mostly sensitive to antineutrinos through the reaction

$$\bar{\nu}_e + p \rightarrow e^+ + n \quad . \tag{9.46}$$

For a supernova at 10 kpc distance and a 1 kton water detector, one expects O(200) events, without taking into account the detector efficiency. For comparison, for a supernova in the Andromeda galaxy ($\sim$ 770 kpc), O(1) event is expected.

Given the random character and frequency of a supernova explosion near the Earth, detectors, telescopes, and satellites should be ready.
To this end, the SNEWS (SuperNova Early Warning System) collaboration was established. The goal of SNEWS is to provide the astronomical community with an alert signal of the occurrence of a core-collapse event. SNEWS is also engaged in downtime coordination, and global sensitivity optimization to a supernova signal. SNEWS has been automatically running since 2005. Currently, the following neutrino experiments are involved: Super-K (Japan), LVD (Italy), Ice Cube (South Pole), KamLAND (Japan), Borexino (Italy) Daya Bay (China), and HALO (Canada). Alerts of possible supernova neutrinos are sent from the experiments to the SNEWS computer at Brookhaven National Laboratory. Multiple detectors would see supernova neutrinos simultaneously, so the probability of a false alarm is extremely low.
A supernova emits about half its neutrinos in a couple of seconds, while the first electromagnetic signal may not come for many hours or even

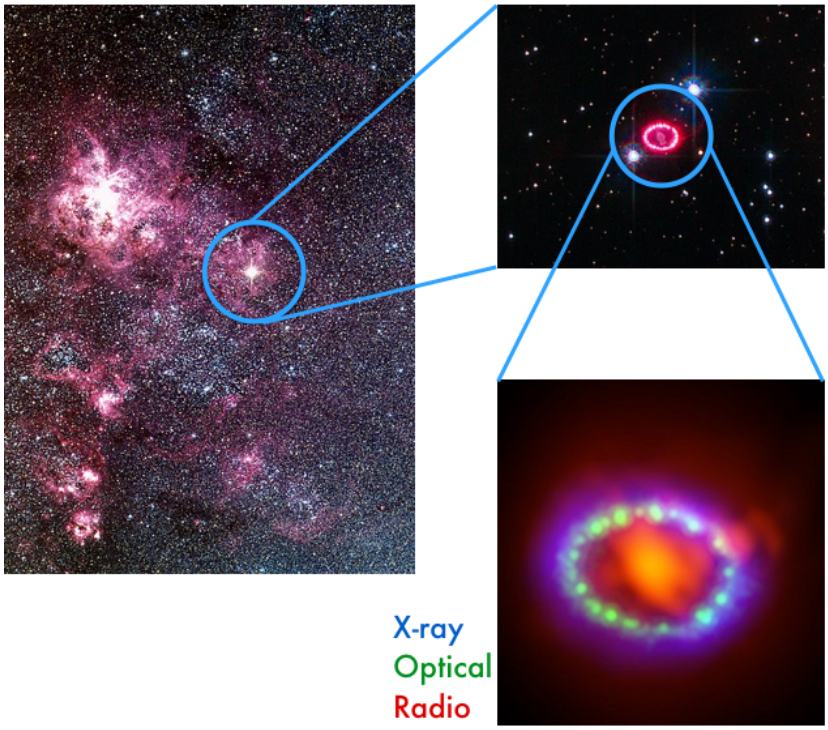

Figure 9.9: The SN1987A supernova observed at various wavelenghts.

days, depending on the outer layers of the star and dust between Earth and the star. That's why the neutrino detectors and the SNEWS system offer the possibility of an early detection of a supernova's birth.
Calculations show that neutrinos from supernovae in other galaxies will be too weak for these facilities to detect, so SNEWS will alert us for events happening in the Milky Way or nearby.
The SNEWS alert can be received signing up for a mailing list. Up to now (2020) no alerts has been issued.

9.12 SN 1987A

The supernova SN 1987A in the Large Magellanic Cloud, a satellite of our Milky Way Galaxy, is the first for which neutrinos were detected (Fig. 9.9). The supernova explosion prior to 1987 and visible with nacked eye happened in 1604 ("Kepler's Supernova", $\sim$6 kpc.).

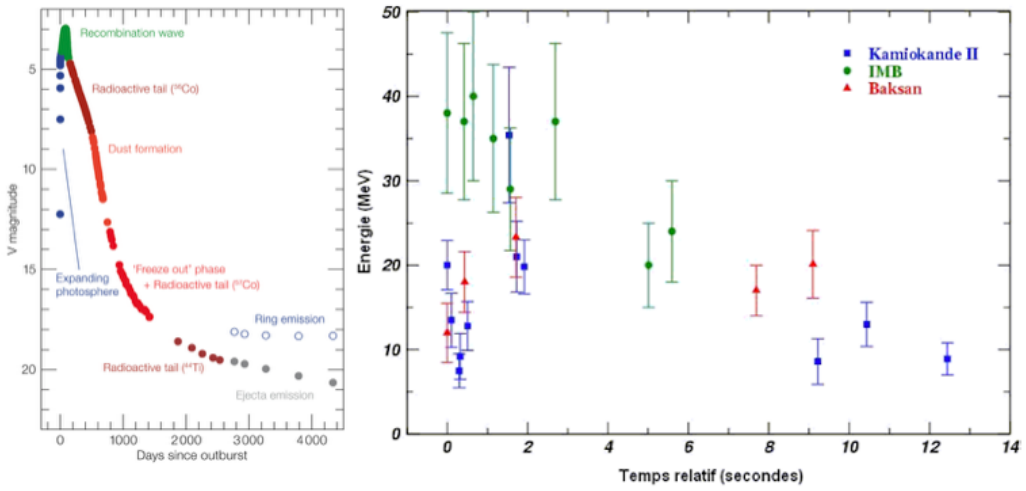

Figure 9.10: **(Left):** The SN1987A supernova light curve. **(Right):** Early neutrino measurements associated to SN1987A.

The progenitor of SN 1987A was Sanduleak-69202: a heavy (16-22 solar masses) blue super-giant star at a distance of 50 ± 5 kpc from Earth. After the explosion was indeed verified that Sanduleak-69202 disappeared from the sky.

The Hubble Space Telescope has taken images of the supernova regularly since August 1990 without detecting the neutron star remnant. It could be that the remnant is covered by dust clouds, or that the remnant is not a neutron star but a black hole.

The neutrino detectors at the time collected only few events (Fig. 9.10) but they were sufficient for an overall proof of the core-collapse picture. Looking at the time distribution of the events, they are in agreement with a $\sim$ 10 s burst, in agreement with theoretical models. The energy distribution of the events is consistent with a neutrinosphere temperature of about 4 MeV and the average energy of the detected neutrinos was $\sim$15 MeV.

The number of events detected was in agreement with a 3×10^{53} erg liberated energy (Baksan: 5 events, Super Kamiokande: 12 events, IMB: 8 events).

The neutrino arrival time distribution allowed also a measurement of the neutrino masses, resulting in $m_\nu < 10$ eV and in a test of the neutrino

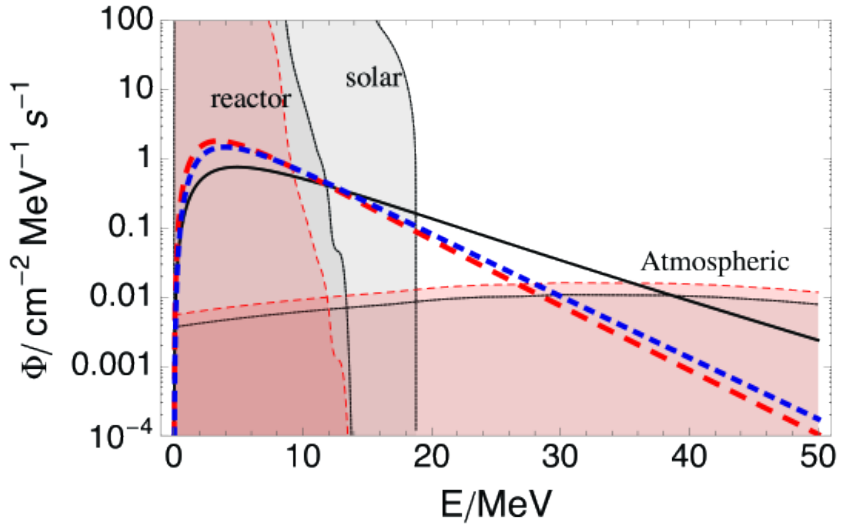

Figure 9.11: Backgrounds in a diffuse supernova neutrino search. The window of opportunity between 20 and 40 MeV is visible. (Figure from Lunardini/Sholberg)

speed: $|v_\nu - c|/c < 2 \times 10^{-9}$.

9.13 Diffuse Supernove Neutrino Background

It is expected that all the supernovae in cosmic history gives rise to a diffuse neutrino background (DSNB), calles also relic supernova neutrino flux. The DSNB flux depends on the historical rate of core-collapses, average neutrino production, cosmological redshift effects and neutrino oscillation effects. For neutrino energies above ∼19 MeV, estimates of the $\bar{\nu}_e$ flux are 0.1-1 cm^{-2}s^{-1}.
The detection techniques are the same as for burst neutrinos, however in the DSNB case the problems are the background.
At low energies, solar and reactor neutrinos dominate the background while at higher energies, atmospheric neutrino backgrounds dominate. The atmospheric and reactor backgrounds vary by detector location. There is an energy window at ∼ 20-40 MeV in which the DSNB dominates over the other neutrino fluxes and there is an opportunity for an experimental observation (see Fig. 9.11).

Chapter 10 | Dark Matter

Already in 1932, Jan Hendrik Oort found some discrepancies between the observed rotation curve (the velocity of the stars as a function of the galactic radius) of our own galaxy and the expected one from luminous matter.From this observation, he was not able to exclude that this discrepancy may have been caused by an underestimate of luminous matter due to the presence of absorbing matter. In 1933, Fritz Zwicky's studies of the Coma cluster pointed to a significant discrepancy between the amount of matter deduced from the knowledge of the typical mass-to-light ratio of galaxies, and the gravitation properties of the system. Under the supposition that the Coma system has reached, mechanically, a stationary state, the Virial Theorem implies

$$\langle E_{kin} \rangle = \frac{1}{2} \langle V_g \rangle \tag{10.1}$$

where $\langle E_{kin} \rangle$ and $\langle V_g \rangle$ denote average kinetic and potential energies. Zwicky assumed an uniform mass distribution and a cluster radius R$\sim$ 1 Mly with 800 galaxies with M $\sim$109 solar masses. The total mass estimate was $\sim 1.6 \times 10^{45}$g. The average gravitational potential energy was therefore $\langle V_g \rangle = (3/5)GM/R$. Using the virial theorem (Eq. 10.1), the average mean squared velocity can be extracted:

$$\sqrt{\langle v^2 \rangle} \approx 80 \frac{\text{km}}{\text{s}} \tag{10.2}$$

This result has to be compared to the observed value of the average Doppler effect of $\sim$1000 km/s. The conclusion was that the average density of the Coma system would have to be at least 400 times larger than that derived from the observations on luminous matter. Zwicky himself commented:

If this would be confirmed we would get the surprising result that **dark matter** *is present in much greater amount than luminous matter.*

10.1 Galaxy Rotation Curves

Until the 1970s, there was not much progress towards the understanding of this discrepancy attributed to some from of non-luminous matter, until Vera Rubin and coworkers published their work on rotation curves of spiral galaxies.
The measurements showed convincingly that the rotational velocities of the stars as a function of the radius R of the galaxies did not follow the expected Kepler's law

$$v(R) = \sqrt{\frac{GM(R)}{R}} \tag{10.3}$$

but they rather stayed about constant out to very large R, as showed in Fig. 10.1. This implied that galaxies were surrounded by a large amount of invisible matter.

10.2 Barionic Mass Estimation with X-ray Halos

Galaxy clusters are composed by abundant barionic matter which usually does not emit radiation. If this matter is present within strong gravitational potentials, bremsstrahlung photons can be emitted (usually in the X-ray band). Measuring these X-rays can lead to an estimation of the amount of barionic matter contained in a cluster, thus providing a tool for measuring its dark matter content by subtraction, if the total gravitational mass could be estimated in another way.
Approximating the cluster as a spherically symmetric system in equilibrium ($\bar{v} = 0$) the hydrodynamical Euler equation

$$\rho \frac{d\bar{v}}{dt} = -\nabla P - \rho \nabla \phi \quad , \tag{10.4}$$

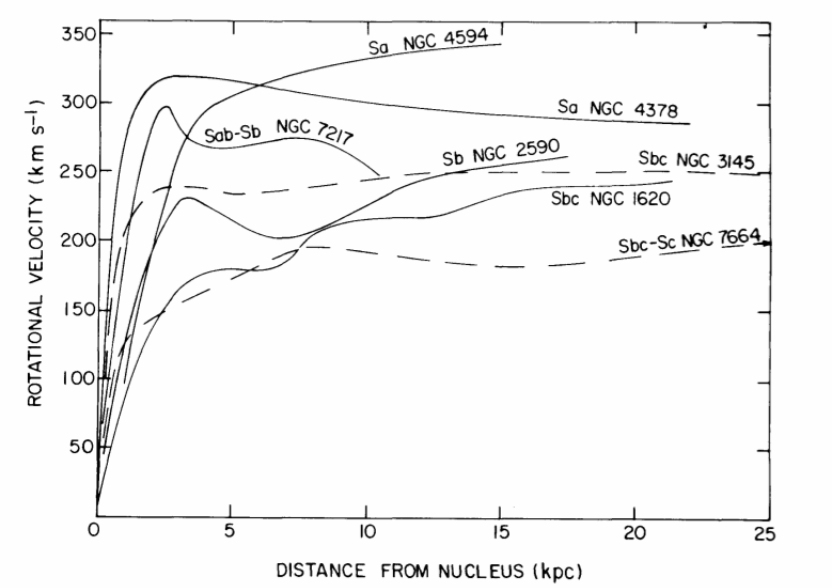

Figure 10.1: Rotational curves for different galaxies as measured by Rubin *et al* in V.C. Rubin *et al.*, Astrophys. Journal, 255, 107 (1978).

where P is the pressure, ρ the density, and ϕ the gravitational potential, becomes

$$\frac{dP}{dr} = -\frac{GM(r)}{r^2}\rho \quad . \tag{10.5}$$

$M(r)$ is the amount of matter contained within the radius r. Connecting the pressure $P(r)$ with the temperature $T(r)$ through the law of ideal gases $P = \rho k_B T/m$ and considering only protons for simplicity ($m = m_P$), after some algebra we obtain

$$M(r) = \frac{k_B T r}{G m_P}\left(-\frac{d\ln\rho}{d\ln r} - \frac{d\ln T}{d\ln r}\right) \quad . \tag{10.6}$$

The previous equation allows the measurement of the mass profile $M(r)$ through the measurement of the temperature and density profiles $T(r)$ and $\rho(r)$.
The temperature is determined via the shape of the frequency spectrum of the X-ray radiation, or through the strength of the emission lines. The

gas density $\rho(r)$ is proportional to the square root of the *luminosity density*, which is another directly measured quantity.

10.3 Gravitational Mass Estimation with Weak Lensing

Galaxies and clusters of galaxies act as gravitational lenses for the light coming toward us. This means that the deflection of light must be affected by the total gravitational mass of the astrophysical object under consideration, including the possible presence of dark matter.
Weak gravitational lensing (WGL) is the deflection of light emitted from sources behind a massive object (like a galaxy or a cluster of galaxies). Since the distortion of light is not very strong (in contrast to *strong gravitational lensing*, where light is so bended to form the characteristic "arcs"), many measurements of different background objects are needed, so that a WGL measurement is an inherently statistical process.
Let's start with looking how a light ray would be bent if we use Newtonian gravity.
The acceleration in the direction orthogonal to the direction observer-source (z) is (for small deflections)

$$g_\perp = \frac{GMb}{(b^2+z^2)^{3/2}} \quad , \tag{10.7}$$

where M is the lens'mass and b the impact parameter. The orthogonal velocity is

$$v_\perp = \int g_\perp dt = \int g_\perp \frac{dz}{c} = \frac{2GM}{bc} \quad . \tag{10.8}$$

The deflection angle is then

$$\alpha = \frac{v_\perp}{c} = \frac{2GM}{bc^2} \quad . \tag{10.9}$$

We will see that the general-relativistic calculation will give a factor 2 larger deviation angle. This effect was famously verified during a solar eclipse giving one of the first striking confirmation of general relativity.
The weak-field approximation metric is

$$ds^2 = c^2\left(1+2\frac{\phi}{c^2}\right)dt^2 - \left(1-2\frac{\phi}{c^2}\right)dr^2 \quad . \tag{10.10}$$

For a light ray, $ds^2 = 0$, and the last equation, evaluated at the first order for $\phi/c^2 \ll 1$ gives the effective speed of light in a weak gravitational field

$$c' = |\frac{dr}{dt}| \approx c\left(1 + \frac{2\phi}{c^2}\right) \quad . \tag{10.11}$$

We can also introduce the effective index of refraction at first order $n \approx c/c' \approx 1 - 2\phi/c^2 > 1$ (since $\phi < 0$).
Fermat's principle implies the following variational problem

$$\delta \int_a^b nx(l)dl = \delta \int_{\lambda_a}^{\lambda_b} nx|\frac{dx}{d\lambda}|d\lambda = \delta \int_{\lambda_a}^{\lambda_b} L(\dot{x}, x, \lambda)d\lambda = 0 \quad , \tag{10.12}$$

where λ is some arbitrary curve parameter and L is the legrangian. The solution to the variational problem (a and b are fixed) is given by the Euler-Lagrange equation

$$\begin{array}{l} \frac{d}{d\lambda}\frac{\partial L}{\partial \dot{x}} - \frac{\partial L}{\partial x} = 0 \quad \text{with} \quad \frac{\partial L}{\partial \dot{x}} = n\frac{\dot{x}}{|\dot{x}|} \quad \frac{\partial L}{\partial x} = |\dot{x}|\frac{\partial n}{\partial c} \quad \text{and} \\ \Rightarrow \frac{d}{d\lambda}(n \cdot x) - \nabla n = 0 \Rightarrow n\ddot{x} = \nabla n - \cdot x(\nabla n \cdot x) \quad . \end{array} \tag{10.13}$$

In the last equation, we have the spacial derivative if n minus the "parallel" derivative along the light path: this subtraction is thus equivalent to the derivative perpendicular to the light path. Rearranging the terms

$$\ddot{x} = \nabla_\perp \ln(n) \quad , \tag{10.14}$$

and substituting the approximate value for n

$$\ddot{x} \approx -\frac{2}{c^2}\nabla_\perp \ln(n) \quad . \tag{10.15}$$

The total deviation angle α is the integral along the light path of the gradient of n perpendicular to the light path (from the source λ_a to the observer λ_b), since $\theta = \int \ddot{x}d\lambda$

$$\alpha = \int_{\lambda_a}^{\lambda_b} ds\nabla_\perp n = \frac{2}{c^2}\int_{\lambda_a}^{\lambda_b} d\lambda\nabla_\perp\phi \quad , \tag{10.16}$$

where the gradient is taken only along the two coordinates orthogonal to the light ray (gravity acts only there, while longitudinally along z the contributions sum up to zero) and therefore ϕ in the last integral is viewed

as a vector with 2 components instead of three. Considering the simplified case where the deviating mass is point-like, $\phi = -GM/r$ with $r = \sqrt{x^2+y^2+z^2} = \sqrt{b^2+z^2}$ ($b^2 = x^2+y^2$ is the impact parameter). Evaluating Eq. 10.16

$$\alpha = \frac{2GM}{c^2}(\hat{x},\hat{y})\int_{-\infty}^{+\infty}\frac{dz}{(b^2+z^2)^{3/2}} = \frac{4GM}{c^2}(x,y)\left[\frac{z}{b^2(b^2+z^2)^{1/2}}\right]_0^{\infty} = \frac{4GM}{c^2 b}(\cos\varphi,\sin\varphi) \tag{10.17}$$

Some interesting points about the deviation due to a gravitational field are the following

- α is linear wrt the mass M, so the effects of more masses just add together to the total deviation.
- The same calculation using Newton's gravity would return an angle smaller by a factor of two.
- Introducing the Schwartzschild radius $R_s = 2GM/c^2$, we can rewrite $\alpha = 2R_S/b$.

10.4 Dark Matter from Astrophysical Measurements

Weak gravitational lensing provides a method for estimating the total mass of an astronomical object, while X-ray surveys are sensitive mostly to the baryonic content. If these two mass estimation methods do not agree, the difference among them should be due to some kind of non-baryonic matter. The today's baryonic density parameter is $\Omega_b^0 = \rho_b^0/\rho_c$ and measurements at different red-shifts are related by $\rho_b/\rho_c = \Omega_b^0/a^{-3}$. Expressing the baryonic density as $\Omega_b h^2$, where h is the Hubble's constant in 100 km/s/Mpc, we have the following different measurements

- From X-ray surveys, $\Omega_b h^2 \sim 0.02$.
- From light absorption from far-away quasars (with higher uncertainty), $\Omega_b h^2 \sim 0.02$.

- From the CMB anisotropy measurements, $\Omega_b h^2 = 0.02225 \pm 0.00023$ (Planck satellite). The density of baryonic matter is deduced from the relative height of the of the odd and even acoustic peaks. If Ω_b is enhanced, also the fist peak is enhanced, while the second is suppressed. The enhancement of Ω_b shifts also the peaks to higher l.

- Another method for estimating Ω_b is based on the predictions of the nucleosynthesis models based on our knowledge of nuclear physics. The predicted abundances of light elements match quite well the observations.

In summary, the surprising result $\Omega_b h^2 \sim 0.02$ follows from a variety of observations which are consistent with each other.
Weak lensing is instead sensitive to Ω_m, measuring $\Omega_m h^2 \sim 0.3$ as also other methods:

- Measure for different objects of the mass-to-light ratio as a function of the scale. This ratio saturates to a limiting value past the galaxy cluster scale ($\sim Mpc$). From this, the $\Omega_m h^2 \sim 0.3$ result can be deduced.

- Large-scale surveys for mapping the spectrum of the distribution of galaxies lead to $\Omega_m h^2 \sim 0.2$. While this number is quite different from 0.3, it is still much bigger than the baryonic density.

- The mapping of the cosmic velocity field combined with the distribution of galaxies leads also to $\Omega_m h^2 \sim 0.3$.

- The CMB provides directly $\Omega_m h^2 = 0.308 \pm 0.012$ (Planck satellite, Ade et al, Planck Results XIII, Astron.Astroph. 594, A13 (2015)).

The surprising result is that baryons constitute only about 5% of the critical density, while the total matter content about 30%. Both numbers are surprising: we would have expected that matter constitutes the bulk of the Universe's content, while baryons should have constituted the bulk of the matter content. Both these expectations are put into question by many different measurements, which are quite consistent with each other. Neutrinos are very abundant in the Universe, and as non-baryonic matter, they could be the solution to the puzzle. Unfortunately, their contribution is estimated to be $\Omega_\nu h^2 \sim 0.0025$ making them irrelevant in the total

balance for Ω_m.
In summary, different measurements point to the existence of additional gravitating matter the exact nature of which we do not know yet.

10.5 Dark Matter and Structure Formation

Although indirect, a very strong argument for the existence of dark matter is based on considerations related to structure formation. The structures we observe today (galaxies, clusters of galaxies) should represent inhomogeneities in the early Universe which acted as "seeds" for gravitational instability and aggregation of matter. These density inhomogeneities $\delta\rho/\rho$ can be observed measuring the $\delta T/T$ anisotropies in the CMB. It turns out that $\delta\rho/\rho \sim 10^{-4}$ and $\delta\rho/\rho \sim a$ where a is the scale factor, which has grown by a factor equal to the red-shift since recombination time ($z \sim 1100$).
Today, $\delta\rho/\rho \gg 1$, but since recombination, not enough time has passed for going from $\delta\rho/\rho \sim 10^{-4}$ to the needed size of the perturbations.
This tells us that considering only barions, there was not enough time for structures to form and create what we observe today. Therefore, we need some kind of matter which decoupled from the primordial plasma much earlier and started to clump and form in time the required density perturbations.

10.6 Dark Matter Properties

Having estimated by different methods how much Dark Matter (DM) is present in the Universe, we would like now to know what are its properties, in the case DM is really a new kind of particle(s).

- **Mass:** This parameter is not very well constrained and, depending from the model, can vary within tens of orders of magnitude. Simply estimating the de Broglie wavelength for a particle confined on galactic scales (kpc) with a typical escape velocity of 100km/s, we can derive a lower limit of 10^{-22} eV.

- **Interaction:** DM should be indeed "dark", *i.e.* it should not interact electromagnetically. If DM can interact with known particles, it

also depends from the specific model. Since DM cannot radiate, it is believed to be rather dissipationless: this would restrict its ability to clump or accrete around compact objects like black holes with respect to barionic matter. Some models of DM based on the existence of a "dark sector" propose an interaction with the Standard Model photon to some level and in this sense some electromagnetic interaction is allowed. Other models predict the possibility for DM to annihilate into Standard Model particles and this might represent a possible astrophysical signal to detect.

- **Self-Interaction:** Limits to the self-interaction of DM allow for cross-sections of the order of the strong ones.

10.7 Dark Matter as a Thermal Relic

The idea of *thermal decoupling* is an appealing framework for the description of DM. Thermal decoupling assumes that DM was in thermodynamical equilibrium in the early Universe. As the Universe expanded and cooled down, DM density dropped to the point that annihilation basically stopped, *freezing out* DM to the density we observe today.
A slightly more quantitative description is the following. As the density dropped via the expansion, the rate

$$\Gamma = n \cdot \sigma \cdot v \tag{10.18}$$

of the reaction keeping DM in equilibrium becomes smaller. The Hubble time $1/H(T)$ as a function of the temperature T is a measure of the age of the Universe and the inverse of the reaction rate $1/\Gamma$ tells how long does it take for the reaction to happen on average. So, if $\Gamma \ll H(T)$ is, then the reaction keeping the equilibrium is too slow, since less than one reaction happens in one age of the Universe. In other words, the rate of the reaction does not keep up to the expansion rate of the Universe. The **freeze-out** temperature T_{fo} is the temperature at which expansion and reaction rate are equal

$$\Gamma(T_{fo}) = H(T_{fo}) \quad . \tag{10.19}$$

While the Universe expands, $\Gamma > H$, until T_{fo} is reached. After that, $\Gamma < H$ and the DM density is "frozen" and then it will keep decreasing

with the expansion.

10.8 Hot Thermal Relics and the Example of Neutrinos

If thermal relics are relativistic at the decoupling time, they are called *hot thermal relics*. Neutrinos are an example of such particles: given their almost vanishing mass they move at almost the speed of light at the decoupling. If they have to be thermal relics, they should have been in thermodynamical equilibrium, for example through a reaction like

$$\nu + \bar{\nu} \longleftrightarrow f + \bar{f} \quad , \tag{10.20}$$

where $\nu(\bar{\nu})$ is a neutrino (antineutrino) and $f(\bar{f})$ is a fermion (antifermion). Taking $E \sim T_\nu$ and for the cross-section the Fermi approximation [1] $\sigma \sim G_F^2 T_\nu^2$, at the freeze-out temperature T_ν we require ($v = c = 1$)

$$n(T_\nu) \cdot \sigma(T_\nu) = H(T_\nu) \Rightarrow T_\nu^3 G_F^2 T_\nu^2 = \frac{T_\nu^2}{M_P} \quad . \tag{10.21}$$

where we used the Friedmann equation $H^2 = \frac{8\pi G}{3}\rho$ and $\rho \sim T^4$ for relativistic particles. Solving for the freeze-out temperature

$$T_\nu = (G_F^2 M_P)^{-1/3} \approx 1 \text{ MeV} \quad . \tag{10.22}$$

This result is consistent with the relativistic condition $m \ll T$ assumed at the beginning, so neutrinos are really an example of hot relics.

10.9 Cold Thermal Relics and WIMPs

Cold thermal relics are non-relativistic at freeze-out, so the appropriate approximation for the density is

$$n \sim (mT)^{3/2} e^{-\frac{m}{T}} \quad , \tag{10.23}$$

[1] $G_F \sim 10^{-5}\text{GeV}^{-2}$ and we assume $E \ll m_W$.

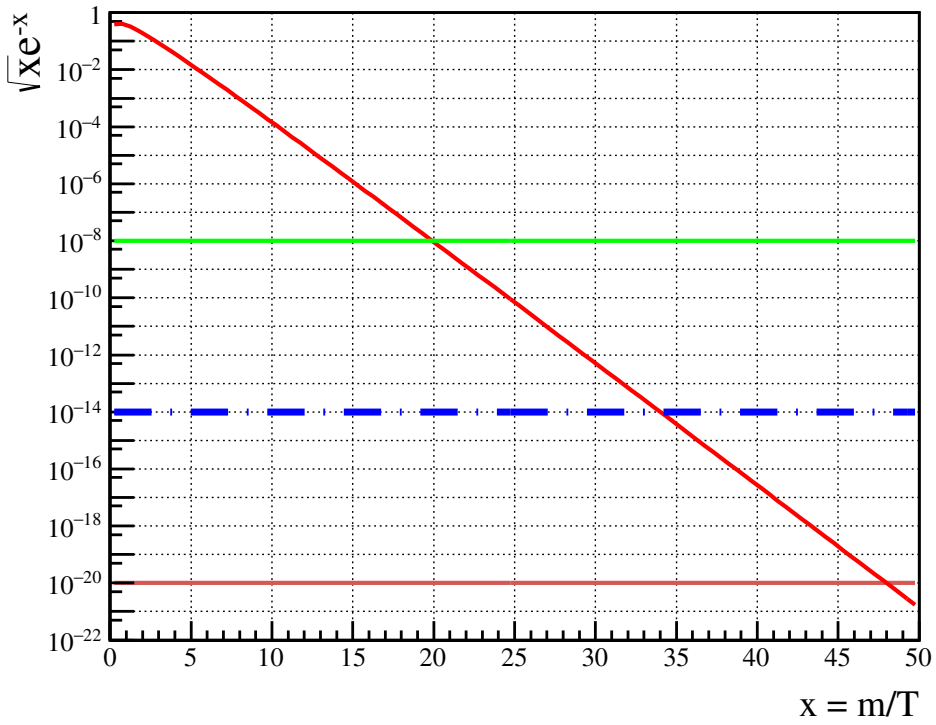

Figure 10.2: Plot of the two sides of Eq. 10.24. The blue dashed line corresponds to the WIMP case $1/(m \cdot M_P \cdot \sigma) = 10^{-14}$, calculated with the weak scale "miracle" values $m_\chi = 100$ GeV and $\sigma = G_F^2 m_\chi^2$. Other two horizontal lines at 10^{-8} and 10^{-20} are added for reference.

The freeze-out condition $n\sigma \sim H$ (we still consider $v \sim c$ up to some factor) in the radiation-dominated phase of the Universe implies $n_{fo} \sim T_{fo}^2/(\sigma M_P)$.
Defining $x = m/T$ ($x \gg 1$ then defines the non-relativistic "cold" regime), the freeze-out condition becomes

$$\sqrt{x}e^{-x} = \frac{1}{m \cdot M_P \cdot \sigma} \quad . \tag{10.24}$$

The last equation does not have analytical solutions and must be solved numerically. A graphical representation of the solution is given in Fig 10.8, where $\sqrt{x}e^{-x}$ is reported together with three cases for $1/(m \cdot M_P \cdot \sigma)$: the

solutions are at the intersection points.
Let's try now to calculate the density parameter associated to a cold relic particle with mass m_χ

$$\Omega_\chi = \frac{m_\chi n_\chi(T_0)}{\rho_c} = \frac{m_\chi T_0^3}{\rho_c}\frac{n_0}{T_0^3} \quad . \tag{10.25}$$

Today, $T_0 = 2.7K \sim 10^{-4}$ eV. In an isoentropic FLRW Universe ($aT \sim const.$), for relativistic particles we have $T \sim 1/a$ and $n \sim 1/a^3$, so

$$\frac{n_0}{T_0^3} = \frac{n_{fo}}{T_{fo}^3} \quad . \tag{10.26}$$

Substituting n_0 from the last equation into the density parameter equation and using again the freeze-out condition

$$\Omega_\chi = \frac{T_0^3}{\rho_c M_P}\frac{x_{fo}}{\sigma} \quad . \tag{10.27}$$

The dark matter abundance is measured to be about $\Omega_{DM} \sim 0.2$, so the last equation can be recast in the more suggestive form

$$\frac{\Omega_\chi}{0.2} \simeq \frac{x_{fo}}{20}\left(\frac{10^{-8}\text{GeV}^{-2}}{\sigma}\right) \quad , \tag{10.28}$$

where appropriate numerical values normalize each member to $\mathcal{O}(1)$. In a more exact treatment of the problem, the cross-section of the last equation should be the thermally-averaged cross section $\langle\sigma v\rangle$ for reasons connected to the Boltzmann equation.
Using the equipartition theorem $(3/2)T = (1/2)mv^2$, we can estimate that $v \sim c/3$ for $x \sim 20$ and this leads to the estimate

$$\langle v\sigma\rangle \sim 3 \times 10^{-26}\frac{\text{cm}^3}{\text{s}} \quad . \tag{10.29}$$

This result is often associated to the so-called **WIMP miracle**, which consists in the following coincidence. For various reasons, new physics is expected at the electroweak scale $m \sim E_{EW} \sim 200$ GeV. If we calculate the electroweak pair-annihilation cross-section at freeze-out temperature

$$\sigma_{EW} \sim G_F^2 T_{fo}^2 \sim \left(\frac{E_{EW}}{20}\right)^2 \sim 10^{-8}\text{GeV}^{-2} \quad , \tag{10.30}$$

we obtain the right cross-section which is able to explain the DM abundance. This result is often quoted as an indication that new physics at the electroweak scale might also explain DM in the form of a cold relic from the early Universe. Looking at Fig. 10.8, the dashed line describes about this case with $\sigma_{EW} = G_F^2 m_\chi^2$ and $m_\chi = 100$ GeV, corresponding to $x \sim 35$. Is this really a "miracle"? The previous result was obtained under the assumption of electroweak cross-sections and the cold relic condition $x \gg 1$. In general, following a dimensional argument, a DM annihilation cross-section can be written as $\sigma \sim g^4/m_\chi^2$, where g is some coupling constant. Using Eq. 10.24, $x \gg 1 \Rightarrow m_\chi M_P \sigma \gg 1$, and therefore $m_\chi \gg 0.1$ eV if $\sigma \sim 10^{-8}$ GeV^2. This means that as long as the cross-section is the right one for explaining the DM abundance, the cold relic mass can be very small. The conclusion is that the supposed "miracle" can be realized also without appealing to the electroweak scale.
The argument for understanding the WIMP paradigm can also be restated as following.
As we have seen,

$$\Omega_\chi \propto \frac{1}{\langle v\sigma \rangle} \sim \frac{m_\chi^2}{g_\chi^4} \quad . \tag{10.31}$$

The WIMP miracle states that if we use weak-scale masses and coupling constants, we can roughly reproduce the observed DM abundance. The last equation though fixes only the ratio between couplings and masses and therefore also other combinations might in principle obtain the correct abundance.

10.10 Mass Ranges for Cold Thermal Relics

General limits can be imposed to the allowed mass range of cold thermal dark matter. The requirement of unitarity in the calculation of cross-sections places the approximate bound

$$\sigma < \frac{4\pi}{m_\chi^2} \quad , \tag{10.32}$$

and this, together with Eq. 10.28 approximately implies

$$\frac{\Omega_\chi}{0.2} > 10^{-8}\text{GeV}^{-2} \times \frac{m_\chi^2}{4\pi} \quad . \tag{10.33}$$

Since $\Omega_\chi < 0.2$ we have

$$\left(\frac{m_\chi}{120\ \text{TeV}}\right)^2 < 1 \quad . \tag{10.34}$$

For a lower limit for WIMPs ($\sigma \sim G_F^2 m_\chi^2$), choosing $x_{fo} \sim 20$ we have

$$\Omega_\chi h^2 \sim 0.1 \frac{10^{-8}\text{GeV}^{-2}}{G_F^2 m_\chi^2} \sim 0.1 \left(\frac{10\ \text{GeV}}{m_\chi}\right)^2 \quad . \tag{10.35}$$

This lower limit is known as the **Lee-Weinberg** limit. The overall mass range allowed for WIMPs goes therefore from few GeVs to many TeVs.

10.11 Direct Searches for Dark Matter

The dark matter rate R in a detector containing N_T nuclei is

$$R = N_T \times \langle \Phi_\chi \rangle \quad , \tag{10.36}$$

where $\langle \Phi_\chi \rangle$ is the average flux. The recoil energy spectrum can be further written as

$$\frac{dR}{dE_R} = N_T \cdot n_\chi \cdot \langle v_\chi \frac{d\sigma}{dE_R} \rangle = N_T \cdot \frac{\rho_\chi}{m_\chi} \cdot \langle v_\chi \frac{d\sigma}{dE_R} \rangle \quad , \tag{10.37}$$

where σ is the nucleus-DM cross section, E_R the nucleus recoil energy, and v_χ is the DM velocity. In general the cross section can be dependent from the velocity which has a distribution $f(v)$ over which the cross section is averaged.
From classical mechanics collision theory,

$$E_R = \frac{q^2}{2m_T} = \frac{\mu_T^2}{m_T} v_\chi^2 (1 - \cos\theta) \quad , \tag{10.38}$$

where μ_T is the nucleus-DM reduced mass and θ the scattering angle. Differentiating the last equation ($dE_R = \frac{\mu_T^2}{m_T} v_\chi^2 d(cos\theta)$) and substituting in Eq. 10.37

$$\frac{dR}{dE_R} = N_T \frac{\rho_\chi m_T}{m_\chi \mu_T^2} \int_{v_{min}}^{v_{esc}} d^3v \frac{f(v)}{v} \frac{d\sigma}{d\cos\theta} \quad . \tag{10.39}$$

The integration limits are between the minimal velocity (corresponding to $\cos\theta = -1$) $v_{min} = q/(2\mu_T)$ and the galactic escape velocity v_{esc}.
The velocity distribution $f(v)$, the DM density ρ_χ, and the escape velocity come from astrophysical measurements, the DM mass m_χ is a parameter, while the other quantities are known. The cross section depends from the DM model considered.
The formula is general and can be used for placing upper limits to DM cross sections as a function of the DM particle mass.

10.12 Velocity Distribution Models

The Standard (galactic) Halo Model (SHM) assumes an isotropic thermal distribution for dark matter described by a Maxwell-Boltzmann distribution with a cutoff at v_{esc}

$$f_{SHM}(v) = N_{SHM} \cdot e^{-\frac{1}{2}|v|^2/\sigma^2} \cdot \Theta(v_{esc} - |v|) \quad , \tag{10.40}$$

where N_{SHM} is a normalization constant and $\sigma = |v_0|/\sqrt{2}$ is the DM velocity dispersion for a local reference frame at rest with velocity v_o.
The SHM is a first-order approximation of the DM distribution in the galaxy. The galaxy has different kinds of inhomogeneities and substructures, which can be modeled by

$$f_{sub}(v) = N_{sub} \cdot \exp\left[-(v - \bar{v}_{sub})^T \frac{\sigma_{sub}^{-2}}{2} (v - \bar{v}_{sub}) \right] \times \Theta(v_{esc} - |v|) \quad , \tag{10.41}$$

where v is intended as a 3-dim vector and σ is a 3x3 matrix (the dispersion tensor), and v_{sub} is the average velocity of the particles in the galactic substructure.
The total velocity distribution can be modeled as

$$f_\chi(v) = (1 - \eta) \cdot f_{SHM}(v) + \eta \cdot f_{sub}(v) \quad , \tag{10.42}$$

where the parameter η regulates the proportion of the substructure in the galaxy.
A generic model for the dispersion tensor which can describe "in-falling clumps" structures is $\sigma_{sub} = \mathrm{diag}(v_{rr}, v_{\theta\theta}, v_{\phi\phi})$ with $\langle v_{sub} \rangle = (\langle v_r \rangle, \langle v_\theta \rangle, \langle v_\phi \rangle)$.
In these spherical coordinates, r points towards the center of the galaxy, θ

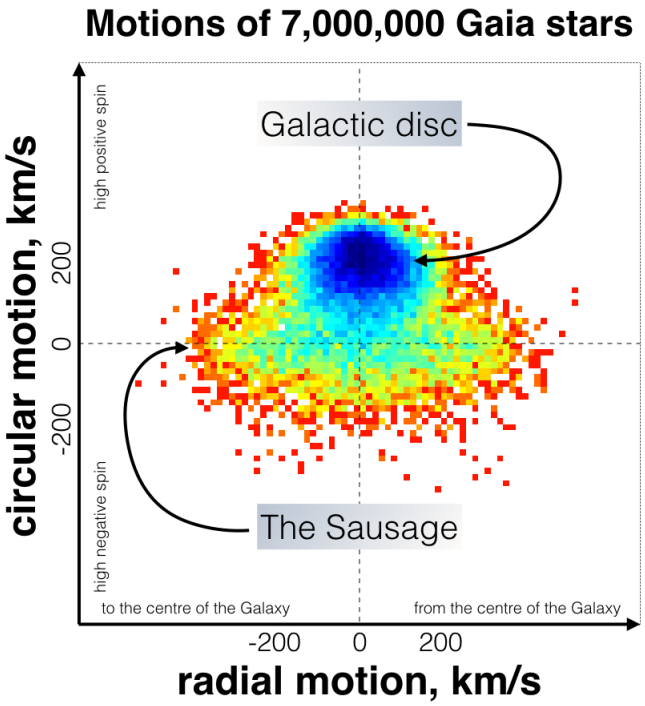

Figure 10.3: Velocity distributions measured by the Gaia mission. The "Sausage" is clearly visible with respect to the distribution of galactic disk stars. The structure is the result of a merger happened O(10) billions of years ago.

is the zenith angle and ϕ is oriented in the direction of the galactic disk's rotation. Condidering the angle α between the velocity vector of the Earth and v, the model assumes

$$\begin{aligned} \langle v_r \rangle &= \langle v_\theta \rangle = \frac{1}{\sqrt{2}} |v| \sin\alpha \\ \langle v_\phi \rangle &= |v| \cos\alpha \\ \sigma_{rr} &= \sigma_{\theta\theta} = \frac{1}{\sqrt{2}} (\sigma_{\parallel} \sin\alpha - \sigma_{\perp} \cos\alpha) \quad . \end{aligned} \tag{10.43}$$

Choosing different model parameters $(\langle v \rangle, \sigma_{\parallel}, \sigma_{\perp})$, the different galactic substructures can be modeled.
A relevant galactic structure recently discovered is the so-called "Gaia Sausage" or Enceladus: it is a merger event happened billions of years ago

where the Milky way merged with another smaller galaxy. The structure was discovered by the Gaia satellite mission which measured distances and velocity of millions of stars in our galaxy. The measured velocity distribution is showed in Fig.10.3.

Chapter 11 | Dark Energy

11.1 Introduction

The Dark Energy "problem" (DE) started in 1998 with the publication of results about 1a supernovae distances: very distant supernova were dimmer than expected suggesting that the universe's expansion was accelerating.
A brief historical account of DE is the following:

1917: Einstein introducd the cosmological constant in his field equations to obtain a static Universe.
1920s: Pauli realized that for a radiation field the vacuum energy would be very large. Ha calculated (unpublished) such an energy using as ultraviolet cutoff the classical electron radius, obtaining a value such that the Universe would have a too large curvature.
1931: Einstein removed the cosmological constant after the discovery of cosmic expansion.
1967: Zeldovich reintroduced the cosmological constant in connection with vacuum fluctuations.
1987: Weinberg published his famous review paper on the problem (Rev. Mod. Phys. 61 (1989) 1)
1998: Based on the analysis of 16 distant and 34 nearby supernovae, Riess *et al.* first discovered the acceleration of the expansion of the Universe. Right after, using 18 nearby supernovae and 42 high-redshift supernovae, Perlmutter *et al.* confirmed the discovery.
2011: Adam Riess, Brian Schmidt, and Saul Perlmutter win the Nobel Prize in physics 2011.

11.2 Cosmological Constant

The presence of a positive cosmological constant can account for the presence of dark energy. In the following we review briefly what the cosmological constant Λ is in the framework of general relativity.
The Einstein equation allows a term proportional to $g_{\mu\nu}$

$$R_{\mu\nu} - \frac{1}{2}g_{\mu\nu}R + \Lambda g_{\mu\nu} = 8\pi G T_{\mu\nu} \tag{11.1}$$

where Λ is a constant. Such term is allowed by the conservation laws ($\nabla_\mu G_{\mu\nu} = 0$ and $\nabla_\mu T_{\mu\nu} = 0$).
If we interpret the new term as an additional form of matter we can rewrite the energy-momentum tensor as

$$T_{\mu\nu} \to T_{\mu\nu} - \frac{1}{8\pi G}\Lambda g_{\mu\nu} \quad . \tag{11.2}$$

If we condider an ideal fluid

$$T_{\mu\nu} = (\rho_\Lambda + P_\Lambda)u_\mu u_\nu + P_\Lambda g_{\mu\nu} \quad , \tag{11.3}$$

then

$$P_\Lambda = -\rho_\Lambda \quad \text{with} \quad \rho_\Lambda = \frac{1}{8\pi G}\Lambda \quad . \tag{11.4}$$

The described fluid is "strange", since if Λ is positive, then pressure is negative. Since the cosmological constant term is proportinal to $g_{\mu\nu}$, it is Lorentz invariant and thus can be interpreted as vacuum energy. Using the FRLW metric, the Einstein equations with the cosmological constant are

$$\frac{\ddot{a}}{a} = -\frac{4\pi G}{3}(\rho + 3P) + \frac{\Lambda}{3} \quad , \tag{11.5}$$

$$H^2 = \frac{8\pi G}{3}\rho - \frac{k}{a^2} + \frac{\Lambda}{3} \quad . \tag{11.6}$$

Sometimes it is useful to introduce the Planck Mass

$$M_P = \sqrt{\frac{1}{8\pi G}} \quad , \tag{11.7}$$

and recast the Friedmann equations in the following form

$$3M_P^2 H^2 = \rho_m + \rho_\Lambda - \frac{3M_P^2 k}{a^2} \quad , \tag{11.8}$$

$$6M_P^2 \frac{\ddot{a}}{\dot{a}} = 2\rho_\Lambda - \rho_m \quad , \tag{11.9}$$

where we assumed $P_m = 0$ and have differentiated between the normal matter density ρ_m and the dark energy density $\rho_\Lambda = M_P^2 \Lambda$. Considering the first equation Eq. 11.8, a static Universe (H=0) without a cosmological constant, would imply a density: $\rho_m = 3M_P^2/a^2$ and k=1 (positive curvature).
Such a result is not consistent with Eq. 11.9, since it implies $\ddot{a}/a < 0$, namely a collapsing Universe.
The latter considerations show that for having a static Universe (H=0 and $\ddot{a}/a < 0$) we need

$$2\rho_\Lambda = \rho_m \quad \text{and} \quad \rho_\Lambda = \frac{M_P^2}{a^2} \quad , \tag{11.10}$$

forcing a fine-tuning of the constant's value. All these problems, together with the instability of a static Universe (see the exercises), and the discoveries of Hubble lead Einstein to abandon the cosmological constant.

11.3 Cosmological Constant and the Vacuum

In the vacuum, quantum fields can have fluctuations even if their mean value is zero. According to quantum field thery, the vacuum is populated by virtual particles which in certain conditions can have even measurable macroscopic effects, like in the case of the Casimir force.
Taking the example a free bosonic field, the creation/annihilation operators satisfy the relation $[a^\dagger, a] = 1$ and the Hamiltonian of the system reads

$$H = \frac{1}{2}\hbar\omega(aa^\dagger + a^\dagger a) = \hbar\omega(a^\dagger a + \frac{1}{2}) \quad . \tag{11.11}$$

The second term of the last member of the equation gives rise to a divergence if all the frequencies are summed up. Going to the continuum limit ($\hbar = 1$) and considering a bosonic field with mass m

$$\frac{1}{2}\sum_i \omega_i = \frac{1}{2}\int \frac{(d^3x)(d^3p)}{(2\pi)^3}\sqrt{k^2+m^2} = V\int \frac{k^2 dk}{4\pi^2}\sqrt{k^2+m^2} \quad , \tag{11.12}$$

where we performed the space integration and used spherical coordinates in momentum space.
The momentum integral diverges as expected, and we can introduce an UV cutoff for obtaining a finite result. The Planck mass seems a good possible choice, and the energy density for the boson field becomes

$$\rho_b = \int_0^{M_P} \frac{k^2 dk}{4\pi^2}\sqrt{k^2+m^2} \approx \int_0^{M_P} \frac{k^3 dk}{4\pi^2} = \frac{M_P^4}{16\pi^2} \approx \frac{1}{2^{10}\pi^4 G^2} \approx 10^{71}\ \text{GeV}^4 \quad , \tag{11.13}$$

where we used the ultra-relativistic approximation $k \gg m$.
In our universe, the energy density corresponding to the cosmological constant term is smaller than the critical density ρ_c

$$\rho_\Lambda < \rho_c \approx 10^{-46}\ \text{GeV}^4 \quad . \tag{11.14}$$

Instead, our rough estimate of the vacuum energy contribution from a quantum field leads to

$$\frac{\rho_b}{\rho_c} \approx 10^{117} \quad , \tag{11.15}$$

which is quite surprising: if the cosmological constant were so large, the Universe would be much different with respect to how it looks like today. A possibility is that supersymmetry exists: in this case the bosonic contributions are counter-balanced by the fermionic superpartners. We still did not observe supersymmetry, but even if we use a cut-off at the electroweak scale (or the scale at which supersymmetry should be broken) like ≈ 100 GeV, still we have $\rho_b/\rho_c \approx 10^{52}$.
The latter estimates show the difficulties in interpreting the cosmological constant as vacuum energy. Up to now (2020), the nature of dark energy remains elusive and we only observe its effects on the dynamics of the Universe.

11.4 Modified Gravity

Another possibility is that gravity is described by higher-order terms in the Einstein-Hilbert action. The Einstein equations can be obtained varying the following (relatively simple) action

$$S = \frac{1}{16\pi G}\int d^4x\sqrt{-g}R + S_{\text{matter}} \quad , \tag{11.16}$$

which could be modified including higher-order terms like R^n. For example, S. Carroll and collaborators proposed

$$S = \frac{1}{16\pi G}\int d^4x\sqrt{-g}\left(R - \frac{\mu^4}{R}S_{\text{matter}}\right) \quad , \tag{11.17}$$

resulting in the following equations of motion

$$\left(1+\frac{\mu^4}{R^2}\right)R_{\mu\nu} - \frac{1}{2}\left(1-\frac{\mu^4}{R^2}\right)g_{\mu\nu}R + \mu^4(g_{\mu\nu} - \nabla_{(\mu}\nabla_{\nu)})R^{-2} = 8\pi G T_{\mu\nu} \tag{11.18}$$

If $\mu = 0$ the last equation reduces to the Einstein one.
Considering the energy-momentum tensor T of a fluid, the Friedmann "Hubble" equation becomes

$$3M_P^2H^2 - \frac{\mu^4M_P^2}{12(\dot{H}+2H^2)^3}(2H\ddot{H} + 15H^2\dot{H}^2 + 6H^4) = \rho \quad . \tag{11.19}$$

A careful analysis of the last equation shows that there is the possibility of an accelerated expansion, although this version of modified gravity violates the equivalence principle.
In general, one could in principle consider the general class of theories

$$S = \frac{1}{16\pi G}\int d^4x\sqrt{-g}f(R) + S_{\text{matter}} \quad , \tag{11.20}$$

and see which ones give accelerated expansions. Such theories should anyhow respect the existing experimental constraints favouring the simpler Einstein-Hilbert action.

11.5 Coupling gravity with quantum fields

Models of the so-called *Quintessence* consider a scalar field

$$S = \int d^4x\sqrt{-g}\left[-\frac{1}{2}g^{\mu\nu}\partial_\mu\phi\partial_\nu\phi - V(\phi)\right] \quad , \tag{11.21}$$

which, varying with respect to $g_{\mu\nu}$ gives the energy-momentum tensor

$$T_{\mu\nu} = \partial_\mu\phi\partial_\nu\phi - g_{\mu\nu}\left[\frac{1}{2}\partial^\lambda\phi\partial_\lambda\phi + V(\phi)\right] \quad . \tag{11.22}$$

Comparing with the usual fluid energy-momentum tensor, we can conclude (co-moving frame)

$$\rho = \frac{1}{2}\dot{\phi}^2 + V(\phi) \quad , \quad P = \frac{1}{2}\dot{\phi}^2 - V(\phi) \quad , \tag{11.23}$$

and the Friedmann equations are

$$3M_P^2 H^2 = \frac{1}{2}\dot{\phi}^2 + V(\phi) \quad , \tag{11.24}$$

$$-2M_P^2 \dot{H} = \dot{\phi}^2 \quad . \tag{11.25}$$

Considering $a \propto t^n$, where with n=1 there is no acceleration, while $n > 1$ implies acceleration, the Friedmann equations imply a potential of the form

$$V = V_0 exp\left(-\sqrt{\frac{2}{n}}\frac{\phi}{M_P}\right) \quad . \tag{11.26}$$

This means that all the potentials "flatter" than the previous one with $n = 1$ can give rise to accelerated expansion. The quintessence scenario can be realized with scalar fields like axions, dilatons, or the Higgs field. There is a large variety of scenarios where gravity is coupled to one (or more) fields for trying to explain dark energy and here we mentioned only one out of many possibilities.

11.6 Dark Energy Measurements

Type 1a Supernovae
The Dark Energy effect was discovered in 1998-99 using observations on peculiar stars: Type Ia supernovae. These "stars" are actually binary systems (two stars orbiting one another) in which one of the stars is a white dwarf. The other star type can be anything from a giant star to a smaller white dwarf.
When a carbon/oxygen white dwarf accretes matter from a companion, it can exceed the Chandrasekhar limit of ≈1.44 solar masses: beyond this point, it cannot support itself with electron-degeneracy pressure (Pauli exclusion principle). The white dwarf eventually collapses to form a neutron star.

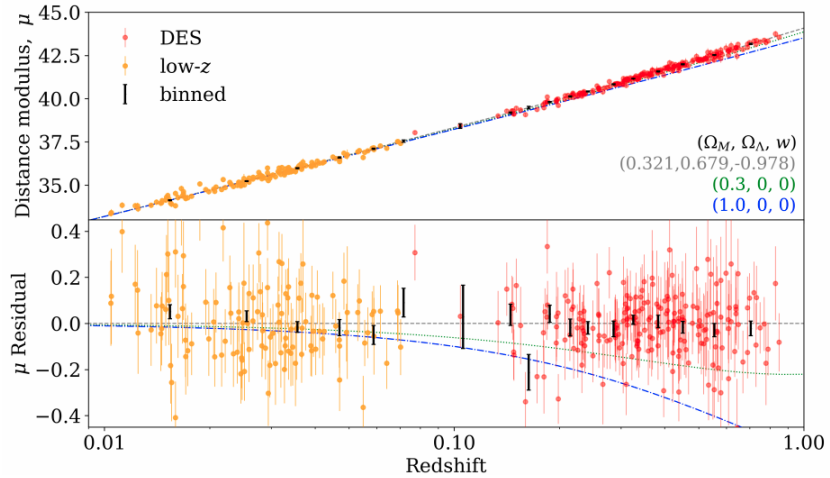

Figure 11.1: Supernova Type 1a distance measurements from the DES collaboration. The gray line and values represent the best fit to the data. In the lower panel are reported the residuals with respect to the best fit line.

The type Ia category of supernovae produces a consistent peak luminosity because the mass at explosion is fixed by the Chandrasekhar limit. This fixed value allows these stars'explosions to be used as standard candles: this allows to measure the distance of their host galaxies from us.

Distance Measurements

Dark Energy surveys measure the luminosity distance d_L of the supernovae as a function of the redshift and in particular the relevant variable is the *distance modulus* μ

$$\mu = m - M = 5 \log_{10} \left(\frac{d_L}{10 \text{ pc}} \right) \quad , \tag{11.27}$$

where m is the apparent magnitude and M the absolute magnitude. The absolute magnitude is defined as the apparent magnitude of an object when seen at a distance of 10 parsecs.

The luminosity distance is connected to the measurable light flux (power/surface) Φ: $d_L = \sqrt{L/(4\pi\Phi)}$, where L is the intrinsic luminosity of the object.

d_L is further connected to the cosmological parameters through

$$d_L = (1+z)c \int_0^z \frac{z'}{H(z')} \quad , \tag{11.28}$$

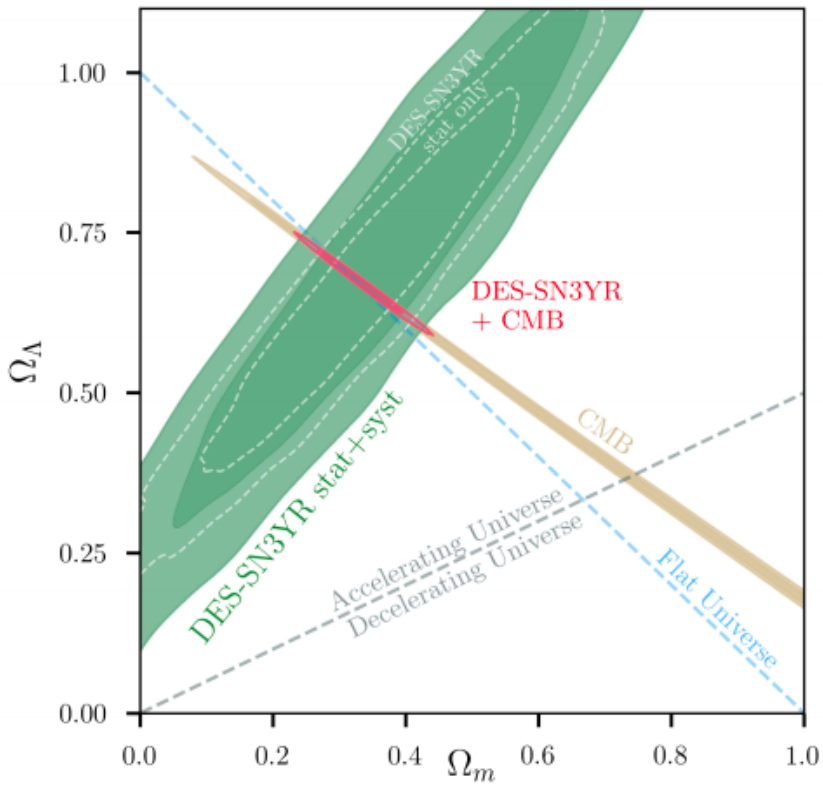

Figure 11.2: Constraints to the ΛCDM model with 68% and 95% confidence intervals.

where the Hubble parameter, through the Friedmann equations is expressed as a function of the red-shift

$$H(z) = H(0)\sqrt{\Omega_m(1+z)^3 + \Omega_\Lambda(1+z)^{3(1+w)}} \quad . \tag{11.29}$$

In Fig. 11.1 are reported the results of the DES dark energy survey collaboration. The very distent supernovae show a statistically significant deviation from models without dark energy. The best fitting model has $\Omega_m = 0.321$ and $\Omega_\Lambda = 0.679$ with an equation of state parameter $w = -0.978$. The result is consistent with a ΛCDM model with significant fraction of dark energy. In Fig. 11.2 the dark energy survey results are plotted together with the results from CMB. Together, they constrain even more the cosmological parameters and are consistent with an almost-flat Universe dominated by dark energy and accelerating expansion rate.

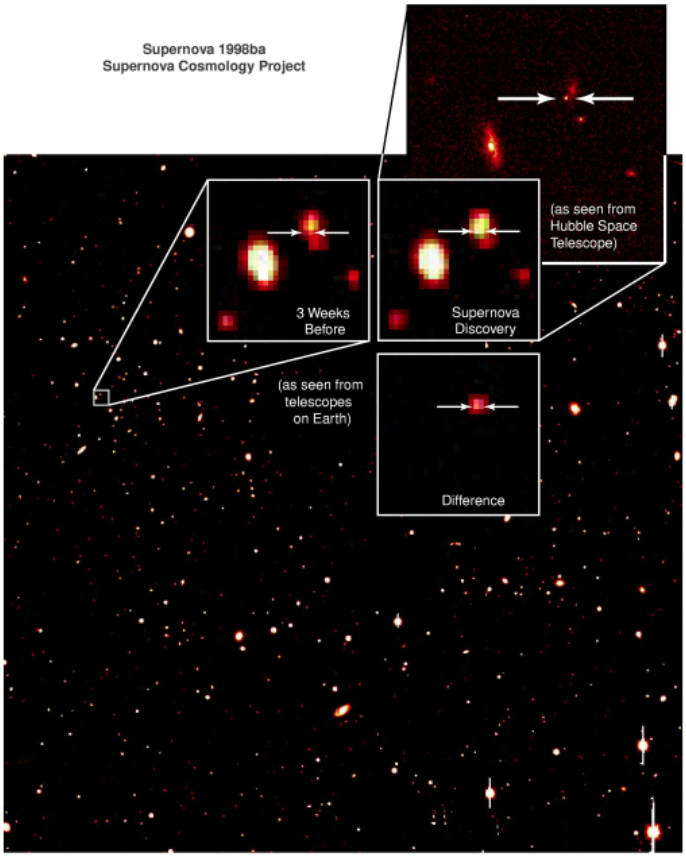

Figure 11.3: Supernova 1998ba observed during the supernova survey that lead to the discovery of Dark Energy and to the 2011 Nobel Prize won by S. Perlmutter, B.P. Schmidt, and A. Riess.

11.7 Experimental Details

Ia supernovae, are the brightest of the supernova types (by a factor ~ 6): that's why they are condidered as standard candles for very high distances measurements.
The glow of a Type 1a supernova lasts a few weeks and it faded away within a few months. The measurements use the magnitude at peak, which has a very consistent brightness (after calibration procedures). Since one can never predict a supernova explosion and supernovae only ex-

plode a couple of times per millennium in any given galaxy, the search for these objects must be carefully planned in order to obtain observation time at the best telescopes.
In practice, astronomers observe wide fields of sky out from the galactic plane. These patches of sky contain O(100) distant galaxies. After having observed O(10000) galaxies, after a period of 3 weeks, the same galaxies are observed again. The comparison between images allows the discovery of Type 1a supernovae. An example of obtained images is showed in Fig. 11.3

Chapter 12 | Gravitational Waves

12.1 Brief History

After the striking first verifications of the prediction of GR (Mercury's perihelion precession, bending of light rays from the Sun), **Einstein** worked on another consequence of the theory, namely gravitational waves. Unfortunately, the first 1916 paper Einstein wrote on the subject, contained mathematical errors that were only corrected in 1918. In 1922, **Eddington** pointed out (in addition to another mathematical mistake), that some of the wave solutions in Einstein's paper allowed speeds higher than that of light, sarcastically commenting that "the only speed of propagation relevant to them is the speed of thought". Now understood that the problem noticed by Eddington was due to artefacts of the coordinate system that Einstein used and therefore they were unphysical.
Eddington's critical remarks were reinforced by Einstein himself and his assistant **N. Rosen** which started to be convinced that gravitational wave emission was not possible.
The story ended only 35 years after: in 1957, **Felix Pirani** was finally able to show how gravitational waves were able to affect other bodies and later Hermann Bondi showed that gravitational waves were able to transport energy (like electromagnetic waves).
After that, **J. Wheeler** and **J. Weber** started to think that gravitational waves could be detectable.
In 1967, radio pulses were discovered from rotating neutron stars: these "pulsars" motivated **Joseph Taylor** to measure binary sytems composed by couples of such stars. The orbital properties of binaries are important because, according to GR, gravitational waves carry energy away from the system, forcing it to slow down its rotation. In 1974, Taylor and his graduate student **Russell Hulse** discovered the first binary pulsar and in

1993 were awarded the Nobel Prize in Physics for the discovery.
In 1981, orbital-period slow-down was measured in that system, with a magnitude exactly consistent with GR (within a small uncertainty).
J. Weber (U. of Maryland) tackled the experimental problem of detecting gravitational waves and came to the conclusion that two techniques were viable: resonant detectors and laser interferometers.
Resonant detectors were more affordable adn in 1965 Weber build his first detector: a 1.5-tonne, 1 m $\times$ 2 m cylindrical bar made of aluminium that would resonate is excited by a gravitational wave of the right frequency.
The Weber's cylinders had a resonance frequency of 1660 hertz and the piezoelectric sensors had to be very sensitive, since they had to detect a change in the cylinders' lengths by about 10^{-16} m.
In 1969 Weber announced the detection of a gravitational wave in two bars separated by 1000 km (Chicago-Maryand). Unfortunately, these results could not be reproduced by other experimental groups and the data analysis procedure was questioned.
Although the detection failed, the work of Weber stimulated the community and developed new technology. **Rainer Weiss** at MIT started to think about detecting gravitational waves and in 1972 he wrote a 23-page note in a MIT's quarterly newsletter describing for the first time the main experimental design for a laser interferometer. The Weiss design would later become the foundation of the **Laser Interferometer Gravitational-wave Observatory (LIGO)**.

12.2 Linearized General Relativity

For weak gravitational fields, we can linearize the metric tensor around the flat Lorentz spacetime $\eta_{\mu\nu}$

$$g_{\mu\nu} = \eta_{\mu\nu} + h_{\mu\nu} \quad \text{with} \quad |\eta_{\mu\nu}| \ll 1 \quad \text{and} \quad |\frac{\partial h_{\mu\nu}}{\partial x_\xi}| \ll 1 \quad . \tag{12.1}$$

Important relations the perturbation h must fulfill are

$$\begin{aligned} & h_{\mu\nu} = h_{\nu\mu} \quad , \\ & h^{00} = h_{00} \quad , \quad h^{ij} = h_{ij} \quad , \quad h^{0i} = -h_{i0} \quad , \\ & h^\chi_\nu = g^{\chi\mu} h_{\mu\nu} = (\eta^{\chi\mu} - h^{\chi\mu}) h_{\mu\nu} \approx \eta^{\chi\mu} h_{\mu\nu} \quad , \\ & h \equiv h^\nu_\nu \quad , \\ & \bar{h}_{\mu\nu} \equiv h_{\mu\nu} - \eta_{\mu\nu} \tfrac{h}{2} \quad . \end{aligned} \tag{12.2}$$

We introduce now small changes on the coordinates, which in GR are equivalent to a gauge transformation. "Small" changes means $|\xi^\mu \ll 1|$ and $|\partial\xi^\mu/\partial\xi_\beta| \ll 1$ with the properties

$$\begin{aligned}
&x^{\alpha'} \equiv x^\alpha + \xi^\alpha[x^\beta] \quad , \\
&x^\alpha = x^{\alpha'} - \xi^\alpha[x^\beta] = x^{\alpha'} - \xi^\alpha[x^{\beta'} - \xi^\beta] \approx x^{\alpha'} - \xi^\alpha[x^{\beta'}] \quad , \\
&\frac{\partial\xi^\alpha}{\partial\xi_\beta} = \frac{\partial x^{\alpha'}}{\partial x_{\beta'}}\frac{\partial x^{\beta'}}{\partial x_\beta} = \frac{\partial x^{\alpha'}}{\partial x_{\beta'}}\frac{\partial(x^\beta+\xi^\beta)}{\partial x_\beta} \approx \frac{\partial\xi^\alpha}{\partial\xi_{\beta'}} \quad , \\
&\frac{\partial x^\alpha}{\partial x_{\beta'}} = \frac{\partial x^{\alpha'}}{\partial x_{\beta'}} - \frac{\partial\xi^\alpha}{\partial\xi_{\beta'}} = \delta^\alpha_\beta - \frac{\partial\xi^\alpha}{\partial\xi_\beta} \quad , \\
&\frac{\partial x^{\alpha'}}{\partial x_\beta} = \frac{\partial x^\alpha}{\partial x_\beta} + \frac{\partial\xi^\alpha}{\partial\xi_\beta} = \delta^\alpha_\beta + \frac{\partial\xi^\alpha}{\partial\xi_\beta} \quad , \\
&g_{\alpha'\beta'} = \eta_{\alpha'\beta'} + h_{\alpha'\beta'} = \eta_{\alpha\beta} + h_{\alpha'\beta'} \quad .
\end{aligned} \tag{12.3}$$

We expect that δ does not change at first order and indeed

$$\delta^{\alpha'}_{\beta'} = \frac{\partial x^{\alpha'}}{\partial x_{\beta'}} = \frac{\partial(x^\alpha + \xi^\alpha)}{\partial x_\beta}\frac{\partial x^\beta}{\partial x_{\beta'}} = (\delta^\alpha_\beta + \frac{\partial\xi^\alpha}{\partial\xi_\beta})\frac{\partial(x^{\beta'} - \xi^\beta)}{\partial x_{\beta'}} \quad , \tag{12.4}$$

and performing the derivative in the second half of the last part of the latter equation and multiplying we have

$$\delta^{\alpha'}_{\beta'} = \delta^\alpha_\beta = \frac{\partial x^\alpha}{\partial x_\beta} \quad , \tag{12.5}$$

which proves also that $\eta_{\alpha'\beta'} = \eta_{\alpha\beta}$.
With the above properties, it can also be proved that

$$\begin{aligned}
h_{\alpha\beta} &= h_{\alpha'\beta'} + \frac{\partial\xi_\alpha}{\partial\xi_\beta} + \frac{\partial\xi_\beta}{\partial\xi_\alpha} \quad , \\
h_{\alpha'\beta'} &= h_{\alpha\beta} - \frac{\partial\xi_\alpha}{\partial\xi_\beta} - \frac{\partial\xi_\beta}{\partial\xi_\alpha} \quad .
\end{aligned} \tag{12.6}$$

The above results follow considering the tensor transformation laws

$$g_{\mu'\nu'}(x') = \frac{\partial x^\alpha}{\partial x^{\mu'}}\frac{\partial x^\beta}{\partial x^{\nu'}}g_{\alpha\beta}(x) \quad . \tag{12.7}$$

Substituting the definition of the coordinate transformation ($x' = x - \xi$)

$$g_{\mu'\nu'}(x') = (\delta^\alpha_{\mu'} - \frac{\partial\xi^\alpha}{\partial x_{\mu'}})(\delta^\beta_{\nu'} - \frac{\partial\xi^\beta}{\partial x_{\nu'}})[g_{\alpha\beta}(x') - \frac{\partial g_{\alpha\beta}}{\partial x_\sigma}(x')\xi^\sigma] \tag{12.8}$$

and simplifying

$$g_{\mu'\nu'}(x') = g_{\mu\nu}(x) - \frac{\partial \xi^\alpha}{\partial x_\mu} g_{\alpha\nu} - \frac{\partial \xi^\beta}{\partial x_\nu} g_{\mu\beta} - \frac{\partial g_{\mu\nu}}{\partial x_\sigma} \xi^\sigma \quad . \tag{12.9}$$

The last term of the previous result can be neglected in the case of the Minkowski spacetime and the obtained formula shows how also $h_{\mu\nu}$ transforms under a coordinate transformation.
The obtained transformation property shows that the perturbation tensor h is not unique but it remains small even if changed by a gauge transformation: the idea is to choose the best transformation for simplifying the calculations in the linearized regime.
For the linearization of the Einstein equations, we need to linearize the Ricci tensor, which is function of derivatives and products of Christoffel symbols. The products can be discarded, since they are of higher order, while the linearization of the derivatives become

$$\frac{\partial \Gamma^\chi_{\beta\mu}}{\partial x_\nu} = \frac{1}{2}\eta^{\sigma\chi}\left[\frac{\partial^2 h_{\beta\sigma}}{\partial x_\mu \partial x_\nu} + \frac{\partial^2 h_{\mu\sigma}}{\partial x_\beta \partial x_\nu} - \frac{\partial^2 h_{\beta\mu}}{\partial x_\sigma \partial x_\nu}\right] \quad , \tag{12.10}$$

$$\frac{\partial \Gamma^\chi_{\beta\nu}}{\partial x_\mu} = \frac{1}{2}\eta^{\sigma\chi}\left[\frac{\partial^2 h_{\beta\sigma}}{\partial x_\mu \partial x_\nu} + \frac{\partial^2 h_{\nu\sigma}}{\partial x_\beta \partial x_\mu} - \frac{\partial^2 h_{\beta\nu}}{\partial x_\sigma \partial x_\mu}\right] \quad , \tag{12.11}$$

Substituting in the Riemann curvature tensor

$$R_{\alpha\beta} = g_{\alpha\chi} R^\chi_{\beta\mu\nu} = g_{\alpha\chi}\left[\frac{\partial \Gamma^\chi_{\beta\mu}}{\partial x_\nu} - \frac{\partial \Gamma^\chi_{\beta\nu}}{\partial x_\mu} + \Gamma^\chi_{\gamma\mu}\Gamma^\gamma_{\beta\nu} - \Gamma^\chi_{\gamma\nu}\Gamma^\gamma_{\beta\mu}\right] \approx g_{\alpha\chi}\left[\frac{\partial \Gamma^\chi_{\beta\mu}}{\partial x_\nu} - \frac{\partial \Gamma^\chi_{\beta\nu}}{\partial x_\mu}\right] \tag{12.12}$$

we finally obtain

$$R_{\alpha\beta\mu\nu} = \frac{1}{2}\eta_{\alpha\chi}\eta^{\sigma\chi}\left[\frac{\partial^2 h_{\nu\sigma}}{\partial x_\beta \partial x_\mu} - \frac{\partial^2 h_{\beta\nu}}{\partial x_\sigma \partial x_\mu} - \frac{\partial^2 h_{\mu\sigma}}{\partial x_\beta \partial x_\nu} + \frac{\partial^2 h_{\beta\mu}}{\partial x_\sigma \partial x_\nu}\right] \quad . \tag{12.13}$$

Multiplying the Lorentz metrix tensors in front of the last equation

$$R_{\alpha\beta\mu\nu} = \frac{1}{2}\left[\frac{\partial^2 h_{\nu\alpha}}{\partial x_\beta \partial x_\mu} - \frac{\partial^2 h_{\beta\nu}}{\partial x_\alpha \partial x_\mu} - \frac{\partial^2 h_{\mu\alpha}}{\partial x_\beta \partial x_\nu} + \frac{\partial^2 h_{\beta\mu}}{\partial x_\alpha \partial x_\nu}\right] \quad , \tag{12.14}$$

we can also calculate the Ricci tensor

$$R_{\beta\nu} = g^{\alpha\mu} R_{\alpha\beta\mu\mu} = \eta^{\alpha\mu} R_{\alpha\beta\mu\nu} \tag{12.15}$$

and threfore

$$R_{\beta\nu} = \frac{1}{2}\left[\frac{\partial^2 h^{\mu}_{\nu}}{\partial x_\beta \partial x_\mu} - \eta^{\alpha\mu}\frac{\partial^2 h_{\beta\nu}}{\partial x_\alpha \partial x_\mu} - \frac{\partial^2 h}{\partial x_\beta \partial x_\nu} + \frac{\partial^2 h_{\alpha\beta}}{\partial x_\alpha \partial x_\nu} \quad .\right] \quad . \tag{12.16}$$

In the last equation, the second term is just the wave equation in disguise

$$-(\nabla^2 - \frac{\partial^2}{\partial t^2})h_{\beta\nu} \quad , \tag{12.17}$$

and this shows already where we will end with this calculation. We still need the Ricci scalar for having the complete Einstein equations: renaming some indices we have

$$R = g^{\beta\nu} R_{\beta\nu} = \eta^{\beta\nu} R_{\beta\nu} = \frac{\partial^2 h_{\mu\alpha}}{\partial x_\mu \partial x_\alpha} - \frac{\partial^2 h_{\alpha\mu}}{\partial x_\mu \partial x_\alpha} \quad . \tag{12.18}$$

We have now all the ingredients for calculationg the Einstein tensor

$$G_{\beta\nu} = R_{\beta\nu} - \frac{1}{2} g_{\beta\nu} R \approx G_{\beta\nu} = R_{\beta\nu} - \frac{1}{2}\eta_{\beta\nu} R \approx \tag{12.19}$$

$$\frac{\partial^2 h^{\mu}_{\nu}}{\partial x_\beta \partial x_\mu} - \eta^{\alpha\mu}\frac{\partial^2 h_{\beta\nu}}{\partial x_\alpha \partial x_\mu} - \frac{\partial^2 h}{\partial x_\beta \partial x_\nu} + \frac{\partial^2 h^{\alpha}_{\beta}}{\partial x_\alpha \partial x_\nu} - \frac{\eta_{\beta_\nu}}{2}\left(\frac{\partial^2 h^{\mu\alpha}}{\partial x_\mu \partial x_\alpha} - \eta^{\alpha\mu}\frac{\partial^2 h}{\partial x_\mu \partial x_\alpha}\right) \quad . \tag{12.20}$$

The last equation can be rewritten with the trace-inverse $\bar{h}$ instead of h

$$G_{\beta\nu} = \frac{1}{2}\left[\frac{\partial}{\partial x_\beta}\frac{\partial \bar{h}^{\mu}_{\nu}}{\partial x_\mu} - \eta^{\alpha\mu}\frac{\partial^2 \bar{h}_{\beta\nu}}{\partial\alpha\partial\mu} + \frac{\partial}{\partial x_\nu}\frac{\partial \bar{h}^{\alpha}_{\beta}}{\partial x_\alpha} - \eta_{\beta\nu}\eta^{\mu\xi}\frac{\partial}{\partial x_\mu}\frac{\partial \bar{h}^{\alpha}_{\xi}}{\partial x_\alpha}\right] \quad . \tag{12.21}$$

Analogously to the case of electrodynamics, we can choose a *Lorentz gauge*[1]

$$\frac{\partial \bar{h}^{\chi}_{\sigma}}{\partial x_\chi} = 0 \quad . \tag{12.22}$$

[1]It looks like historically this gauge choice was due to Ludvig Valentin Lorenz (Denemark), and not Hendrik Antoon Lorentz (Dutch). Likely, due to the similarity of the names, the error propagated through the literature. We will keep using "Lorentz" in the following.

After this choice, the Einstein tensor reduces to

$$G_{\beta\nu} = \frac{\eta^{\alpha\mu}}{2}\frac{\partial^2 \bar{h}_{\beta\nu}}{\partial x_\alpha \partial x_\mu} \quad , \tag{12.23}$$

which is nothing less but the wave equation. Substituting this result for the Einstein tensor into the Einstein equation

$$(\nabla^2 - \frac{\partial}{\partial t^2})\bar{h}^{\beta\nu} = -16\pi T^{\beta\nu} \quad . \tag{12.24}$$

The result tells us that the linearized version of the Einstein equation is the wave equation with the energy-momentum tensor as the source term. This equation thus describes gravitational waves which travel at the speed of light, and there is no restriction to the allowed frequencies.

12.3 Plane Waves

In empty space, all the components of the energy-momentum tensor are zero and the obtained wave equation has solutions of the form

$$\bar{h}_{\mu\nu} = A_{\mu\nu}\exp(ik_\chi x^\chi) = A_{\mu\nu}e^{ik_i x^i}e^{-i\omega t} \quad , \tag{12.25}$$

where A is the (tensor) amplitude and k is the wave vector and both quantities are constant. It can be verified that

$$\frac{\partial \bar{h}_{\mu\nu}}{\partial x_\beta} = ik_\beta \bar{h}_{\mu\nu} \quad , \tag{12.26}$$

$$(\nabla^2 - \frac{\partial}{\partial t^2})\bar{h}_{\mu\nu} \equiv \Box\bar{h}_{\mu\nu} = -(k_\beta k^\beta)\bar{h}_{\mu\nu} = 0 \quad , \tag{12.27}$$

$$k_\beta k^\beta = 0 \quad \Rightarrow \quad \omega = \pm\sqrt{k_1^2 + k_2^2 + k_3^2} \quad . \tag{12.28}$$

The wave vector is $k = (k_0, \vec{k}) = (\omega, \vec{k})$ and the wave travels in the direction of $\vec{k}$. The Lorentz gauge condition implies also

$$k_\nu A^\nu_\mu = 0 \quad , \tag{12.29}$$

which is an *orthogonality* restriction on the components of the amplitude tensor.

12.4 The TT gauge

We can further choose a more convenient coordinate transformation for understanding gravitational waves. In general, the Einstein equations are 10 and up to now we just choose the Lorentz gauge which gives four constraints: we still have 6 degrees of freedom left. We can further choose a coordinate transformation such that

$$\Box\xi_\mu = 0 \quad , \tag{12.30}$$

so that the Lorentz gauge is still respected. We choose $\xi_\mu = B_\mu \exp(ik_\chi r^\chi)$, which respects the gauge constraints. This produces a solution called ${}^{TT}\bar{h}_{\mu\nu}$ which is called the *transverse-traceless* solution (see next) and we have also ${}^{TT}\bar{h}^\mu_\mu = \bar{A}^\mu_\mu = 0$, where $\bar{A}$ is the amplitude of the TT solution.
We know already how h transforms, so we can use the new coordinate transformation on it

$$\bar{h}_{\mu'\nu'} \equiv^{TT} \bar{h}_{\mu\nu} = \bar{h}_{\mu\nu} - \frac{\partial\xi_\mu}{\partial x_\nu} - \frac{\partial\xi_\nu}{\partial x_\mu} + \eta_{\mu\nu}\frac{\partial\xi^\chi}{\partial x_\chi} \quad , \tag{12.31}$$

Inserting the coordinate transformation

$$\bar{A}_{\mu\nu} = A_{\mu\nu} - i(B_\mu k_\nu + k_\mu B_\nu - \eta_{\mu\nu}B^\chi k_\chi) \tag{12.32}$$

$$\bar{A}^\alpha_\mu = A^\alpha_\mu - i(B_\mu k^\alpha + k_\mu B^\alpha - \delta^\alpha_\mu B^\chi k_\chi) \tag{12.33}$$

and the traceless condition becomes

$$0 = \bar{A}^\mu_\mu = A^\mu_\mu - i(B_\mu k^\mu + k_\mu B^\mu - 4B^\chi k_\chi) = A^\mu_\mu + 2iB_\mu k^\mu \Rightarrow iB^\mu k_\mu = -A^\mu_\mu/2 \quad . \tag{12.34}$$

If the trace of A is not zero ($A^\mu_\mu \neq 0$), we can choose B_μ in the coordinate transformation such that the trace of $\bar{A}$ is zero (and therefore ${}^{TT}\bar{h}^\mu_\mu = 0$). This amounts to add four additional constraints (on top of the Lorentz gauge) and reduce the degrees of freedom to two. We can choose the B_μ component such that

$$h^{0\mu} = 0 \quad , \quad h^i_i = 0 \quad , \quad \frac{\partial h^{ij}}{\partial x_i} = 0 \quad . \tag{12.35}$$

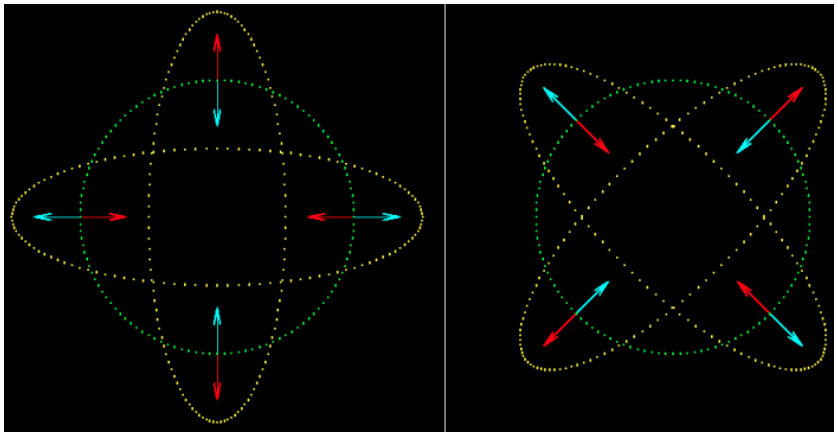

Figure 12.1: Effect of a GW on a ring of massive particles for the two polarization states.

The last equations fully define the tranverse-traceless gauge (TT).
Taking a GW propagating along the z direction ($k_\mu = (\omega, 0, 0, -\omega)$) the solution is

$$ {}^{TT}h^{\mu\nu} = \begin{pmatrix} 0 & 0 & 0 & 0 \\ 0 & h_+ & h_\times & 0 \\ 0 & h_\times & -h_+ & 0 \\ 0 & 0 & 0 & 0 \end{pmatrix} \cos[\omega(t-z)] \quad . \tag{12.36} $$

The two degrees of freedom left are associated to the two polarization states of the GW each with amplitudes h_+ and $h_\times$.
The line element associated with h is (with $\phi = \omega(t-z)$)

$$ ds^2 = -dt^2 + (1 + h_+ \cos\phi)dx^2 + (1 - h_+ \cos\phi)dy^2 + 2h_\times \cos\phi dxdy \quad . \tag{12.37} $$

12.5 Effect on Particles

Assuming $\tau \approx t$, the linearized geodetic equation is

$$ \frac{du^\mu}{dt} = -\frac{1}{2}\left(\frac{\partial h_{\mu\alpha}}{\partial x_\beta} + \frac{\partial h_{\beta\mu}}{\partial x_\alpha} - \frac{\partial h_{\alpha\beta}}{\partial x_\mu}\right) u^\alpha u^\beta \tag{12.38} $$

Considering a static particle, its four-velocity will be $u^\mu = (1,0,0,0)$ and the last equation reduces to

$$\frac{du^\mu}{dt} = -\left(\frac{\partial h_{\mu 0}}{\partial x_0} - \frac{1}{2}\frac{\partial h_{00}}{\partial x_\mu}\right) \quad . \tag{12.39}$$

Remembering the TT gauge ($h_{00} = h_{\mu 0} = 0$), we have $\frac{du^\mu}{dt} = 0$: a GW does not affect an isolated particle at first order.
If instead we consider two particles at a space points $-x_0$ and x_0 with a GW travelling in the z direction, the distance between the points will be described by

$$ds^2 = -g_{11}dx^2 = (1-h_{11})(2x_0)^2 = (1-h_+)(2x_x)^2 \Rightarrow \Delta s \approx \left(1 - \frac{1}{2}h_+ \cos\omega t\right)(2x_0) \quad . \tag{12.40}$$

Analogously for two points on the y axis, we will have

$$s \approx \left(1 + \frac{1}{2}h_+ \cos\omega t\right)(2x_0) \quad . \tag{12.41}$$

Considering a ring of particles, according to the rotation in the xy plane of the last two distances, the result of the change in their positions as a function of time can be seen in Fig. 12.1.
It is worth noting that this result was obtained in the TT gauge, but it is actually gauge-independent. The gauge freedom allows to choose a coordinate system for simplifying the calculations but the observable consequences are independent from this choice.

12.6 Observation of gravitational waves with laser interferometers

The last formula can be approximately rewritten as a fractional lenght change

$$\frac{\delta L}{L} \approx \frac{1}{2}h_+ \quad , \tag{12.42}$$

and sometimes the amplitude h is called the *wave strain*. This fractional change is relevant in interferometric experiments measuring gravitational

waves.
GW interferometers use laser light sent in two different directions towards suspended mirrors. The reflected light from the two paths is tuned to destructively interfere and give a zero signal on a light detector. Phase differences are induced by the passage of a GW (which changes the relative length of the two paths) which makes an interference pattern appear and the light detector can pick it up.
The GW induces the accumulation of an extra phase

$$\delta\phi = 4\pi\frac{\delta L}{\lambda} \quad , \tag{12.43}$$

where λ is the wave length and δL is the distance change between the mirror and the beam-splitter. The last formula is valid if the metric perturbation does not change much during the light travel in the interferometer. A more detaild analysis is needed for high-frequency GWs: this case is relevant for space-based detectors.
Considering L-shaped interferometers along the x and y directions as in the case if LIGO, using the strain formulas derived before, we can write for the fractional change of the two arms

$$\frac{\delta L_x}{L} \approx \frac{1}{2}h_+ \quad , \tag{12.44}$$

$$\frac{\delta L_y}{L} \approx -\frac{1}{2}h_+ \quad . \tag{12.45}$$

From these deformations, we see that the GW acts tidally, shortening one arm and stretching the other with a time variation given approximately by a sinusoidal function.
The $h_\times$ polarization component acts in a similar way, just rotated by 45° with respect to the interferometer's x-y reference frame. In general, since the GW can have polarization axes which are not aligned with the interferometer's arms, we have to expect a GW with a weighted combination of the two polatization components.
The general working principle of GW interferometers like LIGO is showed in Fig. 12.2.

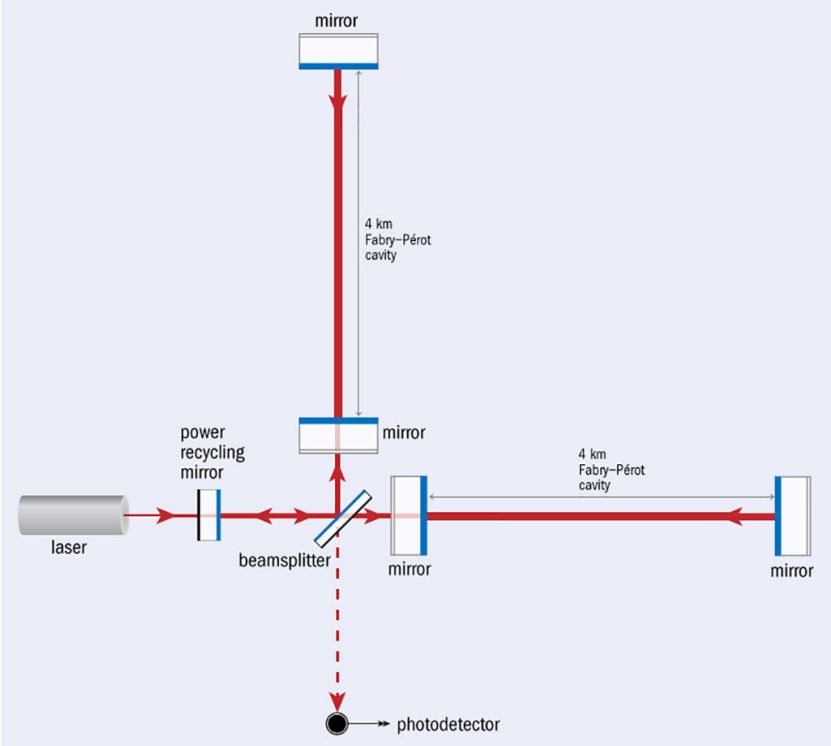

Figure 12.2: Working principle of the LIGO interferometer.

12.7 Gravitational wave energy and amplitude

The energy flux carried by a GW with frequency f and typical amplitude (for both polarizations) h is

$$F_{GW} = \frac{\pi}{4} f^2 h^2 \quad . \tag{12.46}$$

Restoring the c and G factors and rescaling to realistic values

$$F_{GW} = 3 \frac{\text{mW}}{\text{m}^2} \left(\frac{h}{10^{-22}} \right)^2 \left(\frac{f}{1\ \text{kHz}} \right)^2 \quad . \tag{12.47}$$

By comparison, this energy flux is comparable (even higher) to the one emitted by the full moon.
If we now integrate over a sphere of radius R and assume an emission

duration T, we have for the typical amplitude

$$h = 10^{-21} \left(\frac{E_{GW}}{0.01 M_{sun} c^2} \right)^{1/2} \left(\frac{R}{20 \text{ Mpc}} \right)^{-1} \left(\frac{f}{1 \text{ kHz}} \right)^{-1} \left(\frac{T}{1 \text{ ms}} \right)^{-1/2} \quad . \tag{12.48}$$

The latter amplitude is normalized to numbers fitting a gravitational collapse within the Virgo cluster and it also set the sensitivity scale for interferometric gravitational wave detectors.
The same formula can be applied to binary systems radiating energy with GWs increasing the parameter T.

12.8 Gravitational Wave Sources

Let's start considering an "artificial" source of GWs: an aluminum bar with 1 m width, length L=20 m, and weight 490 tons. Given the properties of aluminum and the width of the bar, the maximum rotation speed (i.e. a higher speed will break the bar) around an axis orthogonal to the bar's axis and going through its center is $\omega = 28$ rad/s. The rotational energy of such a system is $E_{rot} = (1/2) I \omega^2$ and the power is

$$P_{rot} = E_{rot} \cdot \omega = \frac{1}{24} M L^2 \omega^3 \tag{12.49}$$

where we used the moment of inertia of a bar $I = (1/12) M L^2$.
In natural units, the power is a dimensionless quantity and general relativity says that the gravitational wae power is approximately

$$P_{GW} \approx P_{rot}^2 \quad . \tag{12.50}$$

For restoring the normal units, we need the conversion factor

$$P_0 = \frac{c^5}{G} \approx 3.6 \cdot 10^{59} \text{ arg/s} = 2 \times 10^5 \times M_{sun} c^2 / \text{sec} \quad . \tag{12.51}$$

Combininig the last three equations

$$P_{GW} \approx (10^{-41})^2 \cdot P_0 \approx 10^{-23} \text{ erg/s} \quad . \tag{12.52}$$

With some effort such GWs could be created in a laboratory experiment, but as it is clear from the number, the radiated power will be incredibly

small and hardly measurable.
We can try again considering an astrophysical system of mass M and typical spatial extension R.
The virial theorem says that the average kinetic energy of the system will be $K \sim M^2/R$ and therefore the typical time (e.g. the orbital time of two pulsars or black holes) will be

$$T \sim \frac{R}{\sqrt{M/R}} = \sqrt{\frac{R^3}{M}} \quad . \tag{12.53}$$

The rotation power of the system is therefore

$$P_{rot} \sim \frac{K}{T} \sim \left(\frac{M}{R}\right)^{5/2} \quad . \tag{12.54}$$

Since GR says that the GW power is the square of the rotation power, in c.g.i units we have

$$P_{GW} \sim \left(\frac{M}{R}\right)^5 P_0 \quad . \tag{12.55}$$

If the considered system is rather symmetric, the quadrupole moment will be reduced and so will be also for the radiated power which will be lower than the one estimated with the last formula.
Looking more closely the case of two astrophysical bodies with masses m_1 and m_2 separated by a distance a and rotating around a common center of mass, Kepler's law says that

$$\omega^2 a^3 = m_1 + m_2 \equiv M \quad . \tag{12.56}$$

The kinetic energy K and the potential energy V are connected by

$$K = -\frac{1}{2}V = \frac{1}{2}\frac{m_1 m_2}{a} \quad . \tag{12.57}$$

Defining the reduced mass $\mu = m_1 m_2/M$, the radiated power as GWs is $P_{GW} \sim K\omega$:

$$P_{GW} \sim \frac{\mu^2 M^3}{4a^5} P_0 \quad , \tag{12.58}$$

in c.g.s units. The exact result based on GR is

$$P_{GW} = \frac{32}{5}\frac{\mu^2 M^3}{a^5} f(\epsilon) P_0 \quad , \tag{12.59}$$

with

$$f(\epsilon) = \left(1 + \frac{73}{24}\epsilon^2 + \frac{37}{96}\epsilon^4\right)\left(1 - \epsilon^2\right)^{-7/2} \quad . \tag{12.60}$$

The parameter ϵ is the eccentricity of the orbit. Neglecting GR, our classical estimate is wrong by roughly one order of magnitude, which is not too bad, given the intensity of the involved gravitational fields.
The emission of GWs brings the two objects in an inspiraling trajectory. The change of kinetic energy due to GW emission is

$$\frac{dK}{dt} = \frac{1}{2}\frac{\mu M}{a^2}\frac{da}{dt} = -L_{GW} = -\frac{32}{5}\frac{\mu^2 M^3}{a^5} \quad . \tag{12.61}$$

Solving the differential equation by separation of variables we can obtain the variation of the orbital radius with time

$$a = a_0\left(1 - \frac{t}{\tau}\right)^{1/4} \quad , \tag{12.62}$$

with

$$\tau = \frac{5}{256}\frac{a_0^4}{\mu M^2} \quad . \tag{12.63}$$

It is interesting to compare some inspiral times due to GW emission:

System	Period	Spiral time	P_{GW} (erg/s) (erg/s)	Flux on Earth (erg/s/cm^2)
Sun-Jupiter	11.86 yr	2.5×10^{23}yr	5.2×10^{10}	~ 0
Sirius A/B	49.94 yr	7.2×10^{21}yr	1.1×10^{15}	1.3×10^{-24}
Black holes	12 sec	3.2 yr	3.2×10^{41}	2.7×10^{-3}

The black holes in the table are one solar mass each and at a distance of 1kpc from the Earth. From these values, it is clear that only for extreme astrophysical objects we have a chance of detecting directly the emitted gravitational waves.

Chapter 13 | Cosmological Perturbations

13.1 Introduction

Assuming there was an inflationary phase after the birth of the Universe, right after very small perturbations in the matter density should have been present. The gravitational force made these initially small perturbations grow and eventually became the structures we observe today (stars, galaxies, clusters of galaxies,..). Gravitation acts on matter during expansion and thus we have to develop a theory for the evolutions of density perturbations in a Friedmann Universe.

13.2 Classical Newton's theory for non-relativistic matter

In a non-relativistic setting, $v \ll c$ and the evolution of a self-gravitating gas with density $\rho(r,t)$, velocity $v(r,t)$, and gravitational potential $\phi(r,t)$ is described by the fluidodynamical equations

$$\frac{\partial \rho}{\partial t} + \nabla \cdot (\rho v) = 0 \quad \text{Continuity Equation} \quad , \tag{13.1}$$

$$\frac{\partial v}{\partial t} + (v \cdot \nabla) v = -\frac{\nabla P}{\rho} - \nabla \phi \quad \text{Euler Equation} \quad , \tag{13.2}$$

$$\nabla^2 \phi = 4\pi G \rho \quad \text{Poisson Equation} \quad . \tag{13.3}$$

In the previous equations and in the following, the position r and velocity v are intended as 3-vectors

Let's now consider the expansion with the Hubble law $v(r,t) = (\dot{a}/a)r = H(t)r$. The continuity equation becomes

$$\frac{\partial \rho}{\partial t} + \rho \nabla \cdot v + (v \cdot \nabla)\rho = \frac{\partial \rho}{\partial t} + \rho \nabla \cdot v = 0 \quad . \tag{13.4}$$

Noticing that $\nabla \cdot v = \nabla(Hr) = 3H$ we have

$$\frac{\partial \rho}{\partial t} + 3H\rho = 0 \quad . \tag{13.5}$$

The term $3H\rho$ accounds for the expansion of the Universe.
The last result should be familiar since it follows also from evaluating

$$\frac{1}{a^3}\frac{d}{dt}(\rho a^3) = 0 \quad , \tag{13.6}$$

which simply states that $\rho \propto a^{-3}$, as we expect from the diluition of a gas in an expanding volume.
Considering now a spherically symmetric distribution, in the radial spherical coordinate, the Poisson equation reads

$$\nabla^2 \phi = \frac{1}{r^2}\frac{\partial}{\partial r}\left(r^2 \frac{\partial \phi}{\partial r}\right) = 4\pi G \rho \quad , \tag{13.7}$$

and the solution is $\phi = (2\pi G/3)\rho r^2$. Inserting now the Hubble relation $v = Hr$ in the Euler's equation for a "cold" gas (P=0) (and $\dot{r} = 0$, where r is the modulus of the position vector)

$$r\frac{\partial H}{\partial t} + H^2(r \cdot \nabla)r = (\dot{H} + H^2)r = -\nabla \phi \quad , \tag{13.8}$$

and inserting the solution for the gravitational potential and remembering that $\dot{H} + H^2 = \ddot{a}/a$ we have

$$\frac{\ddot{a}}{a} = -\frac{4\pi G}{3}\rho \quad , \tag{13.9}$$

which is the Friedmann "acceleration" equation. In this sense, the classical result is not different from the general relativistic result.
If we are in presence of relativistic matter or radiation, then $P \neq 0$ and we have to substitute in the previous calculations $\rho \to \rho + P/c^2$.

13.3 First order perturbations for non-relativistic matter

For understanding the propagation of fluctuations, we consider small first-order perturbations around average values denoted with the subscript "0" (which are the solutions obtained from the homogeneous expanding Universe of the previous section)

$$\rho(r,t) = \rho_0(t) + \delta\rho(r,t) \tag{13.10}$$
$$v(r,t) = v_0(r,t) + \delta v(r,t) \tag{13.11}$$
$$\phi(r,t) = \phi_0(r,t) + \delta\phi(r,t) \tag{13.12}$$

With the perturbed quantities, the continuity equation becomes

$$\frac{\partial\rho_0}{\partial t} + \frac{\partial\delta\rho}{\partial t} + \rho_0\nabla\cdot v_0 + \rho_0\nabla\cdot\delta v + \delta\rho\nabla\cdot v_0 + v_0\cdot\nabla\delta\rho = 0 \tag{13.13}$$

Recognizing the continuity equation for ρ_0 and v_0 in the last expression we have (remembering $v = Hr$)

$$\frac{\partial\delta\rho}{\partial t} + \rho_0\nabla\cdot\delta v + 3H\delta\rho + v_0\cdot\nabla\delta\rho = 0 \quad . \tag{13.14}$$

For the Euler equation,

$$\frac{\partial v_0}{\partial t} + \frac{\partial\delta v}{\partial t} + v_0\cdot\nabla v_0 + v_0\cdot\nabla\delta v + \delta v\cdot\nabla v_0 + \frac{\nabla\delta P}{\rho_0} + \nabla\phi_0 + \nabla\delta\phi = 0 \quad . \tag{13.15}$$

Again identifying the Euler equation for v_0 we have

$$\frac{\partial\delta v}{\partial t} + v_0\cdot\nabla\delta v + \delta v\cdot\nabla v_0 + \frac{\nabla\delta P}{\rho_0} + \nabla\delta\phi = 0 \quad . \tag{13.16}$$

The same can be done with the Poisson equation

$$\nabla^2\phi_0 + \nabla^2\delta\phi - 4\pi G\rho_0 - 4\pi G\delta\rho = \nabla^2\delta\phi - 4\pi G\delta\rho = 0 \quad . \tag{13.17}$$

We now change the variables with a small abuse of notation:

$$\delta \equiv \frac{\delta\rho}{\rho_0} \quad . \tag{13.18}$$

This implies that

$$\dot{\delta} = \frac{\partial \delta\rho/\rho_0}{\partial t} = \frac{1}{\rho_0}\frac{\partial \rho}{\partial t} - \frac{\delta\rho}{\rho_0^2}\frac{\partial \rho_0}{\partial t} = \frac{1}{\rho_0}\frac{\partial \rho}{\partial t} + 3H\frac{\delta\rho}{\rho_0} \tag{13.19}$$

$$\nabla\delta = \frac{1}{\rho_0}\nabla\delta\rho \tag{13.20}$$

$$(\delta v \cdot \nabla)v_0 = (\delta v_0 \cdot \nabla)(Hr) = H\delta v \tag{13.21}$$

Using the new variable δ and its properties, the continuity, Euler and Poisson equations become

$$\dot{\delta} + \nabla \cdot \delta v + v_0 \cdot \nabla\delta = 0 \tag{13.22}$$

$$\frac{\partial \delta v}{\partial t} + H\delta v + (v_0 \cdot \nabla)\delta v + c_s^2\nabla\delta + \nabla\delta\phi = 0 \tag{13.23}$$

$$\nabla^2\delta\phi = 4\pi G\rho_0\delta \quad , \tag{13.24}$$

where we introduced the adiabatic (constant entropy) speed of sound c_s defined as $c_s^2 = \partial P/\partial\rho$.

13.4 Linear perturbations in comoving coordinates

Introducing "comoving" coordinates which follow the Hubble flow:

$$x = \frac{r}{a(t)} \quad , \tag{13.25}$$

and the comoving velocity perturbation

$$u = \frac{\delta v}{a(t)} \quad , \tag{13.26}$$

we have now the identifications

$$\frac{\partial}{\partial t} = \frac{\partial}{\partial t}|_{x=\text{const}} \tag{13.27}$$

$$\nabla_r = \frac{1}{a}\nabla_x \quad . \tag{13.28}$$

The new time derivative is comoving with the Hubble flow

$$\frac{\partial}{\partial t} \rightarrow \frac{\partial}{\partial t} + v_0 \cdot \nabla_r = \frac{\partial}{\partial t} + Hx \cdot \nabla_x \quad . \tag{13.29}$$

With the new coordinates, the continuity equation becomes

$$\dot{\delta} + \nabla \cdot u = 0 \quad . \tag{13.30}$$

For transforming the Euler equation it is useful first to see how the derivative of the velocity perturbation changes

$$\frac{\partial \delta v}{\partial t} \rightarrow \frac{\partial \delta v}{\partial t} - Hx \cdot \nabla_x \delta v = a\frac{\partial u}{\partial t} + aHu - aHx \cdot \nabla_x u \quad . \tag{13.31}$$

Using the last result, th Euler equation becomes

$$a\frac{\partial u}{\partial t} + aHu - aHx \cdot \nabla_x u + aHu + (v_0 \cdot \nabla_x)u + \frac{c_s^2}{a}\nabla_x \delta + \frac{1}{a}\nabla_x \delta\phi = 0 \quad . \tag{13.32}$$

Factorizing and simplifying

$$a\left(\frac{\partial u}{\partial y} + 2Hu\right) + \frac{1}{a}\left(c_s^2 \nabla_x \delta + \nabla_x \delta\phi\right) = 0 \quad . \tag{13.33}$$

Summarizing, the final form of the evolution equations with comoving variables (dropping the variables indices: $\nabla_x \equiv \nabla$) are

$$\dot{\delta} + \nabla \cdot u = 0 \quad , \tag{13.34}$$

$$\dot{u} + 2Hu = -\frac{c_s^2 \nabla\delta + \nabla\delta\phi}{a^2} \quad , \tag{13.35}$$

$$\nabla^2 \delta\phi = 4\pi G \rho_0 a^2 \delta \quad . \tag{13.36}$$

13.5 Perturbations Analysis

We study now how perturbations evolve in time, obtaining for the last system of equations an evolution equation for δ. For doing that we have to eliminate the other variables. Let's start taking the divergence of the Euler equation (dropping the second-order term $\delta\nabla c_s^2$)

$$\nabla \cdot \dot{u} + 2H\nabla \cdot u = -\frac{c_s^2 \nabla^2\delta + \nabla^2\delta\phi}{a^2} \quad . \tag{13.37}$$

Substituting now into the last result the continuity equation and the Poisson equation to eliminate u and $\delta\phi$

$$\ddot{\delta} + \underbrace{2H\dot{\delta}}_{\text{expansion}} = \underbrace{\frac{c_s^2\nabla^2\delta}{a^2}}_{\text{pressure}} + \underbrace{4\pi G\rho_0\delta}_{\text{gravity}} \quad . \tag{13.38}$$

Here we see that the expansion term acts like a damping term, while the opposing pressure and gravity terms are responsible for the wave propagation.
The last equation is a second order linear equation and can be analyzed decomposing it in plane waves (Fourier tranform)

$$\delta(x,t) = \frac{1}{(2\pi)^3}\int \hat{\delta}(k,t)e^{-ik\cdot x}d^3k \quad . \tag{13.39}$$

Substituting the parturbation trasformed in momentum space, the initial equation becomes

$$\ddot{\hat{\delta}} + 2H\dot{\hat{\delta}} = \left(4\pi G\rho_0 - \frac{c_s^2k^2}{a^2}\right)\hat{\delta} \quad . \tag{13.40}$$

Separating the time component of the wave from the spacial one

$$\hat{\delta}(k,t) = \delta(k)e^{i\omega t} \quad , \tag{13.41}$$

and substituting into the wave equation we obtain the dispersion relation

$$\omega^2 - 2i\omega H = -\left(4\pi G\rho_0 - \frac{c_s^2k^2}{a^2}\right) \quad . \tag{13.42}$$

Defining the famous "Jeans length"

$$\lambda_J = \frac{2\pi}{k_J} = \frac{2\pi c_s}{a\sqrt{4\pi G\rho_0}} \quad , \tag{13.43}$$

the dispersion relation becomes

$$\omega^2 - 2i\omega H = -\frac{c_s^2}{a^2}\left(k_J^2 - k^2\right) \quad . \tag{13.44}$$

The last equation implies that

$$k > k_J \quad (\lambda < \lambda_J) \quad \Rightarrow \quad \omega^2 > 0 \tag{13.45}$$

$$k < k_J \quad (\lambda > \lambda_J) \quad \Rightarrow \quad \omega^2 < 0 \tag{13.46}$$

The $\omega^2 > 0$ case represents oscillatory solutions, while $\omega^2 < 0$ represents exponential decay or growth solutions.
Physically, perturbations on a small scale (below the Jeans wavelength) tend to oscillate, while perturbations on a large scale (larger than the Jeans wavelength) tend to grow exponentially (the exponential decays are not interesting in this context since they just disappear).
The growing modes can thus be written as

$$\hat{\delta}(k,t) = \delta(k) e^{\gamma t} \quad , \tag{13.47}$$

with

$$\gamma = \sqrt{4\pi G\rho_0 - \frac{c_s^2 k^2}{a^2}} = \frac{c_s}{a}\sqrt{k_J^2 - k^2} \quad , \tag{13.48}$$

for $k < k_J$. The typical time scale for the growth of a perturbation mode (the "e-folding" time) is $\tau = 1/\gamma$. If a gas is very cold, $c_s \sim 0$ and $\tau \sim 1/\sqrt{4\pi G\rho_0}$: the larger the density, the faster the perturbation will grow, as expected.

13.6 Large perturbations in an expanding matter-dominated Universe

We would like to investigate how the perturbations exactly grow in an expanding Friedmann Universe. Focusing on large scales, where $k_J \ll k$, we can neglect the k^2 term in Eq. 13.40

$$\ddot{\hat{\delta}} + 2H\dot{\hat{\delta}} = \left(4\pi G\rho_0 - \frac{c_s^2 k^2}{a^2}\right)\hat{\delta} \approx 4\pi G\rho_0 \hat{\delta} = \frac{3}{2}H^2\hat{\delta} \quad . \tag{13.49}$$

where we substituted the critical density $\rho_0 = \rho_c = 3H^2/8\pi G$ which is a reasonable choice for the matter-dominated era, where we know aready

that $H = 2/(3t)$. Substituting in the previous equation, the equation describing the evolution of the perturbations becomes

$$\ddot{\hat{\delta}} + \frac{4}{3}\frac{\dot{\hat{\delta}}}{t} = \frac{2}{3}\frac{\hat{\delta}}{t^2} \quad . \tag{13.50}$$

For solving the last equation, we can take a power-law *ansatz* solution like $\hat{\delta} \sim t^n$

$$n^2 + \frac{1}{3}n = \frac{2}{3} \quad , \tag{13.51}$$

which has two possible solutions: $n = -1$ and $n = 2/3$.
Discarding the negative solution which describes decaying modes we have

$$\hat{\delta} \sim t^{2/3} \sim a \quad . \tag{13.52}$$

The last result shows that within our approximations, the growing modes are independent from the frequency and they are linearly proportional to the scale factor. Therefore, in an expanding Universe, perturbations do not grow exponentially with time, but slower, following a power-law. These conclusions remain true also in the presence of a cosmological constant.

13.7 Large perturbations in an expanding radiation-dominated Universe

In the case of radiation domination, we have to perform all the calculations again, since we cannot neglect the pressure, which actually is $P/c^2 = \rho/3$.
The pressure gradient term can be neglected and in the large-scale approximation $k \ll k_J$ we obtain the following equation for the perturbation dynamics

$$\ddot{\hat{\delta}} + 2H\dot{\hat{\delta}} = 4H^2\hat{\delta} \quad . \tag{13.53}$$

From the Friedmann equations, in the radiation-dominated era $H = 1/2t$ and the equation simplifies to $n^2 = 1$ with solutions $n = \pm 1$. Considering only the positive solution

$$\hat{\delta} \sim t \sim a^2 \quad . \tag{13.54}$$

Chapter 14 | The Cosmic Microwave Background

The Cosmic Microwave Background (CMB) is a relic electromagnetic radiation from the early Universe. It was predicted before its discovery in 1948 by R. Alpher and R.Herman. The CMB was finally measured by A. Penzias and R. Wilson in 1964 with a ground-based antenna, winning the Nobel price for the discovery in 1978.
Nowadays very precise measurements of the CMB are done with satellites.
The CMB originated at the time where the temperature of the Universe, through expansion, dropped at the point of allowing the capture of electrons by nuclei. The Universe then bacame transparent to the electromagnetic radiation, which then was red-shifted from the time of its production until now. The cosmological red-shift predicts a much colder relic radiation today with respect to its original temperature. Alpher and Herman gave 5K as the first estimate, which turned out to be not far away to the presently known value.
The CMB has today a density of about 514 photons per cm^3 and they traveled for 99.7% of the age of the Universe until they reached our detectors. At the time when the CMB was produced, the Universe was about 1000 times smaller and 1000 warmer than now.
The CMB appears as a rather uniform radiation compatible with a blackbody distribution with a temperature of about 2.7K. What is actually interesting are the deviations from this mean temperature as a function of the angular scale of the sky.
After reading this chapter you have definitely to google "Planck CMB simulator" or go to "http://strudel.org.uk/planck" and look interactively how the comological parameters affect the CMB.

14.1 Recombination

14.2 Multipole Decomposition of the CMB

The CMB has an average temperature (mediated over the whole sky) of about T_0=2.7K. After subtracting this average temperature, we can consider the relative fluctuations around the mean

$$\frac{\delta T}{T_0} = \frac{T - T_0}{T_0}(\theta, \phi) \quad , \tag{14.1}$$

which depend on the two angles θ and ϕ which constitute a coordinate system describing the sky around us. Since we are dealing with small fluctuations on the surface of a sphere (the sky), we can expand the relative fluctuations on the spherical harmonics basis $Y_{l,m}$ (this is analogous to a Fourier series expansion in a "flat" case on the sin / cos basis)

$$\frac{\delta T}{T_0}(\theta, \phi) = \sum_{l,m} a_{l,m} Y_{l,m}(\theta, \phi) \quad . \tag{14.2}$$

Since $Y_{l,m}$ is an orthonormal set of functions [1], we can invert the previous equation obtaining

$$a_{l,m} = \int Y^*_{l,m}(\theta, \phi) \frac{\delta T}{T_0}(\theta, \phi) d\Omega \quad , \tag{14.3}$$

where the integral in $d\Omega$ is done over all angles.
Since we subtracted the average temperature T_0 and $Y_{0,0}$=const, we should have $a_{0,0} = 0$ for the lowest multipole ($l = 0$). For $l = 1$ we have the *dipole contribution* which is due to the Doppler effect caused by the motion of the Earth with respect to the CMB.
Therefore, the interesting part of the CMB which should contain information about its origin at the decoupling time must be contained in the $l > 1$ multipoles.
The (in general, complex) components $a_{l,m}$ represent fluctuations around zero, therefore $\langle a_{l,m} \rangle = 0$. If they represent Gaussian random variables, the whole information about them should be contained in the variances

[1] $\int Y_{l,m} Y^*_{l',m'} d\Omega = \delta_{l,l'} \delta_{m,m'}$

$\langle |a_{l,m}|^2 \rangle$ which are connected to the power of the specific (l, m) mode. Given the isotropic nature of the CMB, we expect the variance to be dependent only from l, which is related to the angular size of the anisotropy pattern. Remembering the closure relation $\sum_m |Y_{l,m}|^2 = (2l+1)/4\pi$ for the spherical harmonics, we can define the **angular power spectrum**

$$C_l = \frac{1}{2l+1} \sum_m \langle |a_{l,m}|^2 \rangle \quad , \tag{14.4}$$

which is also called the **TT power spectrum**. Sometimes C_l is indicated as C_l^{TT}. If we assume that the $a_{l,m}$ are independent random variables, we have for the correlations

$$\langle a_{l,m} a_{l',m'} \rangle = \delta_{l,l'} \delta_{m,m'} C_l \quad . \tag{14.5}$$

If we assume that the spectrum of the density perturbations in the early Universe was Gaussian, the angular power spectrum contains all the statistical information about the CMB anisotropies and therefore we can proceed in calculating

$$\begin{aligned} \frac{\delta T}{T_0} = \langle \sum_{l,m} a_{l,m} Y_{l,m} \sum_{l,m} a^*_{l,m} Y^*_{l,m} \rangle = \sum_{l,l',m,m'} Y_{l,m} Y^*_{l,m} \langle a_{l,m} a^*_{l,m} \rangle = \\ \sum_l C_l \sum_m |Y_{lm}|^2 = \sum_l \frac{(2l+1)}{4\pi} C_l \quad . \end{aligned} \tag{14.6}$$

A subtle point here is the following: the averaging $\langle\rangle$ should be done over an ensemble of Universes, while we have only one realization of it. We can imagine that averaging over different directions might represent an averaging over an ensemble of different Universes. In practice, the *observed* power spectrum is calculated as follows

$$\frac{1}{4\pi} \int \left(\frac{\delta T}{T} \right)^2 d\Omega = \sum_l \frac{2l+1}{4\pi} \hat{C}_l \quad , \tag{14.7}$$

with $\hat{C}_l = \sum_m |a_{l,m}|^2/(2l+1)$.
So if the theoretical power spectrum the angular average spectrum were the same, we should have $\langle \hat{C}_l \rangle = C_l \Rightarrow \langle \hat{C}_l - C_l \rangle = 0$. The averaged

squared difference between theory and observation is called **cosmic variance** and a direct calculation yields

$$\langle (\hat{C}_l - C_l)^2 \rangle = \frac{2}{2l+1} C_l^2 \quad . \tag{14.8}$$

The last formula shows that the variance is smaller for large l (small scales), while it is large for small l (large scales). The cosmic variance represents a limit on the accuracy of the comparison between theory and experiment.

14.3 Angular Scales

As we anticipated in the previous section, the multipole number l is connected to the angular scale in the sky. The spherical harmonics have an oscillatory pattern on the sphere in the following (approximate) sense: in a full great circle on the spherical surface, there are l wavelengths of oscillations. This means that the angular scale corresponding to the mode l is $\theta = 2\pi/l$. We can define the angular resolution as the angle connected to the distance from a crest and a valley of a wave $\theta_{res} = \pi/l$. A detector must have a resolution at least equal to θ_{res} in order to resolve scales up to l.
For comparison, the first high-resolution satellite mission (COBE) had $\theta_{res} = 7^\circ \Rightarrow l < 26$. The follow-up experiment (WMAP) had $\theta_{res} = 0.23^\circ \Rightarrow l < 783$. The latest (at the time of writing) and most precise satellite mission (Planck) improves the angular resolution about three times over WMAP.
The question we would like to answer now is: if there were density perturbations in the early Universe characterized by (comoving) wavenumbers k (*i.e.* a comoving wavelength $\lambda = 2\pi/k$), to which CMB multipole l will contribute the most? In other words, we would like to link the primordial perturbations to the pattern measured in the CMB.
Let's define the **angular diameter distance** as $d_A = D/\theta$, which is the same as defining the angle θ subtended by an object of width (length perpendicular to the line of sight) D placed at a distance d_A from us. Taking into account the expansion of the Universe we can define the comoving

version of the angular diameter distance

$$d_A^c = \frac{D^c}{\theta} = \frac{(a_0/a)D}{\theta} = \frac{(1+z)D}{\theta} = (1+z)d_A \quad . \tag{14.9}$$

Considering now the comoving wavelength λ (associated with the comoving wavenumber k) of a density perturbation, the mode should be visible in the CMB at an angular size of

$$\theta_\lambda = \frac{\lambda}{d_A^c} = \frac{2\pi}{k d_A^c} = \frac{2\pi}{l} \quad , \tag{14.10}$$

which gives the relation $l = k d_A^c$. This result follows from a rather simplified treatment, since clearly it is not possible that a single density perturbation mode contributes to just one single CMB harmonic. The full calculation must take into account all the modes but the basic result we obtained still holds, in the sense that only the modes close to k contribute significantly.

14.4 CMB Polarization

The CBM can be polarized because of different reasons. Thomson scattering is surely present (scattering of photons from charged particles that took place at the last scattering surface) and contributes up to $\sim$ 5% level which in terms of temperature fluctuations corresponds to few μK. Thompson (linear) polarization was indeed experimentally detected.
The Thompson cross section is proportional to the photon polarization direction before ($\hat{\epsilon}$) and after the scattering ($\hat{\epsilon}'$)

$$\frac{d\sigma}{d\Omega} \propto |\hat{\epsilon} \cdot \hat{\epsilon}'|^2 \quad . \tag{14.11}$$

Pictorially, the incident photon makes the charged particle (e.g. an electron) oscillate in the direction of the polarization. The oscillation creates radiation with polarization mostly parallel to the initial polarization. If the incident radiation has quadrupole anisotropies, this will result in an emitted linearly polarized radiation (this can be seen since the incident orthogonal components are suppressed in Eq. 14.11).
A photon can be polarized only in the two directions orthogonal to its

propagation. The polatization can always be decomposed in two othogonal modes which are both orthogonal to the direction of propagation. The superposition of the two polarization states given in general an elliptical polarization, and linear or circular polarizations are special cases.
Defining the polarization vector $\hat{\epsilon} = \vec{E}/|E|$ where E is the electric field, the **polarization tensor** is defined as the time average (considering E as an oscillating field in complex representation)

$$p_{ij} = \langle \hat{\epsilon}_i \hat{\epsilon}_J^* \rangle \quad . \tag{14.12}$$

The polarization tensor is traceless

$$Trp = p_{ii} = \langle \hat{\epsilon}_i \hat{\epsilon}_i^* \rangle = \langle |\epsilon| \rangle = 1 \tag{14.13}$$

and Hermitian $(p_{ij})^* = p_{ji}$. An orthogonal basis for Hermitian matrices is provided by the three 2×2 Pauli matrices σ_k. The last observation, combined with the fact that Pauli matrices are trace-less but $Trp = 1$ leads to the following decomposition

$$p_{ij} = \frac{1}{2} \left(I + Q\sigma_1 + U\sigma_2 + V\sigma_3 \right) \tag{14.14}$$

where I is the identity matrix and

$$\sigma_1 = \begin{pmatrix} 1 & 0 \\ 0 & -1 \end{pmatrix} \quad ; \quad \sigma_2 = \begin{pmatrix} 0 & 1 \\ 1 & 0 \end{pmatrix} \quad ; \quad \sigma_3 = \begin{pmatrix} 0 & -i \\ i & 0 \end{pmatrix} \quad . \tag{14.15}$$

The numbers Q,U,V are called *Stokes parameters* and their nice property is that they are measurable. For example, if we take a linear polarization filter and pass polarized light through it and measure the intensity of light F as a function the filter θ (F_θ) we can verify that $Q = F_0 - F_{90}$, $U = F_{45} - F_{135}$. The "chirality" (the direction where the polarization is rotating) is $V = 2F_C - F$ where F_C is the intensity of the light after passig through a filter which passes circularly polarized light in a certain direction and F is the total incident intensity. Stokes parameters are usually defined between -1 and 1, so Q, U, V are normalized to F.
The degree of polarization is sometimes given as $r = \sqrt{Q^2 + U^2 + V^2}$. The Stokes parameters vary on a spherical surface referred as the Poincare' sphere.

The **intensity tensor** which tells how much intensity there is in each polarization mode is analogously defined as

$$\rho_{ij} = \langle E_i E_j^* \rangle = \frac{1}{2} \left(J \cdot I + Q\sigma_1 + U\sigma_2 + V\sigma_3 \right) \quad . \tag{14.16}$$

In this case we did not normalize by the electric field vector length and thus we have the new factor

$$J = \delta_{ij}\rho_{ij} = |E_x|^2 + |E_y|^2 \tag{14.17}$$

for a certain choice of orthogonal axes x, y while z is the propagation direction of the wave. J is obviously a geometric invariant (independent from the coordinate choice). A second invariant is

$$V = \epsilon_{ij}\rho_{ij} \quad , \tag{14.18}$$

while the Stokes parameters Q and U change with the change of coordinates.
Electromagnetic interactions are parity-conserving and this demands that the helicity must vanish: V=0.
Furthermore, there are two differential invariants (independent from the orientation of the axes)

$$\begin{aligned} S &= \nabla^2 P_E = \partial_i \partial_j \rho_{ij} \\ P &= \nabla^2 P_B = \epsilon_{ik} \partial_i \partial_j \rho_{jk} \end{aligned} \tag{14.19}$$

called scalar and pseudo-scalar invariants, respectively. We consider second-derivatives also because we are dealing with a rank-2 tensor. The other notation ($P_{E/B}$) refers to the so-called "E-modes" and "B-modes" respectively, in analogy to the Helmholtz decomposition of a vector V in a curl-free (irrotational) and divergence-free (solenoidal) parts using a scalar function ψ and a vector function A: $\vec{V} = \vec{\nabla}\psi + \vec{\nabla} \times \vec{A}$.
Actually, the polarization tensor can indeed be decomposed using two scalar functions A and B: $\rho_{ij} = (\partial_i \partial_j - \frac{1}{2}\partial^2)A + (\partial_i \partial_k \epsilon_{kj} + \partial_j \partial_k \epsilon_{ki})B$. We defined already the TT power spectrum related to the correlation function of the temperature fluctuations. We can now define also correlation functions for the polarization fluctiations. Using the decomposition of

the polarization in E and B modes, the only non-vanishing correlation functions (including TT calculated before) are

$$\begin{aligned}
\langle T(\hat{n})T(\hat{n}')\rangle &= \frac{1}{4\pi}\sum_{l=0}^{l=\infty}(2l+1)C_l^{TT}P_l(\cos\theta) \\
\langle T(\hat{n})E(\hat{n}')\rangle &= \frac{1}{4\pi}\sum_{l=0}^{l=\infty}(2l+1)C_l^{TE}P_l(\cos\theta) \\
\langle E(\hat{n})E(\hat{n}')\rangle &= \frac{1}{4\pi}\sum_{l=0}^{l=\infty}(2l+1)C_l^{EE}P_l(\cos\theta) \\
\langle B(\hat{n})B(\hat{n}')\rangle &= \frac{1}{4\pi}\sum_{l=0}^{l=\infty}(2l+1)C_l^{BB}P_l(\cos\theta) \quad .
\end{aligned} \tag{14.20}$$

Having E and B opposite parity properties, their cross-correlations vanish. The origin of the E/B notation comes from electromagnetism, since an electric (E) field can be written as the gradient of a scalar field, while the magnetic field (B) can be written as the curl of a vector field.
Thompson scattering, being a purely electromagnetic process (parity-conserving), can induce only E-mode polarizations.
B-modes can arise only if $P \neq 0$ and this can happen for example in the case of vector perturbations ($\rho_{ij} = \partial_i V_j - \partial_j V_i \Rightarrow P = \epsilon_{ij}\partial^2\partial_i Vj$: can be caused by magnetized interstellar or intergalactic media), tensor perturbations (e.g. from gravitational waves) or second order scalar perturbations.

14.5 CMB Anisotropies

The spherical harmonic expansion in multipoles of the CMB temperature is formally done from $l = 0$ to $l = \infty$. The $l = 0$ multipole (the *monopole*) is just a constant and its physical interpretation is the average temperature over the whole sky: $T_0 = 2.7255 \pm 0.0006$ K. The temperature can be converted in density of photons n^0, density of mass ρ^0 or density parameter Ω^0_{CMB}:

$$\begin{aligned}
n^0 &= 411 \text{ photons/cm}^3 \\
\rho^0 &= 4.64 \times 10^{-34}\text{g/cm}^3 = 2.6 \times 10^{-10}\text{GeV/cm}^3 \\
\Omega^0_{CMB}h_0^2 &= 2.47 \times 10^{-5} \quad .
\end{aligned} \tag{14.21}$$

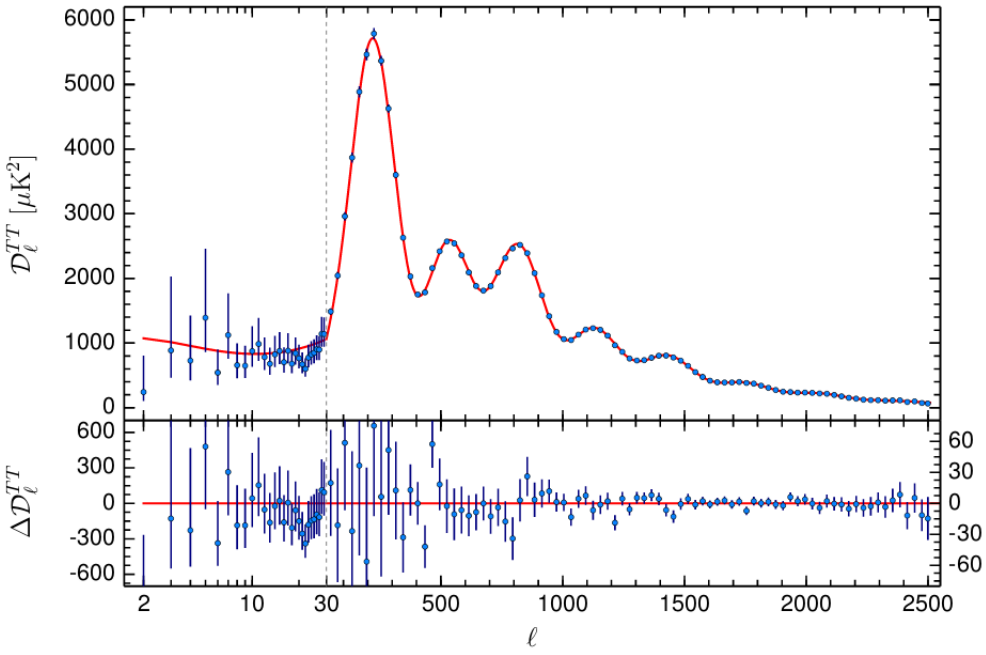

Figure 14.1: Planck Spectrum (arXiv:1502.01589).

The $l = 1$ multipole (the *dipole*) represents fluctuations on an angular scale of order π (or 180°): it is like dividing the sky in two halves and look for differences. The dominant contribution to the dipole term comes from the motion of our detector (ultimately of the earth and the sun) with respect to the CMB frame.
The amplitude of the dipole is $T_1 = 3.355 \pm 0.008$ mK, 10^3 times smaller than the monopole: this shows already the rather high uniformity of the CMB, but the error in the measurement tells us that even small anisotropies can be measured with good accuracy. The dipole amplitude leads to the conclusion that the solar system is moving with velocity $v \sim 370$ km/s with respect to the CMB.
Subtracting the $l = 0$ and $l = 1$ terms whose origin is clear, we conclude that the important cosmological information must be encoded into the $l > 1$ multipoles, up to an l_{max} determined by the experimental resolution. Usually, two classes of fluctuations are considered:
Primary Fluctuations: Produced at the last scattering surface or before. These anisotropies carry information about the early universe. In princi-

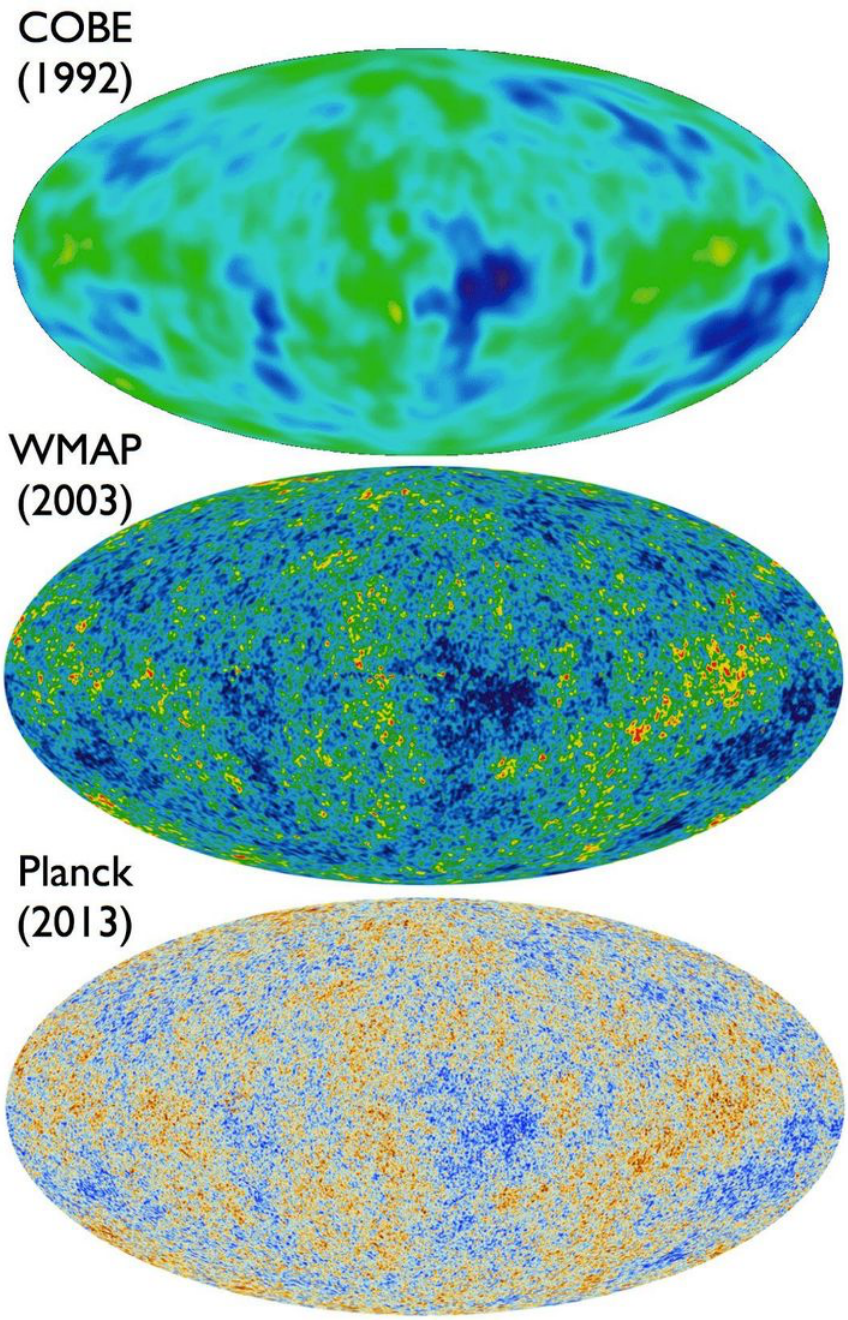

Figure 14.2: Satellite mission for the CMB measurement

ple, these anisotropies can be of the scalar, vector or tensor type. Vector modes are stretched out by the expansion of the universe and are therefore expected to be unobservable. Tensor modes decay as they enter the cosmological horizon, so they are suppressed at angular scales smaller than the one of the last scattering surface ($\sim 1^\circ$). The leave a too small imprint into the TT spectrum to be detected but they might be observed in the BB spectrum.
Secondary Fluctuations: These anisotropies araised after the recombination era: they can provide information about the "normal matter" expansion era.

14.5.1 Primary Anisotropies

Looking at Fig. 14.1, the most prominent characteristic is the presence of peaks at $l > 100$. These peaks are the result of the oscillations of the photon-baryon plasma before recombination. Oscillations happen when two opposing forces are at work. In this case, the gravitational force tending to cluster matter (likely around dark matter concentrations) found opposition from the pressure caused by photons. The amplitude of the resulting density fluctuations is quite small ($\delta\rho/\rho \sim 10^{-5}$). This means that we can consider a linear evolution of these perturbations as a good approximantion and in a linear theory every oscillation mode evolves decoupled from the others.
When an inhomogeneity of certain wavelenght entered the cosmological horizon, plasma oscillations started. In the linear approximation, all the inhomogeneity with the same wavelenght entered the horizon at the same time, thus adding in phase.
The first (and highest) peak in Fig. 14.1 was generated by perturbations which entered the horizon at the recombination time. The (smaller) peaks at higher l are caused by perturbations which entered the horizon before recombination.
An analysis of the cosmological perturbations shows that the perturbation spectrum is flat: this means that every mode should have the same amplitude when entering the horizon. Fig. 14.1 shows that the peaks are decreasing in amplitude: this is due to cosmological expansion, since high-l peaks entered the horizon before and were stretched more. After recombination, no peaks can be produced since there is no oscillating

plasma.
The location and height of the peaks depends from the cosmological parameters. The position of the **first peak** is tightly connected to the total amount of matter/enegy present in the universe today (Ω^0_{tot})

$$l_{1stpeak} \sim \frac{220}{\sqrt{\Omega_m}} \quad . \tag{14.22}$$

A quick inspection of the data in Fig. 14.1 shows that $\Omega^0_{tot} \sim 1$. This means that the Universe today is very close to the critical density and in turn the geometry is very close to the flat one.
The hight of the first peak instead, is tightly connected to the amount of barionic matter Ω^0_B.
Why the position of the first peak has to do with the geometry of the Universe? A physical argument is the following. The size corresponding to the first is known, since it is equal to the cosmological horizon (better: the sound horizon, where the speed of light is replaced with the sound speed in the plasma) at the recombination time. The angle[2] under which the first peak is observed today depends on the geometry. This angle in the case of a flat Universe is about $\sim 1^\circ$ which corresponds to $l \sim 220$: exactly where the first peak is.
The **even peaks** (second, fourth,..)

[2]The angle here is the angle calculated with the triangle given by the distance from us to the last scattering surface and the particle horizon for points at the surfece.